AECL-10748

ATOMIC ENERGY OF CANADA LIMITED

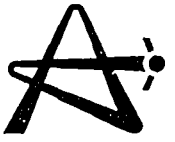

ÉNERGIE ATOMIQUE DU CANADA LIMITÉE

PROCEEDINGS OF THE WORKSHOP ON APPLIED MATHEMATICS

PROCÈS-VERBAL DE LA RÉUNION DE TRAVAIL SUR LES MATHÉMATIQUES APPLIQUÉES

H.C. LEE, M. COUTURE, S. DOUGLAS and H.P. LEIVO

1992 February 7-8, Cockcroft Centre, Deep River

Chalk River Laboratories Laboratoires de Chalk River

Chalk River, Ontario K0J 1J0

October 1992 octobre

AECL Research

PROCEEDINGS OF THE WORKSHOP ON APPLIED MATHEMATICS

1992 February 7-8, Cockcroft Centre, Deep River

Editors: H.C. Lee, M. Couture, S. Douglas, *and* H.P. Leivo

Theoretical Physics Branch
Chalk River Laboratories
Chalk River, Ontario K0J 1J0
1992 October

AECL-10748

EACL Recherche

PROCÈS-VERBAL DE LA RÉUNION DE TRAVAIL SUR LES MATHÉMATIQUES APPLIQUÉES

Rédacteurs-réviseurs: H.C. Lee, M. Couture, S. Douglas et H.P. Leivo

RÉSUMÉ

La séance de travail sur les mathématiques appliquées a eu lieu au Centre Cockcroft à Deep River en Ontario les 7 et 8 février 1992. Le but de la séance de travail a été de permettre un forum de spécialistes de mathématiques appliquées pour étudier l'utilisation des mathématiques appliquées et examiner leur avenir à EACL Recherche.

Cinquante sept personnes se sont inscrites pour participer à la séance de travail dont quatre personne ne faisant pas partie d'EACL, quatre faisant partie des Laboratoires de Whiteshell et le reste faisant partie des Laboratoires de Chalk River. Les personnes d'EACL Recherche représentaient 22 services et groupes différents. Il y a eu, au total, huit causeries de 30 minutes et 25 causeries de 15 minutes qui ont englobé une très grande variété de sujets.

Le nombre de personnes y ayant participé a été beaucoup plus grand qu'on ne l'avait d'abord prévu. L'ambiance, au cours de celle-ci, a été pleine d'entrain, vive et toute simple. Pour beaucoup de personnes, la réunion a été une occasion rare et agréable de parler de leur travail avec leurs confrères et consoeurs d'EACL Recherche et de savoir ce que les autres font. La bonne volonté, l'intérêt et l'enthousiasme ont été manifestes pendant les deux jours d'activités. De nombreuses nouvelles relations ont été établies et il se pourrait bien qu'il en résulte une collaboration entre les diverses disciplines engageant des personnes de différents services.

Les points de vue quant à la fréquence des futures réunions de ce genre varient; on a suggéré un intervalle de un à cinq ans entre celles dont le sujet est aussi général que celle qui a eu lieu il y a quelque temps; les réunions de travail sur des sujets plus particuliers pourraient avoir lieu plus fréquemment; en outre, certaines personnes ont exprimé le besoin de cours théoriques de mathématiques supérieures.

La séance de travail a été patronnée et en partie financée par l'unité organisationnelle de Sciences physiques.

Service de Physique théorique
Laboratoires de Chalk River
Chalk River (Ontario) K0J 1J0
1992 octobre

AECL-10748

AECL Research

PROCEEDINGS OF THE WORKSHOP ON APPLIED MATHEMATICS

Editors: H.C. Lee, M. Couture, S. Douglas, *and* H.P. Leivo

ABSTRACT

The Workshop on Applied Mathematics was held at the Cockcroft Centre, Deep River, Ontario, 1992 February 7-8. The purpose of the workshop was to provide a forum for applied mathematicians to survey the use and to discuss the future of applied mathematics at AECL Research.

There were 57 registered participants at the workshop, including four from outside AECLResearch, four from Whiteshell Laboratories and the balance from Chalk River Laboratories. The AECL Research participants came from 22 different branches and units. A total of eight 30-minute and 25 15-minute talks, covering a very wide range of topics, were presented.

The number of participants was significantly greater than first anticipated. The atmosphere at the workshop was lively, spontaneous and informal. For many, the meeting was a rare and refreshing opportunity to discuss their work with peers within AECL Research and to find out what others are doing. Goodwill, interest and enthusiasm were evident throughout the two-day event. Many new contacts were made, and it is not unlikely that interdisciplinary collaboration involving people from different branches will result.

Opinions on how frequently similar meetings should be held vary; suggested intervals between meetings of a scope as general as in the one just held range from one to five years. Workshops on more specific topics could be held more frequently; some participants also expressed a need for formal courses on advanced mathematics.

This workshop was sponsored and partially funded by the Physical Sciences Organizational Unit.

Theoretical Physics Branch
Chalk River Laboratories
Chalk River, Ontario K0J 1J0
1992 October

AECL-10748

DEDICATION

We are deeply saddened by the sudden death of Bernard Lidicky in a tragic car accident. Bernard was an IAEA visiting fellow from Czechoslovakia attached to AECL Research and a participant at the workshop. This volume is dedicated to his memory.

TABLE OF CONTENTS

APPROACHING MULTIPHASE FLOWS FROM THE PERSPECTIVE OF COMPUTATIONAL FLUID DYNAMICS

ANDRZEJ O. BANAS
Thermalhydraulics Development Branch
AECL Research, Chalk River Laboratories

ABSTRACT

Thermalhydraulic simulation methodologies based on subchannel and porous-medium concepts are briefly reviewed and contrasted with the general approach of Computational Fluid Dynamics (CFD). An outline of the advanced CFD methods for single-phase turbulent flows is followed by a short discussion of the unified formulation of averaged equations for turbulent and multiphase flows. Some of the recent applications of CFD at Chalk River Laboratories are discussed, and the complementary role of CFD with regard to the established thermalhydraulic methods of analysis is indicated.

1. Limitations of Thermalhydraulic Simulation Methodologies

Multidimensional computations of internal flows and heat transfer in nuclear reactor components rely at present on two main methodologies for spatial discretization: porous-medium and subchannel approaches.[1,2] Even though both are considered to be advanced computational tools, aimed at accommodating models for single and multiphase flows, these approaches target only relatively crude resolution of flow details, and their underlying theoretical bases rest firmly on hydraulic concepts. Methods of this kind are ideally suited for the geometries of densely-packed rod bundles and tube banks, widely used in the nuclear reactor systems, but they suffer from serious *inherent* limitations.

The linear dimensions of computational cells, 'porous' control-volumes and subchannels, can be small compared to the scale of equipment size, but they must remain large relative to the scale of local flow-field variations. Whereas any subchannel layout must provide each subchannel with at least some solid-wall boundary, the lower-bound restriction on the sizes of 'porous' control-volumes stems from the requirement that they contain sufficient proportion of the solid matrix in order to smear the flow details over large enough regions. Only then can the wall effects, both mechanical and thermal, be accounted for through hydraulic means (empirical friction factors, heat-transfer coefficients, etc.) in these computational approaches.

In both the porous-medium and subchannel computations, the finite-volume balances embody approximations whose effects cannot be diminished by the use (whenever possible) of finer meshes. The universally employed representation of the fluid-solid forces in terms of distributed resistances is compatible with the control-volume selection, but it precludes the rigorous consideration of momentum diffusion within the fluid, and the no-slip or velocity-profile-based boundary conditions at solid surfaces. Wall boundary conditions for scalars, such as temperature, are similarly avoided, and the effects of near-wall flow patterns on their local gradients cannot be considered. In addition, subchannel arrangements are, in general, non-orthogonal, preventing a rigorous treatment of the transverse momentum balances.

2. Perspective of Computational Fluid Dynamics

In essence, the porous-medium and subchannel methodologies bridge the gap between the system (or component-level) thermalhydraulics and the truly *micro*-approach represented by Computational Fluid Dynamics (CFD). As a rule, the modern CFD algorithms are formulated for arbitrary multidimensional geometries, and accommodate progressively finer approximations to the continuum description of fluid flow, heat and mass transfer. When allotted sufficient numbers of degrees of freedom, the CFD analogues of continuum equations are able to capture at least some of the physics beyond the reach of hydraulics approaches, and therefore provide a framework in which the limitations imposed by the use of the latter methods may be overcome. The CFD methods for internal

flows (based on finite-volume or finite-element discreatizations) adopt meshes that naturally allow for realistic representations of solid geometries, and enable the constraint of the computed fields through imposition of wall boundary conditions. In principle, the resolution of important physical and geometrical scales is then always better than that obtainable with subchannel or porous-media methods, and any empirical input to modelling is introduced at the more local level.

Among the most distinctive and industrially-important CFD methodologies developed to date are the numerical simulation methods for turbulent flows, closely allied with turbulence modelling. The advanced methods for incompressible flows comprise four categories:[3]

- One-point-average formulations are based on a hierarchy of correlation equations obtained through one-point averaging of the Navier-Stokes equations. Closure of a truncated set of these equations must rely on hypotheses regarding higher-order correlations appearing in the equations governing the evolution of lower-order correlations.
- Two-point-average methods are based on two-point averages of the Navier-Stokes equations, and were introduced to allow explicit consideration of scale information in modelling.
- Large-Eddy-Simulation Methods, three-dimensional and time-dependent, proceed with explicit computation of large-scale flow-field structures, while accounting for the small-scale turbulence through the subgrid-scale models.
- Direct (full) simulations of turbulent flows, currently feasible only for flows characterized by relatively small Reynolds numbers, attempt to resolve the flow-field at the Kolmogorov length-scale by solving the discrete analogues of the unaveraged Navier-Stokes equations.

Clearly, for flows characterized by realistic Reynolds numbers, the resolution limitations on present-day computers make it necessary to engage averaged formulations and turbulence models. Complex (and often poorly understood) physics, such as that encountered in the presence of multiple phases, adds additional burden. It has been argued recently by Boris[4] that the CFD methods available today can simulate flow either in complex geometry with simple physics or with complex physics in relatively simple geometry, but they cannot do both. Notwithstanding the difficulties, the goal of extending the CFD approach to multiphase flows continues to be steadily pursued, and general formulations that are not directly linked to any specific geometry, and refrain from using hydraulic concepts at the outset, are still in demand.

3. Averaged Descriptions of Turbulent and Multiphase Flows

The one-point averaging procedures yield turbulent-flow descriptions that form the basis of engineering computations and virtually all the commercially developed CFD simulation software to date. Essentially the same procedures are also used to derive the averaged *multifluid* transport equations, which lead to models underlying a large class of numerical simulation methods for multiphase flows. While all multifluid formulations are based on the treatment of individual phases as interpenetrating continua coexisting in the flow domain, they differ in many details. It appears that most derivations can be put on a common ground by tracing their origin to the distributional form of the local instant (differential) balances for a multifluid continuum.[5,6]

In the Eulerian description of a mixture of Newtonian fluids, the property balances accounting for transport within the bulk fluid are cast as partial differential equations, while transport across the interfaces (treated as singular massless surfaces) is accounted for by supplementary jump conditions. Denoting the density by ρ, the velocity field by $\mathbf{u}$, the diffusive flux by $\mathbf{J}$, and the source density of a given property, ψ, by ϕ, both balances can be written in the generic forms:

$$\frac{\partial(\rho\psi)}{\partial t} + \nabla \cdot (\rho\psi\mathbf{u} - \mathbf{J}) = \rho\phi, \tag{3.1}$$

$$[\![\rho\psi(\mathbf{u} - \mathbf{u}_s) - \mathbf{J}]\!] \cdot \mathbf{n} = \phi_s. \tag{3.2}$$

Eqs. (3.1) and (3.2) yield balances of mass, momentum, and energy, respectively, for $\psi = 1$, $\mathbf{u}$, and e, where e denotes the specific energy. In addition, $[\![\ ]\!]$ denotes the property difference across the interface, $\mathbf{n}$ is the unit vector normal to the interface, $\mathbf{u}_s$ is the interfacial velocity, and ϕ_s is the interfacial source of property ψ (e.g., surface tension).

In the multifluid formulation of n-phase problem, a set of n binary *phase-indicator* functions, θ_k $(k = 1, \ldots, n)$, is introduced to determine which of the phases is present at a given time and position. Considering all differential operations in the distributional sense, the gradient of θ_k and its transport equation may be written as:[6]

$$\nabla\theta_k = -\mathbf{n}a_k, \tag{3.3}$$

$$\frac{\partial\theta_k}{\partial t} + \mathbf{u}_s \cdot \nabla\theta_k = 0, \tag{3.4}$$

where the scalar delta-function, a_k, is conveniently interpreted, in the limit, as the interfacial area per unit volume of the fluid mixture.[6] Using Eqs. (3.3) and (3.4), the distributional balances describing the dynamics of the k-th phase may be cast in the form,

$$\frac{\partial(\theta_k\rho\psi)}{\partial t} + \nabla\cdot[\theta_k(\rho\psi\mathbf{u} - \mathbf{J})] = \theta_k\rho\phi + [-\rho\psi(\mathbf{u} - \mathbf{u}_s) + \mathbf{J}]\cdot\mathbf{n}a_k. \tag{3.5}$$

This set of balances represents the multifluid counterpart of the single-fluid continuity, Navier-Stokes, and energy equations (to which it reduces in the absence of interfaces), and constitutes an ideal starting point for any kind of averaging (temporal, volumetric, statistical, etc.). In fact, Eq. (3.5) permits the development of higher-level approaches (multi-point averages or Large-Eddy-Simulation concepts) for multiphase flows. The averaging operators are usually assumed to satisfy a set of *Reynolds rules*,[5] of which the commutativity with the differential operators, $\partial/\partial t$ and ∇, can be proven for a large class of averaging operations. In general, the action of a one-point averaging operator, $\langle\ \rangle$, on both sides of Eq. (3.5), yields:

$$\frac{\partial\langle\theta_k\rho\psi\rangle}{\partial t} + \nabla\cdot\langle\theta_k\rho\psi\mathbf{u}\rangle - \nabla\cdot\langle\mathbf{J}\rangle = \langle\theta_k\rho\phi\rangle + \langle[-\rho\psi(\mathbf{u} - \mathbf{u}_s) + \mathbf{J}]\cdot\mathbf{n}a_k\rangle. \tag{3.6}$$

Further transformations of Eq. (3.6) must involve expressing the averages of products in terms of products of averages. It is at this step where the traditional approaches to turbulence and multiphase flows diverge. Due to large uncertainties regarding the underlying physics, the correlations of fluctuations have been usually neglected in the three-dimensional modelling of multiphase flows. Only recently has the modelling of correlational terms started to be successfuly addressed within the scope of multifluid closure schemes.[7,8] While this line of development is likely to continue, more experimental work of a fundamental nature is indispensable to assure reasonable validity of any new models.

4. Recent Applications of CFD at Chalk River Laboratories

The utility of CFD-based prediction methodologies, and their complementary role with regard to the more traditional thermalhydraulic analyses, are well illustrated by the recently launched project concerning the assessment of fuel-bundle appendage effects on the pressure drop and heat-transfer characteristics of a typical CANDU fuel channel. While it is well known that the price paid for higher heat-transfer rates (attained on account of bearing pads, spacers, end-plates, etc.) is an increase in pressure drop, an experimental quantification of these effects is difficult even in the single-phase flow regime. Adequate characterization of individual appendage contributions to those effects is required as part of the input information in thermalhydraulic analyses utilizing system and subchannel codes.

The application of CFD tools to predict the integral effects, such as additional pressure drop or a change of average heat-transfer rate, caused by relatively minor perturbations of channel geometry, is a viable alternative to experimental testing. The initial phase of the project has demonstrated that the standard k-ϵ model of turbulence transport (in which the turbulent *Reynolds stresses* are represented by the two-parameter gradient model, and the parameters themselves are computed by solving their modelled transport equations) is adequate for predicting the form drag coefficient for a simple obstacle mounted on a fuel rod. The predicted flow patterns lead in turn to plausible estimates of heat-transfer enhancement, which can be characterized by the correction factor to the average heat-transfer coefficient for an unobstructed-rod surface.

5. Conclusions

The contributions of CFD to thermalhydraulic design are recognized, and continue to gain in importance with the increase of available computing power. As anticipated, modern tools of computer graphics make the CFD analyses more accessible and more widely appreciated by non-specialists. While these factors are expected to steadily enhance the supporting role of CFD, the real hope for its future seems to rest with the incorporation of additional physics into the available mathematical algorithms and computer codes. Only then can some of the thermalhydraulic analysis tools be gradually replaced by the CFD technology in nuclear engineering applications.

6. References

1. M.B. Carver, "Multidimensional computational analysis of flow in nuclear reactor components", *Trans. SCS* 1 (1984) 147.
2. N.E. Todreas, and M.S. Kazimi, *Nuclear Systems*, (Hemisphere, 1990).
3. J.H. Ferziger, "Simulation of incompressible turbulent flows", *J. Comput. Phys.* 69 (1987) 1.
4. J.P. Boris, "New directions in Computational Fluid Dynamics", *Ann. Rev. Fluid Mech.* 21 (1989) 345.
5. D.A. Drew, "Mathematical modelling of two-phase flow", *Ann. Rev. Fluid Mech.* 15 (1983) 261.
6. I. Kataoka, "Local instant formulation of two-phase flow", *J. Multiphase Flow* 12 (1986) 745.
7. S.L. Lee, R.T. Lahey, Jr., and O.C. Jones, Jr., "The prediction of two-phase turbulence and phase distribution phenomena using k-ϵ model", *Jap. J. Multiphase Flow* 3 (1989) 335.
8. M. Lopes de Bertodano, S.J. Lee, R.T. Lahey, Jr., and D.A. Drew, "The prediction of two-phase turbulence and phase-distribution phenomena using a Reynolds stress model", *Trans. ASME, J. Fluids Engng.* 112 (1990) 107.

Acknowledgments

The author thanks Mike Carver for his advice and review of this paper, and acknowledges the help of Peter Leivo and Peter Laughton in making the first encounter with TEX a pleasurable experience.

FINITE ELEMENT METHOD - THEORY AND APPLICATIONS

SALEH BASET
Mathematics and Computation Branch
Chalk River Laboratories

ABSTRACT

A brief summary of the mathematical basis of the Finite Element Method (FEM) has been presented. Attention is drawn to the natural development of the method as an engineering analysis tool into a general numerical analysis tool. A particular application to the stress analysis of rubber materials is presented. Special advantages and issues associated with the method are mentioned.

1.Mathematical Basis of FEM

The FEM is typically viewed as an approximation to the integral form of governing equations. Two distinct procedures are available to achieve such approximation; the *weighted residual method* and *variational method* [1].

1.1 Weighted Residual Method

The starting point here is the set of differential equations and boundary conditions which govern the behaviour inside the domain V and on the surface S,

$$\mathbf{A}(\mathbf{u}) = 0 \qquad \text{in } V \qquad (1.1)$$

$$\mathbf{B}(\mathbf{u}) = 0 \qquad \text{on } S \qquad (1.2)$$

where the dependent variable $\mathbf{u}=\mathbf{u}(x_i,t)$ is a scalar (or vector) function of space and time. The differential operators **A** and **B** are obtained from the physics of the problem.

The above equations can be combined in a single integral form, as follows:

$$\int_V \mathbf{C}^T\mathbf{A}(\mathbf{u})\, dV + \int_S \mathbf{D}^T\mathbf{B}(\mathbf{u})\, dS = 0 \qquad (1.3)$$

If Eq. (1.3) is satisfied for any arbitrary choice of functions C and D, then the differential Eqs. (1.1) and (1.2) would be satisfied at all points. It is usually possible to integrate Eq. (1.3) by parts to yield another integral form known as "the weak integral form". Of course, the shape of the functions **A**, **B**, **C** and **D** will now be different. As a result, the new differential operators **A** and **B** will include a lower order of differentiation, albeit at the expense of higher orders in the arbitrary functions **C** and **D**. This results in loosening the continuity condition on the trial functions in the approximation process. In some problems, it has been found that the boundary term in the weak integral is much simpler than the corresponding term in the original form. Such a simplification of boundary conditions constitutes one of the most impressive advantages of the FEM. It is interesting to note herein that if the integration by parts is continued once more, it is possible to entirely get rid of the domain integral by careful choice of arbitrary functions, which satisfies the differential equations in the domain, and hence reduces the dimensionality of the problem by one order of magnitude. This has led to the development of a new method, called the "Boundary Element Method", in the 1970's[2]. Now, if an approximation to the variable **u** is assumed, Eqs. (1.3) will not be identically satisfied for any arbitrary function unless these functions are chosen to minimize the errors (residuals) to zero. Hence the name of *weighted residual methods.*

1.2 Variational Method

A variational principle is a scalar quantity (functional), which is defined in integral form in terms of the dependent variable (e.g., **u**) and/or its derivatives. The solution to the continuum problem is the function **u**, which makes the functional stationary with respect to any arbitrary variation δu. Such variational principles are called *natural* if the physical aspects of the problem can be stated directly in such a way as to minimize some quantities, such as the potential energy of a mechanical system, energy dissipation in viscous flow, etc. If such a principle exists, standard procedures can be immediately established to approximate the solution[1]. It is easy to show that this procedure is mathematically equivalent to the (Galerkin) *weighted residual method.* More important is the fact that the procedure will result in symmetric FEM equations,

which are attractive from a computational point of view. Unfortunately, the opposite is not true, i.e., a weighted residual procedure does not necessarily produce symmetric equations. In this regard, the *weighted residual method* retains its advantage as a more general method, because it is not possible to find a variational principle for some problems which can otherwise be described by differential equations. Some researchers still like to construct the so-called *contrived* variational principles by introducing additional variables called Lagrange multipliers. In these situations, the gain in having symmetric equations can be upset by having more variables and singular equations, which require special care in solving them.

1.3. Trial (Shape or Interpolation) Functions

The FEM can now be recognized as the special case when the approximation of the variable **u** is expressed in terms of piece-wise (i.e., defined element wise) trial functions, as follows:

$$\mathbf{u} \approx \hat{\mathbf{u}} = \sum_{1}^{n} \mathbf{N}_i \, a_i \; = \mathbf{N} \, \mathbf{a} \tag{1.4}$$

where $\mathbf{N}_i$ are assumed trial function (usually polynomial) and a_i are the values of the variable **u** at the nodal points which constitute a given element in the domain.

As for the weighting functions **C** and **D** in Eq. (1.3), various methods can be used. The most common one is known as the Galerkin method, wherein **C** and **D** are chosen to be the same as the trial functions **N** of Eq. (1.4). It can be seen by now that the most important step in FEM is the choice of trial functions **N**. In general, such functions should be continuously integrable (over a single element) up to the highest order of differentiation in Eq. (1.3). In addition, they should avoid the presence of infinity at the inter-element boundaries. Polynomial functions which are chosen to equal unity at the corresponding nodal point and zero elsewhere are commonly used. They are usually expressed in terms of normalized space (i.e., ranging between -1 and +1). They can then be mapped to the real geometry using standard transformation techniques. Experience has shown that simpler functions produce better results, especially in nonlinear analysis. Figure (1.1) shows some such functions for 2- and 3-node elements in 1-dimension space. Extension to 2- and 3-dimension space is straightforward.

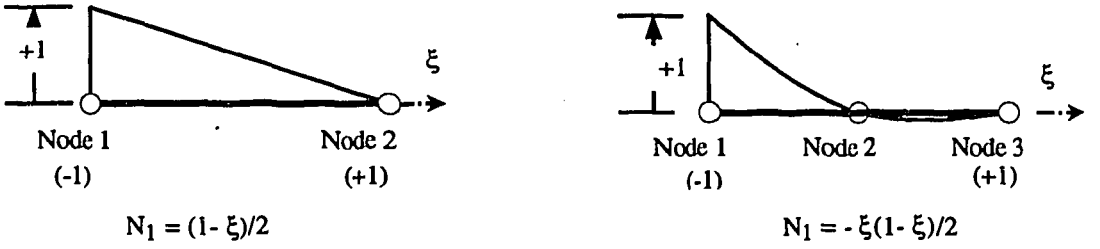

Figure 1.1 Shape Functions for 2-node and 3-node Finite Elements in 1-Dimension Space

If the coordinates x_i are interpolated using the same trial functions **N** of Eq. (1.4), the element is further classified as an *isoparametric* element. Some researchers have shown that by simple relocation of the mid-side node or by changing the trial function itself, it is possible to model such peculiarities as the $1/\sqrt{r}$ singularity of linear fracture mechanics, or to map a semi-infinite domain to a finite space. Except for such peculiarities, experience has shown, however, that the simpler (linear) functions do usually produce better results (for the same degree of discretization), especially in nonlinear analysis. Finally, it is interesting to note that the well-known finite difference method can be viewed as a special case of the weighted residual method, in which the weighting function happens to be the Dirac function applied at grid points.

2. Applications in Solid Mechanics

The most convenient approach in solid mechanics is to write down the potential energy Π of the system as follows:

$$\Pi = \frac{1}{2} \int_V \varepsilon_{ij} \, \sigma_{ij} \; dV - \int_S u_i \, t_i \, dS \tag{2.1}$$

where σ_{ij} and ε_{ij} are the stress and strain tensors inside the domain, while u_i and t_i are the displacement and traction vectors on the boundary, respectively. If the problem is to be reduced to one dependent variable only (e.g., u_i), all other variables have to be expressed in terms of u_i using whatever kinematic and constitutive

material relationship applicable to the problem. For example, in the case of small displacements and linear elastic material, the following relations can be assumed:

$$\sigma_{ij} = E_{ijkl}\,\varepsilon_{kl} \quad , \qquad \varepsilon_{ij} = \frac{1}{2}\left(\frac{\partial u_i}{\partial x_j} + \frac{\partial u_j}{\partial x_i}\right) \tag{2.2}$$

where E_{ijkl} is the generalized Hook's law. Now, by assuming a FEM approximation (similar to Eq. 1.4), the variable **u** and its derivatives can be expressed in terms of nodal variables **a** as follows:

$$\{u\} = [N]\,\{a\} \quad , \qquad \{\delta u\} = [N]\,\{\delta a\} \tag{2.3}$$

$$\{\varepsilon\} = [B]\,\{a\} \quad , \qquad \{\delta\varepsilon\} = [B]\,\{\delta a\} \tag{2.4}$$

The equilibrium of the mechanical system corresponds to the function u which minimizes the functional Π (i.e., $\delta\Pi=0$). By substituting Eqs. (2.2), (2.3) and (2.4) into Eq. (2.1), the variation of functional Π is as follows:

$$\delta\Pi = \{\delta a\}^T \left\{ \int_V [B]^T [E][B]\,\{a\}\,dV - \int_S [N]^T \{t\}\,dS \right\} = 0 \tag{2.5}$$

Since δa is any arbitrary variation, the expression inside the { } brackets should equal zero. This leads to the following set of algebraic equations:

$$[K]\,\{a\} - \{F\} = \{0\} \tag{2.6}$$

where:

$$[K] = \sum_{\text{elements}} \int_V [B]^T [C][B]\,dV \quad , \qquad \{F\} = \sum_{\text{elements}} \int_S [N]^T \{t\}\,dS \tag{2.7}$$

It is understood that the summation in Eq. (2.7) represents the contribution at one node from all the elements connected to it. The formulation of several element matrices can be executed in parallel, making the FEM suitable for modern parallel and vector computer technology.

In the case of rubber analysis, there are many sources of nonlinearities, such as the kinematic and material relationship (Eqs, 2.2), large displacements due to moving boundaries, gap/friction and slip/stick surface conditions, as shown in Figure 2.2. The solution procedure is similar to the above one, with the coefficient matrices **K** and **F** now being functions of the displacement **u** and stress σ. The resulting algebraic equations are nonlinear, and standard numerical linearization procedures (e.g., Newton-Raphson) are usually used for the solution.

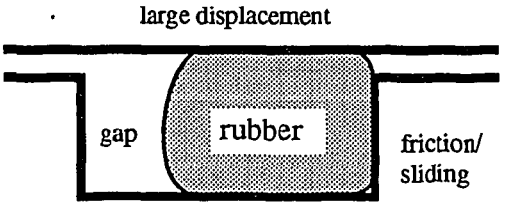

Figure 2.1 Typical O-ring Problem

The general purpose FEM program MARC [3] has been used in the stress analysis of the O-ring of the solid rocket in the space shuttle. The stress, strains, displacements and reactions can be found at different loads, boundary and/or temperature conditions. These results can help the designer determine contact and/or maximum stress locations, which are crucial in operation conditions. The amount of output in a typical FEM analysis is usually very large, and interactive graphics tools[4] have to be used to investigate the results. Figure 2.2 shows a typical colour (reprinted here in gray) contour of stress being superimposed on the deformed mesh.

3- Current Activities in FEM

With the mathematical foundation of FEM being established, a lot of R and D is still going on in this field. Questions such as accuracy, convergence, existence and/or uniqueness of the solution are being addressed. The development of new complicated materials and the need to push operational conditions to new heights

(e.g., high temperatures, supersonic speeds, etc.) have moved research beyond the realm of linear analysis. Automatic -adaptive mesh generation, interactive graphics and animation techniques are becoming indispensable standard tools of numerical analysis. Mixed (hybrid) formulation, wherein several dependent variables are explicitly included, have yielded very accurate results in some particular applications.

4- Conclusions

The FEM has been shown to be based on solid mathematical foundations. This explains the reason why the method has developed from being an intuitive engineering tool in its infancy, to being such a comprehensive numerical method tool now. The successful application of this method to the stress analysis of the O-ring used in the field joints of the solid rocket of the space shuttle has been demonstrated. More development is still taking place to extend FEM to new fields and applications.

References

1. O.C. Zienkiewicz and R.L Taylor, " The Finite Element Method", 4th edition, McGraw-Hill, 1989.
2. C.A. Brebbia and S. Walker, "Boundary Element Techniques in Engineering", Newnes-Butterworth, 1980.
3. Marc Analysis Research Analysis, "MARC general Purpose Finite Element Program", Palo Alto, Cal. 1989.
4. Marc Analysis Research Analysis, "MENTAT - A System for Finite Element Pre- and Post-Processing ", .Palo Alto, Cal. 1989.

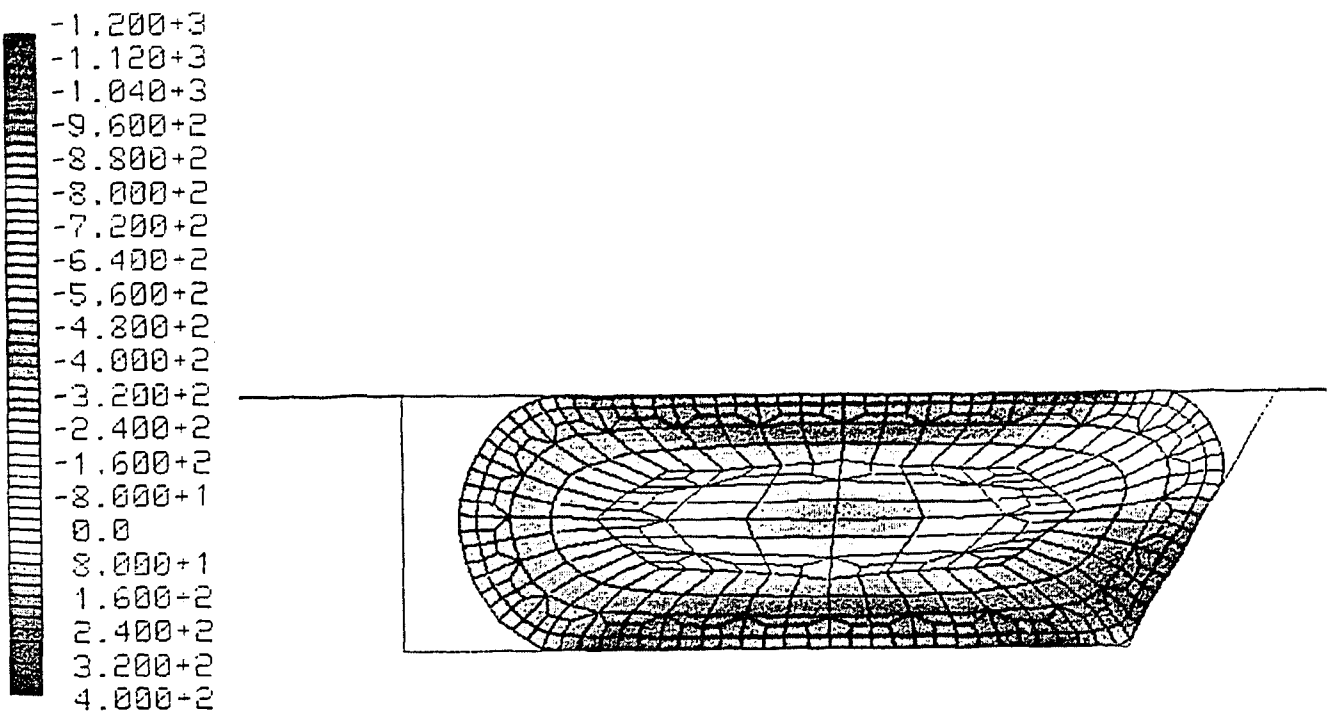

Figure 2.2 Contour of Horizontal Stress in the O-ring under 35% Vertical Compression and Upstream Gas Pressure of 250 psi.

MULTI-DIMENSIONAL TWO-FLUID FLOW COMPUTATION, AN OVERVIEW

M.B. Carver

Advanced Reactor Development Division
Thermalhydraulics Development Branch
Chalk River Laboratories

ABSTRACT

The paper discusses a repertoire of three-dimensional computer programs that have been developed to perform critical analyses of single-phase, two-phase and multi-fluid flow in reactor components. The basic numerical approach to solving the governing equations common to all the codes is presented and the additional constitutive relationships required for closure are discussed. Particular applications are presented for a number of computer codes.

1. Introduction

Because a nuclear reactor system relies entirely on fluid circuits for energy transport, mathematical modeling of thermal-hydraulic phenomena plays a pivotal role in reactor design and development. Methods of improving the accuracy and efficiency of thermal-hydraulic computations are continually sought. Reactor design is supported by a large repertoire of analytical computer programs. These programs embody knowledge accumulated from years of research and development focussed on quantifying fluid flow and heat transfer in single-phase and two-phase systems. Each computer program comprises several areas of expertise, including physical modelling, which selects the appropriate conservation equations to be solved and associated constitutive relationships required to describe energy transfer between the fluid and its boundaries, and mathematical modelling, which chooses an appropriate approximation to the conservation equations and numerical means of solution.

2. Geometric Framework

The first step in any computational analysis is to select a model of the geometries required as a framework for the analysis. The appropriate form is often dictated by the hardware. In most of the coolant circuits of a CANDU reactor, the fluid behaviour may be adequately described by one-dimensional (cross-sectional-averaged) models. However, in the reactor fuel channel, flow must distribute itself among the intricate flow passages of the fuel bundle. In the secondary side of the steam generator, and in the calandria, the flow distribution is also complex. Multi-dimensional analysis is necessary to model detailed local distribution of flows and temperatures in any of the geometrically complex components. All of these components have a similar internal structure; *i.e.*, flow passes through some array of rods or tubes. Alternative computational frameworks for rod array systems are reviewed by Sha [1].

Although the finite-element method lends itself readily to fitting complex external boundaries, it has not often been used for flow systems with complex internal boundaries. Instead, the equations have usually been formulated for finite control volumes and integrated in finite difference form [2].

Except for the 1-D case, the simplest and most natural geometric division of a rod array is a subchannel. Subchannels are readily defined as communicating flow channels bounded by rod surfaces, and fictitious lines between rod centers. Each subchannel is divided into a number of axial control volumes.

An alternative approach is to impose a coordinate system on the entire flow vessel and represent the internal hardware by distributed resistances and heat sources. This classic "porous medium" approach is more suitable for geometries in which rods are densely packed. Information on overall flow distribution inside the rod array is required, rather than details Swithin each control volume. The volume available to the fluid (*i.e.*, not occupied by hardware) and flow area blockages are computed suitably at control volume interfaces.

Note that the porosity and subchannel concepts remain artifacts that do not reduce to the true solution in the limit, as zero velocity cannot be imposed at all solid surfaces. In fact, standard finite-element methods

do not so reduce either. This degree of fidelity can be achieved only by using finely divided body fitted coordinates [1].

The examples in this presentation are restricted to the subchannel and porous medium formulations.

3. Models of Single-Phase Flow

The next step in a computation is to decide on a flow model. As in modelling the geometry, the most complicated available model normally need not be used; simplifying assumptions are frequently valid and may reduce the complexity of the equations to be solved.

Single-phase flow is normally modeled adequately by solving the conservation equations of mass, momentum, and energy. The exact form of the equations will depend on whether the fluid should be considered incompressible or compressible, and inviscid or viscous. These decisions affect both the form of the equations and the behavioural modes of the solution.

The above considerations are common to single or multi-dimensional form. However, the problem of turbulence modeling is peculiar to modeling multi-dimensional flow. The model of turbulence exerts influence only by means of its effects on pressure drop in a 1-D calculation, but in multi-dimensional cases it determines velocity distribution. It is usually modeled by a suitable means of computing the distribution of effective viscosity. This may be introduced by algebraic relationships or the more detailed models involving further differential equations of transport. Note that additional differential equations thus introduced are not governing equations of the flow field, but merely part of the turbulent model.

4. Models of Two-Phase Flow

The assumption of equilibrium produces the simplest model in which the phases are taken to be homogeneously mixed, and to have equal velocity and equal temperature (EVET). The two-phase mixture is treated as a single fictitious fluid having properties determined solely by the relative proportion by weight (quality) of vapour in the mixture. Thus the partial differential equations to be solved are the same as for single-phase flow: conservation of mass, momentum and energy of the mixture, while algebraic relationships cater for the two-phase properties and the equation of state for the mixture. The homogeneous model is suitable for conditions in which departures from mechanical and thermal equilibrium are known to be minimal.

For cases in which gravitational or centrifugal forces are known to induce phases to travel at different speeds, a two-velocity model is required, and an additional relationship is required for relative velocity. Early separated flow models used a void correlation instead of the equation of state, and a simple numeric slip factor to impose the higher velocity of the vapour phase in vertical flow. This was later quantified by relating relative velocity to the rise velocity of vapour bubbles in liquid and the radial distribution of vapour. This simple drift-flux model, also referred to as UVET (unequal velocity equal temperature), uses algebraic relationships for relative velocity, and hence still requires the solution of the same three partial differential equations of conservation, but an additional equation, usually based on gaseous phase continuity, is required for void distribution.

None of the above models permits the temperature of either phase to depart from saturation. To simulate non-equilibrium phenomena such as subcooled boiling, superheated liquid, and flashing, etc., a mechanism that permits these effects must be added. Again, early studies used algebraic relationships, but more rigorous models now use a separate energy equation and equation of state for each phase, and model heat transfer between phases.

The advanced drift flux, unequal-velocity, unequal-temperature model is a combination of both of the above, and therefore requires the solution of five conservation equations: a mixture momentum equation, two continuity equations and two energy equations.

Finally, the full six-equation, two-fluid model abandons the algebraic definition of relative velocity and instead computes phase velocities using two momentum equations containing models of wall-to-fluid and fluid-to-fluid stresses.

It is apparent that with each level of complexity of the two-phase model, additional partial differential equations are added, and hence more involved numerical schemes are required. However, since the basic equations have the same form as for single-phase flow, most advances in numerical techniques for simulation of single-phase flow can be extended to two-phase applications.

The above discussion covers the options in two-phase flow, with boiling and condensation; however, it is frequently necessary to deal with a non-condensable component. For small concentration, when such a component can be considered to travel at the same velocity as the host flow, its distribution can be simulated by a transport equation with appropriate source terms. Otherwise, a separate momentum equation is also required for the component.

5. The Conservation Equations of Two-Fluid Flow

The equations are formulated using the principle of interpenetrating continua, Harlow and Amsden [3]. This permits the equations of each fluid to be written separately, as if each fluid behaved as a continuum, but with additional terms which represent their interaction. This yields for each fluid k; 1 continuity equation, 3 momentum equations, 1 energy equation, 1 state equation, and 1 algebraic constraint. This can be stated in Cartesian Vector form for fluids k and ℓ as follows:

$$\left\{\frac{\partial}{\partial t}(\alpha\rho) + \nabla\cdot(\alpha\rho U)\right\}_k = \Gamma_k \tag{1}$$

$$\left\{\frac{\partial}{\partial t}(\alpha\rho U + \nabla\cdot(\alpha\rho UU)\right\}_k = -\alpha_k\nabla P + (\alpha\rho g)_k + \tau_{k\ell} + \tau_{kw} \tag{2}$$

$$\left\{\alpha\rho\frac{\partial h}{\partial t} + \nabla\cdot(\alpha\rho hU)\right\}_k = -\alpha_k\frac{DP}{Dt} + \left(\frac{\partial Q}{\partial t}\right)_k + \nabla\cdot(\kappa\nabla T)_k + \Phi_k + \phi_{k\ell} \tag{3}$$

$$\alpha_\ell + \alpha_k = 1 \tag{4}$$

$$\rho = \xi(h, P_k) \tag{5}$$

For three dimensional cases, these equations result in a set of 5*2 partial differential equations and 2 constraints. These are to be solved on a grid of at least 10*10*10, which, if converted to ordinary differential equations (ODES) in time, would yield 12 000 simultaneous ODE's. The domain must be discretised into control volumes and the equations integrated over each control volume, using appropriate interpolation functions. As simultaneous solution is impossible, a class of iterative solutions have been developed for 3D 1 fluid flow. They may be extended for 2 fluids [4].

In order to solve the equations, it is necessary to write them in discrete form with reference to finite control volumes. To maintain continuous definition of all variables, it is important that all variables are evaluated correctly where averages across grid points are required, using appropriate interpolation functions or weighting functions. In this area, the finite element, finite difference and finite control volumes overlap somewhat (see [2]); however, finite control volume analyses are predominant.

Most common schemes for multidimensional flow originate from one of two major sources, the ICE [3] procedures developed at Los Alamos National Laboratories and the SIMPLE [5] procedures from Imperial College in London. Both use the staggered grid concept, although the nomenclature is somewhat different. The ICE procedures solve the equations in differential form, whereas SIMPLE users prefer to integrate about the control volume. Both apply equally well to 1, 2, and 3D situations, and the resulting equations are equivalent.

6. Constitutive Relationships

The next most important ingredients in a thermal-hydraulic code are the constitutive relationships required for closure. These are the models of the subprocesses which supply the algebraic relationships necessary for closure, in other words, to balance the number of definitive equations with the number of variables.

In single-phase flow, detailed expressions are required for friction and heat transfer and elements of the turbulence model. In two-phase flow, depending on the model, correlations are needed for void fraction, relative velocity, heat transfer and friction between hardware and each phase and between phases. The question of flow regime affects all of these.

Once a numerical scheme has been developed and exhibited convergence and consistence, the choice of the constitutive relationships determines the detailed results. These must obviously be chosen judiciously. A fairly satisfactory repertoire of relationships has been developed for the homogeneous model. Some doubt exists about the correct choice for the advanced models and further research is continuing.

7. Application Examples

The presentation will discuss examples of modelling three-dimensional two-phase flow in reactor components, including fuel channels, steam generators, and condensers. Some current computational concerns will be discussed.

- ASSERT - Three-dimensional two-fluid analysis of flow and phase distribution in reactor fuel bundles; application to CANDU and MAPLE reactors [6].
- THIRST - Three-dimensional analysis of flow and phase distribution in steam generators; application to steam generators [7].
- THIRST/SLUDGE - Three-dimensional analysis of transport, deposition and entrainment of particulate matter (fouling) in steam generators; application to modelling fouling [8].
- SPOC - Three-dimensional analysis of steam, water and air distribution in power plant condensers application to design of tube banks [9].
- FAITH - Three-dimensional two-fluid analysis of two-component flow in ducts and vessels; application to flows in bends and through broach plates [10].
- FLOW3D - Three-dimensional analysis of flow in arbitrary geometries; application to flow in pool reactors [11].

Further details of the applications are in reference [12], and the above references.

8. Validation

Validation of code predictions against experimental evidence is essential to establish credibility. In order to illustrate that validation is a priority, the presentation will illustrate comparisons with data wherever possible.

9. Acknowledgement

The work described here was partly supported by the COG (CANDU Owners Group), jointly funded by AECL, Ontario Hydro, New Brunswick Power and Hydro Quebec.

10. References

[1] W.T. Sha, (1980), "An Overview of Rod-Bundle Thermal-Hydraulic Analysis", Nucl. Eng. & Des., 62:1-24.

[2] P.F. Galpin, R.G. Huget, G.D. Raithby, (1986), "Fluid Flow Simulations in Complex Geometries", CNS/ANS Conference, Simulation Methods in Nuclear Engineering, Montreal.

[3] F.H. Harlow and A.A. Amsden, (1971), "A Numerical Fluid Dynamics Method for All Speeds", J. Comp. Phys., 8:197-206.

[4] M.B. Carver, (1982), "Numerical Computation of Phase Separation in Two Fluid Flow", ASME paper 82-FE-2.

[5] S.V. Patankar and D.B. Spalding, (1972), "A Calculation Procedure for Heat Mass and Momentum Transfer in Three Dimensional Parabolic Flows", Int. J. Heat & Mass Trans., 15:1787-1801.
[6] M.B. Carver, A. Tahir, D.S. Rowe and S.Y. Ahmad, (1984), "Computational Analyses of Two-Phase Flow in Horizontal Rod Bundles", Nucl. Eng. & Des., 82:21-42.
[7] M.B. Carver, L.N. Carlucci and W.W.R. Inch, (1981), "Thermalhydraulics in Recirculating Steam Generators, THIRST Code User's Manual", AECL Report, AECL-7254.
[8] Y. Liner, M.B. Carver, C.W. Turner and A.O. Campagna, (1992), "Simulation of Magnitite Fouling in Nuclear Steam Generators", 1992 Joint Power Generation Conference, Atlanta.
[9] V.C. Frisina, L.N. Carlucci and A.O. Campagna, (1990), "SPOC: A Computer Program for Simulation of Power Plant Condenser Performance". Proceedings of the EPRI Conference on Condenser Technology, Boston, 1990.
[10] M.B. Carver and M. Salcudean, (1986), "Three-Dimensional Numerical Modelling of Phase Distribution of Two-Fluid Flow in Elbows and Bends", Numerical Heat Transfer, 10, 229-251.
[11] I.P. Jones, J.R. Kightley, C.P. Thompson and N.S. Wilkes, (1985), "Flow3D, A Computer Code for the Prediction of Laminar and Turbulent Flow and Heat Transfer", AERE-R 11825.
[12] M.B. Carver, A.O. Campagna, Y. Liner and B. Lidicky, (1992), "Three-Dimensional Multi-Fluid Analysis of Reactor Components", Proceedings of the 17th CNS Simulation Symposium, Kingston.

Quantum Symmetries

M. Couture
Theoretical Physics Branch
Chalk River Laboratories

The concept of symmetry has played an important role in physics and mathematics. One might think of the close connection between space groups and classes of crystal, Lorentz symmetry and general relativity, Lie groups and gauge symmetries in subatomic physics. It is therefore not surprising that the discovery, approximately ten years ago,[1] of symmetries that are continuous deformations of some of the symmetries mentioned above has caused great excitement among theoretical physicists. Studies have revealed close connections between solvable models in statistical mechanics (for instance, the two-dimensional Ising model) and field theory, knot theory, deformation theory of Lie algebras and noncommutative geometry. The unifying theme in all these seemingly unrelated topics is the Yang-Baxter equation. The following example illustrates the fact that these new symmetries may be viewed as the symmetries of noncommutative spaces.

Consider a set of non-commutative two-dimensional spaces $Q1$ and $Q2$, whose coordinates x_1, x_2 and X_1, X_2 satisfy the following quadratic relations

$$Q1 : x_1 x_2 - q^{-1} x_2 x_1 = 0 \tag{1}$$

$$Q2 : X_1^2 = 0, X_2^2 = 0, X_1 X_2 + q X_2 X_1 \tag{2}$$

where q is some arbitrary parameter known as the deformation parameter. We now define a matrix $Z \equiv \begin{pmatrix} z_1^1 & z_1^2 \\ z_2^1 & z_2^2 \end{pmatrix}$ and impose that the following transformations on $Q1$ and $Q2$

$$\begin{pmatrix} x_1^* \\ x_2^* \end{pmatrix} = Z \begin{pmatrix} x_1 \\ x_2 \end{pmatrix} , \quad \begin{pmatrix} X_1^* \\ X_2^* \end{pmatrix} = Z \begin{pmatrix} X_1 \\ X_2 \end{pmatrix} \tag{3}$$

are such that the x_i^*'s and X_j^*'s still satisfy (1) and (2), respectively. This is possible only if one allows the z_i^j's to be noncommutative. One finds that the relations (1) and (2) are preserved under the transformations (3) provided the z_i^j's satisfy the following quadratic relations

$$z_1^1 z_1^2 = q^{-1} z_1^2 z_1^1, z_1^1 z_2^1 = q^{-1} z_2^1 z_1^1$$
$$z_2^2 z_1^2 = q z_1^2 z_2^2, z_2^2 z_2^1 = q z_2^1 z_2^2$$
$$z_1^2 z_2^1 = z_2^1 z_1^2, z_1^1 z_2^2 - z_2^2 z_1^1 = (q^{-1} - q) z_1^2 z_2^1$$

These relations may be summarized as follows:

$$R(Z \otimes I)(I \otimes Z) = (Z \otimes I)(I \otimes Z)R$$

where I is the two-dimensional identity matrix, $\otimes$ stands for tensor product and

$$R = \begin{pmatrix} 1 & 0 & 0 & 0 \\ 0 & 1-q^2 & q & 0 \\ 0 & q & 0 & 0 \\ 0 & 0 & 0 & 1 \end{pmatrix}$$

The matrix R is a solution of the braid relation

$$(R \otimes I)(I \otimes R)(R \otimes I) = (I \otimes R)(R \otimes I)(I \otimes R)$$

which is one form of the Yang-Baxter equation. Recently, P. Leivo and I found a generalized version of such quantum symmetries.

References

1. E.K. Skyyanin, *Funct. Anal. App.* 16*(1983)263.*

APPLICATION OF NORMAL FORM METHODS TO THE ANALYSIS OF RESONANCES IN PARTICLE ACCELERATORS

W.G. Davies

Nuclear Physics Branch
Chalk River Laboratories

ABSTRACT

The transformation to normal form in a Lie-algebraic framework provides a very powerful method for identifying and analysing non-linear behaviour and resonances in particle accelerators. The basic ideas are presented and illustrated by a simple yet important example.

1. Introduction

In this paper, we will discuss the advantages of using state-of-the-art mathematical tools, in particular normal form methods and maps in a Lie-algebraic framework[1-3], to help us solve very complicated non-linear behaviour in particle accelerators. Although these methods were invented about 100 years ago, they would still have limited utility without the availability of modern computers and considerable mathematical development[3]. Two important developments are the advent of algebraic codes and differential algebra[4].

In general, this is a study of systems of differential equations of the form

$$\dot{x} = f(x, \lambda, t); \quad x \in \mathbf{R}^n, \ \lambda \in \mathbf{R}^m, \ t \in \mathbf{R}. \tag{1.1}$$

In accelerator physics, these equations become Hamilton's equations

$$\zeta' = -[H, \zeta] \tag{1.2}$$

where $f(x, \lambda, t) \Rightarrow H$, $' = d/d\theta$, $t \Rightarrow \theta$, the new "time"; $x \in \mathbf{R}^n \Rightarrow \zeta = (x, p_x, z, p_z, \tau, p_\tau) \in \mathbf{R}^6$, the "canonical variables" and the $[\cdot, \cdot]$ are the familiar Poisson brackets. The relativistic Hamiltonian, H, in cylindrical coordinates will be used for explicitness.

$$H = -e\rho A_\theta - \rho\left\{(\frac{p_0}{c})^2 - m^2c^2 - [p_\rho - eA_\rho]^2 - [p_z - eA_z]^2\right\}^{1/2} \tag{1.3}$$

where $\rho = x + \rho_0$; ρ_0 is the radius of curvature of the central or "design" trajectory, p_0 is the total energy of the system and e is the electronic charge. The magnetic vector potential A has the form

$$A = A(x, z, \tau; \theta); \quad A \in \mathbf{R}^3. \tag{1.4}$$

Equation (1.2) could be solved by brute-force numerical integration, which works up to a point for small systems like cyclotrons, but not for large systems. For example, the main ring of the Superconducting Supercollider has about 10 000 magnets; the Hamiltonian has 20 000 piece-wise continuous sections! Each particle trajectory must be integrated separately. Consequently, exploring phase space is extremely expensive and is accompanied by loss of numerical accuracy. In particular, the *symplectic condition* (conservation of phase space) for Hamiltonian systems is generally not preserved. Alternatively, we can use "state-of-the-art" methods to simplify the problem. This is essential for large systems. A truly enormous simplification of the problem is achieved by employing: 1) maps $\zeta_f = \mathcal{M}(\theta)\zeta_i$; 2) normal forms (reduces the problem to its "simplest" form — isolates resonances); 3) a Lie-algebraic formulation (ensures symplecticity, minimizes the number of terms, enhances understanding).

2. Lie-Algebraic Maps

In the development, we use a Lie-algebraic formulation. The Poisson bracket $[H,\zeta]$ in Hamilton's equations (1.2) satisfies all of the requirements of a Lie algebra, namely, the commutation relation

$$A * B = (A,B) = AB - BA \tag{2.1}$$

and the Jacobi identity

$$(A,(B,C)) + (B,(C,A)) + (C,(A,B)) = 0. \tag{2.2}$$

Note: This Lie algebra is *neither commutative nor associative.*

Traditionally, Taylor-series maps of the form $\zeta_f = \mathcal{M}(\theta)\zeta_i$ have been employed, which when expanded become

$$\zeta_i^{FIN} = R_{ij}\zeta_j^{IN} + T_{ijk}\zeta_j^{IN}\zeta_k^{IN} + U_{ijkm}\zeta_j^{IN}\zeta_k^{IN}\zeta_m^{IN} + \cdots \tag{2.3}$$

where, in general, R, T and U have 36, 126, and 336 terms, respectively. In a Lie-algebraic representation of $\mathcal{M}(\theta)$, we write

$$\mathcal{M} = \mathcal{M}_f; \qquad \mathcal{M}_f = e^{:f:}; \qquad :f:g = [f,g] \tag{2.4}$$

where

$$e^{:f:} \stackrel{\text{def}}{=} \sum_{n=0}^{\infty} \frac{:f:^n}{n!}; \quad :f:^0 = \mathcal{I} = \{\textit{identity map}\}. \tag{2.5}$$

The map $\mathcal{M}_f$ can be factored [1] into

$$\mathcal{M}_f = \mathcal{M}_2\mathcal{M}_3\mathcal{M}_4\ldots = e^{:f_2:}e^{:f_3:}e^{:f_4:}\ldots \tag{2.6}$$

where $\mathcal{M}$ and $\mathcal{M}_n$ are *symplectic maps* and f_n are homogeneous polynomials of degree n; f_2, f_3, and f_4 contain 21, 56 and 126, terms respectively (compare with (2.3)). The maps $\mathcal{M}_n$ are elements of the symplectic group $sp(2n,\mathbf{R})$.

3. Normal Form

The normal form is the transformation $\mathcal{N} = \mathcal{A}\mathcal{M}\mathcal{A}^{-1}$ such that $\mathcal{N}$ is in its "simplest" form; $\mathcal{M}$ must be expanded about a *"centre manifold"* or "closed orbit" (*i.e.* no H_1 term in the Hamiltonian, H), which implies no $\mathcal{M}_1$ term in the map $\mathcal{M}$. The *symplectic map* $\mathcal{A}$ is an n^{th} order canonical transformation that isolates the *tune shifts* and *resonances* to n^{th} order. Using the factored map, we can normalize $\mathcal{M}$ order-by-order to obtain

$$\mathcal{N} = \mathcal{A}_n\cdots\mathcal{A}_4\left\{\mathcal{A}_3\left\{\mathcal{A}_2\mathcal{M}\mathcal{A}_2^{-1}\right\}\mathcal{A}_3^{-1}\right\}\mathcal{A}_4^{-1}\cdots\mathcal{A}_n^{-1}. \tag{3.1}$$

We proceed as follows. From the eigenvectors of the matrix representation R, of $\mathcal{M}_2$, we get a canonical transformation that *rescales and block diagonalizes* R.

$$\mathcal{R} = \mathcal{A}_2 R \mathcal{A}_2^{-1} \Rightarrow \mathcal{R} = \begin{pmatrix} \mathcal{R}_1 & & 0 \\ & \mathcal{R}_2 & \\ 0 & & \mathcal{R}_3 \end{pmatrix}; \mathcal{R}_i = \begin{pmatrix} cos(\mu_i) & sin(\mu_i) \\ -sin(\mu_i) & cos(\mu_i) \end{pmatrix} or \begin{pmatrix} 1 & L_i \\ 0 & 1 \end{pmatrix}. \tag{3.2}$$

Next we normalize $\mathcal{M}_3$

$$\mathcal{N} = \mathcal{A}_3\mathcal{A}_2\mathcal{R}e^{:f_3:}\cdots\mathcal{A}_2^{-1}\mathcal{A}_3^{-1} = e^{:G_3:}\mathcal{R}e^{:g_3:}\cdots e^{-:G_3:} = \mathcal{R}\exp\left\{:-(\mathcal{I}-\mathcal{R}^{-1})G_3 + g_3:\right\}. \tag{3.3}$$

A further simplification results if we expand $(\mathcal{I}-\mathcal{R}^{-1})$ and g_3 in a resonance or complex basis, as follows:

$$h_\pm = x \pm ip_x; \qquad v_\pm = z \pm ip_z. \tag{3.4}$$

Hence,

$$(\mathcal{I}-\mathcal{R}^{-1})|\mathbf{n},\mathbf{m}> = \left[1 - \sum_{\mathbf{n}+\mathbf{m}=3} e^{i(\mathbf{n}-\mathbf{m})\cdot\mu}\right]|\mathbf{n},\mathbf{m}>, \tag{3.5}$$

and

$$g_3 = \sum_{\mathbf{n}+\mathbf{m}=3} A_{\mathbf{nm}}|\mathbf{n},\mathbf{m}> \qquad \text{where} \qquad |\mathbf{n},\mathbf{m}> = h_+^{n_1}h_-^{m_1}v_+^{n_2}v_-^{m_2}\cdots \tag{3.6}$$

and $\mathbf{n},\mathbf{m},\mu$ are vectors with components $(n_1,n_2,\cdots)$ *etc.* Substituting (3.5) and (3.6) into (3.3) and solving for G_3, we obtain

$$G_3 = \sum_{\mathbf{n}+\mathbf{m}=3} \frac{A_{\mathbf{nm}}}{\{1 - exp[i(\mathbf{n}-\mathbf{m})\cdot\mu]\}}. \tag{3.7}$$

All terms in g_3 can be incorporated into G_3 except when $\mathbf{n}-\mathbf{m}=0$ or $(\mathbf{n}-\mathbf{m})\cdot\mu = 2\pi k$; k = integer; *i.e.*, $(n_1-m_1)\mu_x + (n_2-m_2)\mu_z \neq 2\pi k$; $k = 0,\pm1,\pm2\cdots$. In a similar fashion, we could proceed to find G_4, *etc.* A further substitution of $I_x = h_+h_-$, $I_z = v_+v_-,\cdots$ — the *action invariants*— leads to

$$\mathcal{N} = \exp:\left\{(\mu_x + \mu_x'\rho_\tau + \mu_x''p_\tau^2)I_x + (\mu_z + \cdots)I_z + a_xI_x^2 + a_zI_z^2 + \cdots\right\}: \tag{3.8}$$

where we have assumed no acceleration and no explicit resonances; μ are the *phase advances*, μ' and μ'' are the first- and second-order *chromaticities* and all terms proportional to I^n are non-linear *tune shifts*. If explicit resonances occur with $(\mathbf{n}-\mathbf{m})\cdot\mu = 2\pi k$, k = integer, these must be added to (3.8). Finally, the *normal form* has the remarkable property that

$$\mathcal{M}^n = \mathcal{A}^{-1}\mathcal{N}^n\mathcal{A} \tag{3.9}$$

which also results in an enormous saving of work when applicable.

As an example, consider the Hamiltonian for the superposition of a uniform magnetic field with quadrupole and sextupole components. The vector potential for this Hamiltonian up to 3^{rd} order is

$$A_\theta = -\frac{x+\rho_0}{2}B_0 - \frac{1}{\rho_0}\left\{Q_xx^2 + Q_zz^2\right\} - \frac{S_x}{\rho_0}\left\{\frac{x^3}{3} - xz^2\right\}, \tag{3.10}$$

with $A_\rho = A_z = 0$; Q_x, Q_z, S_x are the quadrupole and sextupole strength, respectively. (With a proper choice of parameters, this Hamiltonian models all of the non-linearities of the TASCC superconducting cyclotron magnetic field up to third order.) Because (3.10) is independent of θ, the Hamiltonian (1.3) has the trivial solution

$$\mathcal{M}(\theta) = \exp\left\{-\int_0^\theta :H: d\theta'\right\} \quad \Longrightarrow \quad \mathcal{M}(\theta) = e^{-\theta:H:} \tag{3.11}$$

which can be factored (with some work) into the form of (2.6). Because we are neglecting acceleration, the energy of each particle is conserved and we define $p_\tau = (E_0 - E)/E_0$, where E is the particle energy and E_0 the energy of the central trajectory. If we factor (3.11), we find that f_3 contains 19 complicated terms.

If we carry out the normalization procedure described above and there are no explicit resonances, the normal form contains $g_2 = \mu_x h_+ h_- + \mu_z v_+ v_-$, the "rotation matrix R" and

$$g_3 = \frac{(1-\nu_x)}{4\nu_x\beta} h_+ h_- p_t + \frac{(1-\nu_z)}{4\nu_z\beta} v_+ v_- p_t$$
$$+\pi S_x \frac{k_x^2}{\nu_x\beta} h_+ h_- p_t - \pi S_x \frac{k_x k_z}{\nu_x\beta} v_+ v_- p_t$$
$$+\pi k_x \frac{1-\beta^2}{\nu_x\beta} p_t^3 + 2\pi S_x \frac{k_x^3}{3\nu_x^3\beta^3} p_t^3 \qquad (3.12)$$

which contains 4 *chromaticity* terms proportional to p_τ and two time-of-flight aberration terms proportional to p_τ^3, a substantial simplification. Furthermore, these are the terms that could potentially cause us trouble.

We see from (3.12) that if $\nu_x = \nu_z = 1 \Rightarrow \mu_x = \mu_z = 2\pi$ (that is, we make the system resonant!), then 2 terms disappear and we are left with the terms proportional to S_x. If the remaining *chromaticity* terms can be removed (which they can), then $\mathcal{R}_1 = \mathcal{R}_2 = \mathcal{I}$ or $\mathcal{R}_\perp = \mathcal{I}$. Hence

$$\mathcal{M} = \{\mathcal{A}_3^{-1}\mathcal{A}_2^{-1}\mathcal{N}\mathcal{A}_2\mathcal{A}_3\} = \mathcal{I}e^{-:\alpha p_\tau^3:} \;!! \qquad (3.13)$$

Eq. (3.13) tells us that under these circumstances, all of the non-linearities, except the one proportional to p_τ^3, annihilate each other up to 3^{rd} order in the map! Although one would never want to make the whole accelerator resonant in this way, parts of it can be made so to great advantage.

4. Conclusions

In the design and analysis of particle accelerators, we can achieve truly enormous savings in time and effort by:

1. using *maps*,
2. transforming to *normal form* to study *tune-shifts* and *resonances*, and
3. using the *Lie-algebraic* framework which enhances *insight and understanding.*

Acknowledgements

It is a pleasure to acknowledge many useful discussions with Stephen Douglas and Gordon Pusch.

References

1. A.J. Dragt, F. Neri, G. Rangarajan, D. Douglas, L.M. Healy, and R.D. Ryne, *Ann. Rev. Nucl. Part. Sci.* **38** (1988) 455.
2. E. Forest, M.Berz and J. Irwin, *Part. Accel.* **24** (1989) 91.
3. S. Wiggins, Introduction to Applied Nonlinear Dynamics and Chaos, Springer, 1991, and references therein.
4. M. Berz, *Part. Accel.* **24** (1989) 109.

THE PRESSURE-TUBE SAMPLER - COMMUNICATION THEORY IN MECHANICAL ENGINEERING

R.S. Davis
Reactor Physics Branch
Chalk River Laboratories

ABSTRACT

I became involved in the mechanical engineering of the pressure-tube sampler indirectly after I was assigned related reactor-physics calculations. I discovered a problem in the proposed method of operating a machine inside an operating CANDU reactor, considered it as a problem in communication theory and thus created a number of conceptual solutions to the problem. The role of mathematics in this work has been questioned because the same concepts could have been created in other ways.

1. Introduction

The story of my work on the pressure-tube sampler has two features that are particularly relevant to this workshop's aim of defining the role of applied mathematics in AECL. One such feature is the indirect manner in which an applied mathematician became involved in mechanical engineering - it was not that mechanical engineers decided that they needed a mathematician's help in mechanical engineering. The other such point, which follows from that, is that the customer believes that my work is better described as mechanical engineering than as mathematics. Each member of my audience may decide for himself/herself the degree to which my work is describable as mathematics (and thence the degree to which this report is relevant to this workshop).

The other sections of this report discuss the following topics:

Section 2: The pressure-tube sampler.
Section 3: The indirect route into mechanical engineering.
Section 4: The use of communication theory.
Section 5: The role of communication theory.

2. The Pressure-Tube Sampler

The purpose of the pressure-tube sampler is to monitor the hydriding of pressure tubes in CANDU reactors. This is fundamental to safety, and good monitoring also contributes to economy by avoiding unnecessarily frequent tube replacement. Specifically, the pressure-tube sampler goes right inside a pressure tube, extracts a tiny sample from the inner surface and bears it out so that a laboratory can analyze it.

The goal of the team with which I am working is to make the process more economical, primarily by making it possible while the reactor is at or near full power, and as a corollary minimizing the amount of special tooling required. Clearly, some special tooling is necessary at the sample site, but other than that the in-reactor process is to involve little or no equipment that is not already part of a CANDU station.

This is a challenging goal, because:

(i) the tool's environment is very sensitive to variation from normal operating conditions;
(ii) the tool is subject to many sorts of strong, interfering forces and energy flows;
(iii) the tool is very isolated, inaccessible to, *e.g.*, vision, manipulating tools, or even a cable; and,
(iv) The environment of the tool is very destructive, rapidly making mincemeat of, *e.g.*, hydraulics and electronics.

3. The Transition to Mechanical Engineering

My involvement in this project started when R. Joynes arranged for me to do some reactor physics calculations for the project. They were to determine:

(i) what neutronic effects the tool will have on the reactor, and
(ii) how the tool will be activated by the neutron irradiation.

Since I am in Reactor Physics Branch, these calculations[1] were not out of the ordinary for me.

The first stage in my transition to mechanical engineering came when I asked Joynes about possible detrimental effects of the reactor environment on the materials of the tool. We both considered that question to be out of our respective fields of expertise, but decided that I would ask around about it. I found out that the one potentially important effect was relaxation of springs.[2]

The second stage in my transition to mechanical engineering came when I set out to calculate whether the potential relaxations would be tolerable or not. With CANDU engineering information[3,4] and patient explanation by Joynes of the functions of the springs in the tool, I calculated minimum and maximum loadings that the springs could have. We decided that a better margin was worth pursuing.

The third stage in my transition to mechanical engineering came when I started to suggest corresponding design changes. Because of my experience in Unit 2000, I started with divergent thinking, that is, by listing as many concepts as I could by which to redesign the tool. Although the reference design did not actually need a radical redesign, Joynes decided that we should consider all possible design concepts to ensure that we based our work on the best. Consequently, I prepared a list of all the concepts I could, and of all the combinations thereof that might work. J.M. King and I are now preparing an evaluation of the resulting concepts.[5]

4. The Use of Mathematics

The basic requirements of the tool inside the reactor are:

(i) the raw energy to cut out the sample,
(ii) control to ensure that it takes a sample in the right place (and even more importantly, not in the wrong place), and
(iii) monitoring, so that the operators know how the tool is responding to the controls.

All these requirements are in fact just communication, and the problem is just to find suitable channels. Communication theory is therefore the appropriate tool for the problem. The problem of sensitivity of the environment limits the amplitude of signals, and the interfering forces are noise. The one problem is therefore low signal-to-noise ratio. Communication theory offers two means of overcoming this problem.

(i) Narrow bandwidth - The narrower the bandwidth is, the less noise there is in the communication channel. This is particularly viable for the pressure-tube sampler because, since each mission will take several hours, a delay of several thousand seconds, corresponding to a bandwidth less than a millihertz, would be quite acceptable.
(ii) Redundancy - The channel contains more information than is ideally necessary and, if part of the signal is spoiled by noise, the receiver uses the remaining signal to detect the fact.

Communication theory served as a guide to my divergent thinking (if it is not an oxymoron to speak of guiding divergent thinking). I tried to think of:

(i) every carrier, *i.e.*, everything that passes, or can pass, into or out of the reactor (*e.g.*, coolant flow, fueling machine rams, various fields and the tool itself),
(ii) every way of modulating that carrier,
(iii) every way to restrict the bandwidth upon demodulation, and
(iv) every compatible combination with adequate redundancy.

I found four basic designs in this manner.

One of the designs illustrates the application of the above principles particularly well. The tool integrates coolant flow to determine elapsed time, and uses the same mechanism to power the process. The mechanism is a turbine, reduction gearing, a lead screw, and lost motion between the nut and the cutter. The time delay provides the narrow bandwidth. Since any length of pause may occur during the mission, this design needs redundancy to cope with noise. This may be a brake that stops the turbine when a fueling machine squeezes the tool.

The reference design works entirely by force squeezing the tool. It copes with noise by means of a latch that is triggered by force exceeding a preset level greater than the greatest force the tool will undergo during handling. This is literally a brute-force design, which is possibly still the best approach, although the signal-to-noise ratio is not ample. †

5. Discussion

The difficulty of assessing the role of mathematics in this work is that communication theory was not essential in it (aside from a few simple calculations). It did, however, serve as an effective means of generating ideas. Even more importantly, it provided a means of organizing and cataloguing concepts, so that we can be confident that, after we have invested several years and megabucks in design, we will not then learn of a way we could have done it better.

References

1. R.S. Davis, in preparation.
2. A.R. Causey, G.J.C. Carpenter and S.R. MacEwen. In-reactor stress relaxation of selected metals and alloys at low temperatures. *Jour. of Nucl. Materials* 90 *(1980) 216-223;* also AECL Report, AECL-6740 (1980).
3. N. Prajapati,
4. Bruce Generating Station - Safety report to the Reactor Safety Advisory Committee of Atomic Energy Control Board, Vol. I - Design Descriptions.
5. J.M. King and R.S. Davis, in preparation.

† There was not time at the talk to describe the other two basic designs. They both convey the necessary energy in a spring in the tool, cocked before each mission, and their control signal is to-and-fro axial movement, which occurs very little in normal operation but may safely be performed enough to yield an ample signal-to-noise ratio. The mechanism is a constrained roller, unidirectional drive, reduction gearing and lost motion. To overcome the problem that the tool is actuated while moving, one design uses a tapered dashpot to make the cutter pause for the operators to stop the movement, and the other makes the cut much faster than the tool's movement, using a recoilless mechanism to eliminate recoil force on the adjacent fuel.

EDDY CURRENT SIMULATIONS IN 3D AND APPLICATIONS TO NDT PROBLEMS

N J DISERENS
Mathematics and Computation Branch
Chalk River Laboratories

ABSTRACT

This paper gives a brief summary of the use of the finite element method in the solution of eddy current problems. It outlines one algorithm for 3D analysis and the attempts made at Chalk River Laboratories to apply it to the simulation of crack detection in metal plates and tubes.

1. Introduction

Development of three-dimensional computer programs for the numerical solution of electromagnetic problems has been proceeding over the past 20 years. Prior to that time, a number of two-dimensional codes had been written, mainly utilising analytic or finite difference methods. Limitations in computing power and a need for efficient numerical algorithms made extension to 3D difficult.

With the advent of the Finite Element method, which was originally used for structural problems, it became possible to model intricate geometrical shapes and to use a mesh which mapped on to the surfaces.

Finite Elements were applied first of all to static problems, and a number of successful codes were written which could model both electromagnets and electrostatic devices such as spark chambers. At the same time, improvements in the conjugate gradient method of solution of sparse linear equations by preconditioning gave an efficient way of handling non-linear (iron) problems where the matrix needed to be updated at each iteration.

Other code developers, particularly in France, have concentrated on Boundary Integral methods, where only the material surfaces need to be meshed if the properties are linear. They have applied this technique to eddy current problems and have also developed hybrid boundary/volume methods for non linear cases.

Extension to time-varying problems has been slow. The number of degrees of freedom required to solve even a simple AC problem in three dimensions can be of the order of twenty thousand.

During the past ten years, there has been international collaboration to develop and test algorithms for solving these problems. A series of 'Eddy Current Seminars' at Rutherford Appleton Laboratory in the UK, and the availability of the Felix superconducting coils at Argonne as a test bed, led to the establishment of an organisation known as TEAM[1] (Testing Electromagnetic Analysis Methods).

Three TEAM groups exist: one in Asia, one in Europe and the other in North America. A series of benchmark problems has been devised for developers to test their algorithms. The criterion for a benchmark problem is that either measurements or analytic results must be available. A handbook is available with details of these.

Two algorithms[2] have proved popular among code developers:

(i) The T-Ω method, which solves for magnetic scalar potential W over all regions and for stream function T over conducting regions, (where J = curl T).

ii) The A-ϕ method, which solves for Vector Potential A in conducting regions and scalar potential f elsewhere.

In the field of Non Destructive Testing there has been a great deal of practical measurement, particularly with both ferrous and non ferrous tubes, but very little in the way of 3D computer simulation.

This paper describes the A-ϕ method and the difficulties in applying it to Non Destructive Testing. It reports the progress made in crack simulation at CRL and the requirements for future work.

2. The A-ϕ Method

Starting with Maxwell's Equations, we have:

$$\nabla \times H = J \tag{2.1}$$

$$\nabla \times E = -\frac{\partial b}{\partial t} \tag{2.2}$$

where:

$$B = \mu H = \nabla \times A \tag{2.3}$$

Integrating Equation (2.2) gives:

$$E = -\frac{\partial A}{\partial t} - \nabla V \tag{2.4}$$

where V is an electric scalar potential.

Combining Equations (2.2) and (2.3) gives the operator equation:

$$\nabla \times \frac{1}{\mu} \nabla \times A = -\sigma \left[\frac{\partial A}{\partial t} + \nabla V \right] \tag{2.5}$$

Uniqueness of solution cannot be guaranteed unless a gauge is imposed. This could be done by directly applying the condition that the Divergence of A should be zero. This is known as the Coulomb Gauge. However, there are problems both with the application of boundary conditions on conductors and with the case when two materials with different conducting properties are in contact, when a jump in A across the boundary may occur.

The Lorentz Gauge, Equation (2.6), provides for uniqueness of solution and also gives continuous values of A across material interfaces.

$$\nabla A = -\mu \sigma V \tag{2.6}$$

In the space surrounding the conducting materials, the Laplace Equation:

$$\nabla . \mu \nabla \phi = 0 \tag{2.7}$$

is used, where ϕ is the magnetic scalar potential. Interface conditions must be applied such that the normal component of B and the tangential component of H should be continous, and that the normal component of J should be zero on the external boundaries of conductors.

For regions containing conductors in which drive currents are specified, then, to avoid the problem of m being multivalued, a reduced potential ψ is used, such that:

$$\psi = \phi - \phi_s \tag{2.8}$$

where ψ_s is the magnetic scalar potential due to the drive current, obtained by integration over the conductor, which is not meshed (see Fig. 1).

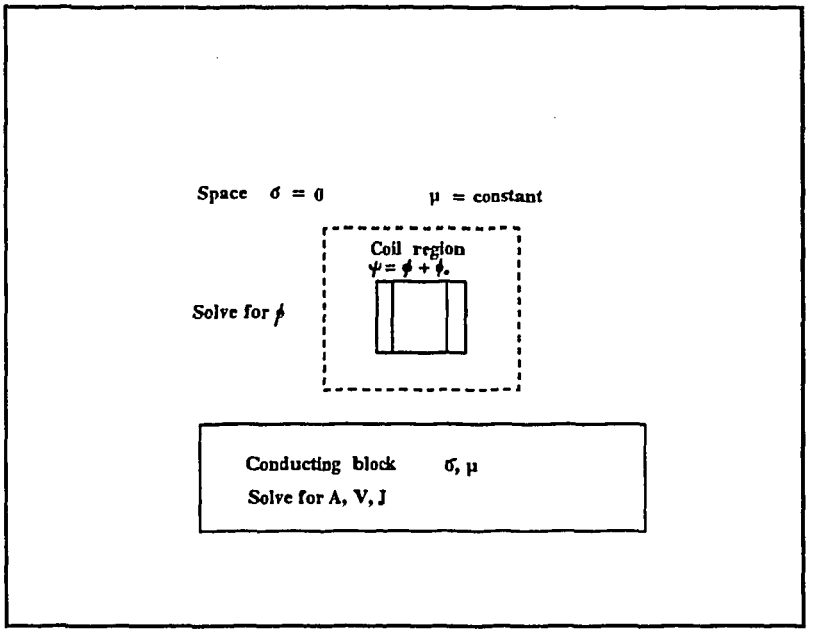

Fig.1 Potential regions for A-ϕ method.

In such cases, the right-hand sides to the equations are provided by the values of fs and its derivatives at the interface between the reduced and total scalar potential regions.

The above equations are solved using Finite Elements, employing the Galerkin weighted residual method for the formulation. Linear (8 node) or quadratic (20 node) brick elements are used.

The equation solver uses a preconditioned conjugate gradient method. A solution is obtained, first for A, ϕ and ψ. Then the values of A are used to obtain a solution for V and J.

3. Crack Simulation Tests on the ELEKTRA Package

Two series of tests have been conducted on this package, which uses the A-ϕ method:

3.1 *Simulation of a Fine Crack in a Non-Ferrous Plate.*

The plate had a resistivity of 50 microhm-cm and a relative permeability of 1. The plate has a surface crack 12.7 mm long, and 0.12 mm wide. Results were required for depths of crack of 1 mm, 0.5 mm and 0.25 mm. The thickness of the plate was 4 mm. The detector probe was set with coil axis normal to the plate surface. The coil was 0.5 mm in axial length and its face was 0.5 mm from the plate. The inner and outer diameters of the probe coil were 2 mm and 3 mm, respectively. The frequency of excitation was 400 kHz.

The experimental results were displayed as complex impedances. The probe scan was transversely across the centre of the crack. At a distance of 10 mm from the crack the probe was lifted. The display was set so that the impedance response was in line with the x axis.

Many models were tried in attempts to simulate the crack, but with a limit of around 40 000 equations on the VAX, the resolution was not fine enough and the results were all 'model sensitive'. Figs. 2a and 2b show the experimental and the best computed results, respectively. (Here we are looking for patterns, not absolute values.)

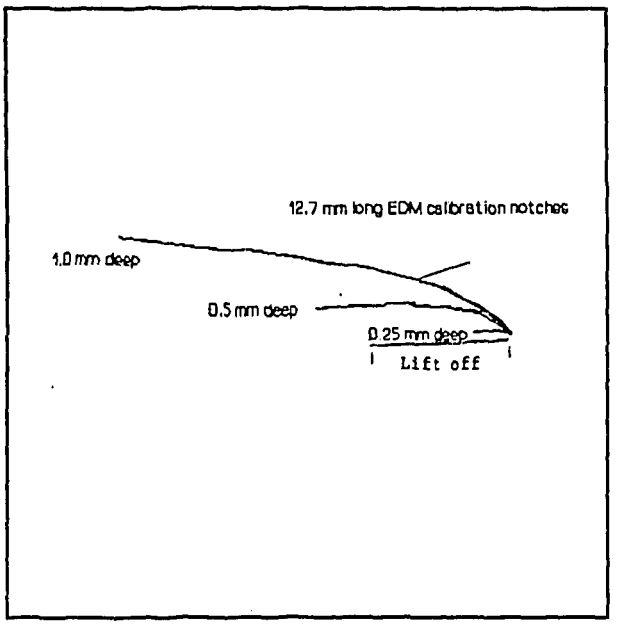

Fig.2a - Experimental.

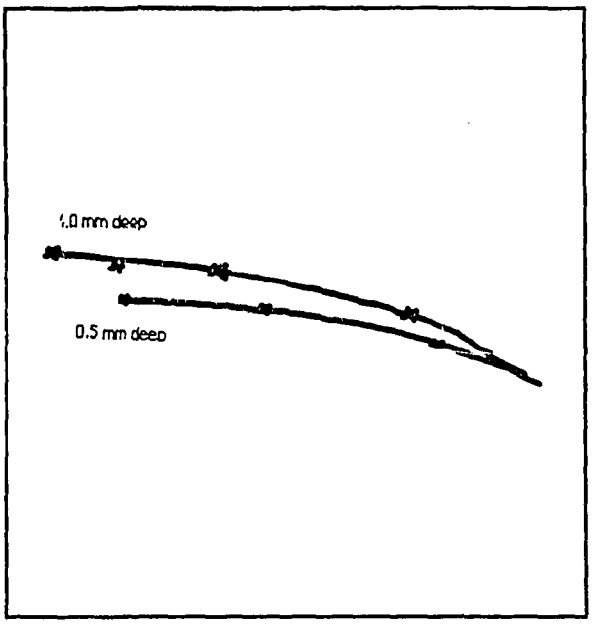

Fig. 2b - Computed.

Impedance plot for crack-in-plate model.

3.2 *Simulation of Crack Detection in Pipes.*

A schematic of an 'RFEC' (Remote Field Eddy Current) pipe inspection scheme is shown in Fig. 3. The field seen by the detector is regarded as being a combination of the direct field from the exciter coil and the indirect field through the wall of the pipe. The region where these cancel is called the 'transition zone'. An abrupt change of phase in the detected signal is seen in this region. Hence the detector coil is generally placed just beyond the transition zone.

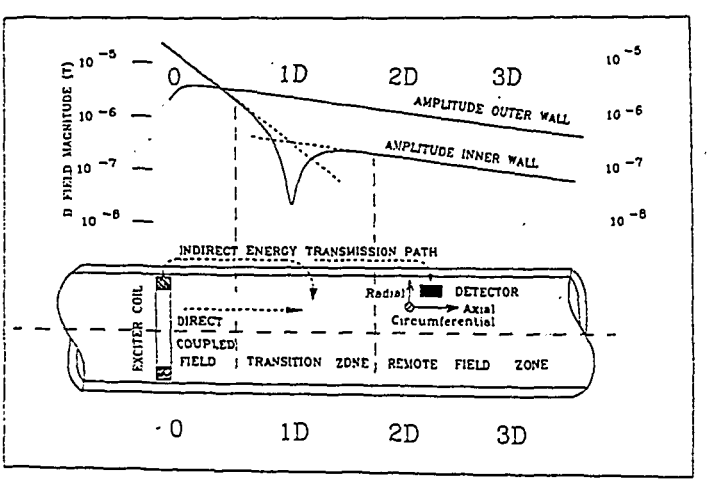

Fig 3. RFEC detector arrangement.

For ferrous tubes it is difficult to detect flaws which run in the longitudinal direction. For non-ferrous tubes circumferential the flaws are most difficult to find.

For this reason, an investigation of the fields due to tilted exciter coils was initiated. Measurements have been made at Queen's University (Kingston, Ontario) with coil tilts of up to 6 degrees in a steel pipe.

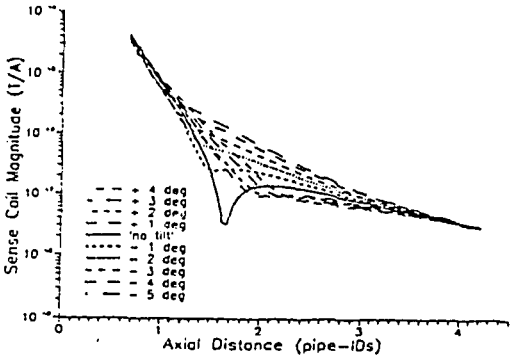

Fig. 4a. Experimental.

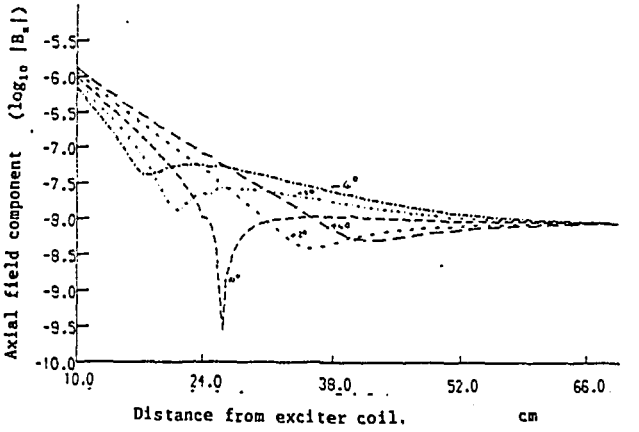

Fig. 4b Computed.

Axial magnetic field component
along inner wall of pipe.

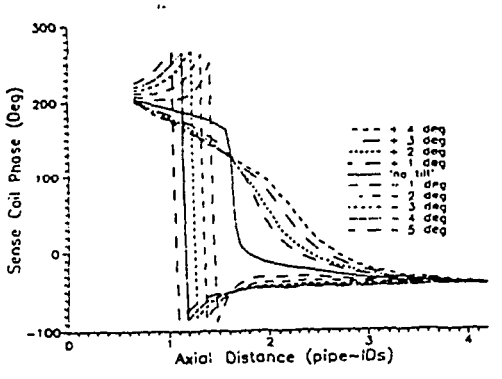

Fig. 5a. Experimental.

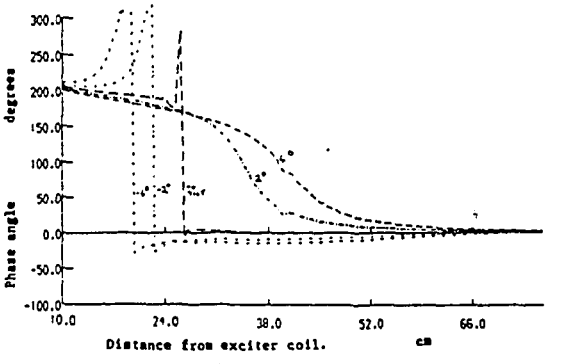

Fig. 5b. Computed.

Phase of axial magnetic field component.

Computer simulations give close agreement. Figs. 4a and 4b show the axial field component and Figs. 5a and 5b the phase variation.

When a longitudinal slot, 10 mm long by 0.2 mm wide, is introduced in the computer model using a 6 degree coil tilt, it appears that the transition zone moves towards the exciter coil (Fig. 6). It is believed that this model is too coarse. More work is required to confirm the effect.

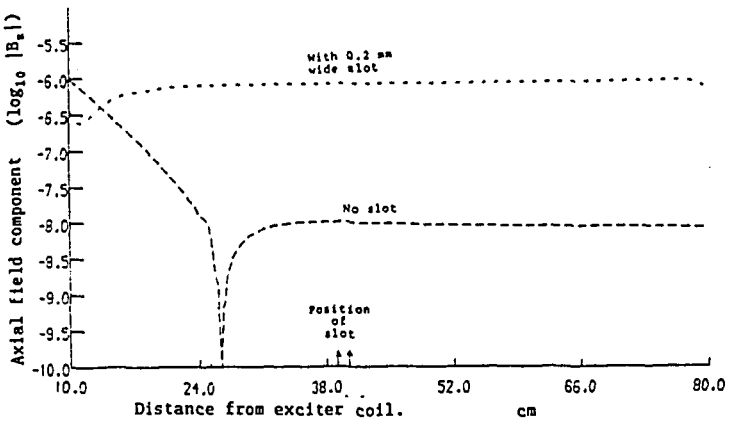

Fig. 6. Shift of transition zone for pipe with slot (computed).

4. Conclusions and Possible Improvements

More nodes are required throughout the model. At present, the practical limit is about 27 000 nodes with about 42 000 degrees of freedom on the VAX 6520, both for the analysis program and for the post processor.

First-order nodes give smoother fields than second-order, using the same number of nodes. This suggests that there may be a coding error, as experience shows that second-order finite elements should give smoother fields.

For the higher frequencies, the usual linear or quadratic shape functions are not appropriate to model the field variation normal to surfaces in materials where skin depth is small. A shape function representing an exponential decay would be much better.

Another way of representing skin effect would be to use impedance elements(3). These would be surface elements having the usual shape functions for the tangential directions, but whose impedance per unit area depends on the material properties, the fields and the frequency. There are difficulties in using this type of element on edges and on plates thinner than the skin depth.

5. Acknowledgements

Acknowledgements are due to Vector Fields Ltd. for use of the ELEKTRA eddy current package; to Prof. David Atherton of Queen's University for supplying the experimental RFEC data; and to Hugh Ghent of NDT Branch, CRL, for impedance data for the plane problem.

6.References

1. Crutzen, Y; Diserens, N J; Emson, C R I and Rodger, D. Proc. *Proc. European TEAM Workshop and International Seminar on Magnetic Field Analysis*, Oxford, UK, 23-25 April 1990. EEC, JRC, Institute for Systems Engineering and Informatics, Ispra, Italy. EUR 12988 EN 1990.
2. Trowbridge, C W. "Introduction to Computer Aided Electromagnetic Analysis". (Vector Fields Ltd. UK. 1990.)
3. Deeley, E M and Xiang, J. "Improved Surface Impedance Methods for Two and Three Dimensional Problems". Trans IEEE MAG-24 (No 1), Jan 1988.

UNUSUAL REPRESENTATIONS OF DISCONTINUOUS CURVES

DAVID JACK
Safety and Environmental Support Branch
AECL Research

Abstract

Representations of curves with discontinuities of position and direction are often made with periodic basis functions, as, for example, in Fourier series, even when the shape of those curves *is aperiodic*. An unusual but perhaps more logical approach is that of using aperiodic basis functions to represent such curves. Examples are used to demonstrate situations where this approach can be used to advantage.

1. Introduction

The physical world abounds with examples of discontinuous curves. Among them are the paths traced out by animate creatures as they locomote, the boundary between water and land along a coastline, and the interaction cross section of a neutron as a function of distance along its path in a heterogeneous medium, to name just a few.

Mathematical representations of discontinuous curves include both continuous and piecewise continuous functions. Representations by Fourier series or integrals are continuous approximations. On the other hand, representations obtained by splicing together various combinations of intervals of algebraic and transcendental functions are piecewise continuous.

The representations which follow are continuous functions but they are unusual in that they are not periodic, like the sin and cos functions of the Fourier series. However, they may be combined in summation or product series to form close approximations to discontinuous curves in a similar manner.

2. Details

A monotonic increasing function of a single variable with constant unequal asymptotes can be made to look like Fig. 1(a) by suitable linear transformations of the dependent and independent variables.

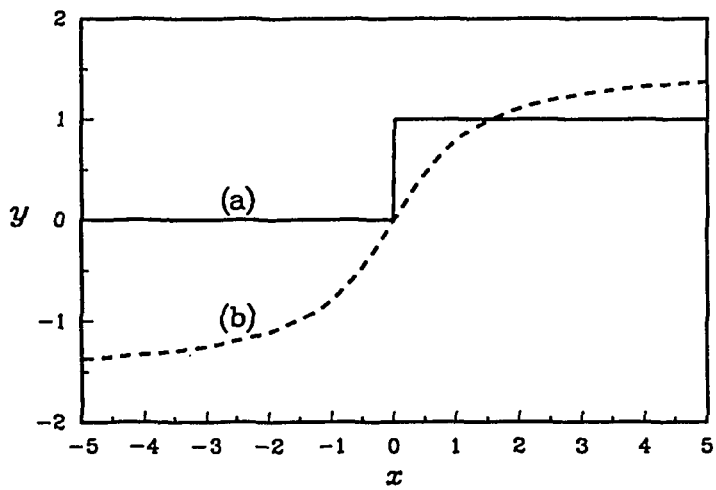

Fig. 1 A continuous function made to look discontinuous.

For example, Fig. 1(b) shows $y = b + A\arctan(mx)$, with $A = m = 1$ and $b = 0$. Fig. 1(a) is the same curve, with $A = 1/\pi$, $m = 10^4$, and $b = \frac{1}{2}$. The large value of m performs a scale transformation along the x axis to produce a curve which has approximations to discontinuities at the points $(0, 0)$,

$(0,1)$. A short list of functions which are candidates for this sort of transformation follows:

$$y = \tanh x, \tag{1}$$

$$y = e^{-e^{-x}}, \tag{2}$$

$$y = \arctan x, \tag{3}$$

$$y = \frac{1}{1+e^{-x}}. \tag{4}$$

They are listed in order of decreasing slope at the origin (following normalization to asymptotes $(-\infty, -\frac{1}{2})$, $(\infty, \frac{1}{2})$ and translated, if necessary, with respect to x, to pass through the origin). All of them, except for (2), possess symmetries which give the same "sharpness" to both the upper and lower approximate discontinuities.

3. Applications

Transformations of discontinuous-looking functions like that of Fig. 1(a) can be added or multiplied together and combined with other functions in potentially useful ways. Two examples are shown in Fig. 2.

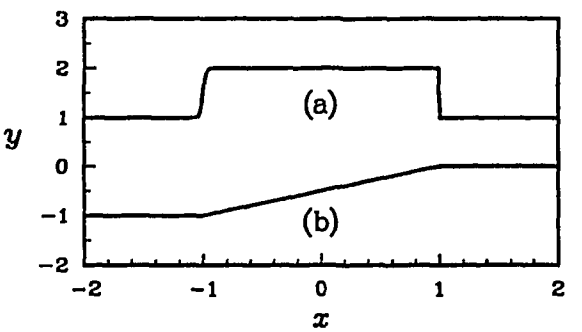

Fig. 2 A single pulse and a finite ramp.

Fig. 2(a) shows a single pulse approximation given by

$$y = 1 + \frac{1}{2}\tanh(40(x+1)) - \frac{1}{2}\tanh(10^5(x-1)). \tag{5}$$

There are no unwanted oscillations near the edges, such as the Gibbs phenomenon found in Fourier integral approximations. Another advantage illustrated in this example is that the sharpnesses of the left and right edges are independent.

In the numerical solution of differential equations describing the evolution of dynamical systems, the use of piecewise continuous ramps as driving functions can sometimes cause convergence problems near the discontinuities. Fig. 2(b) shows a finite ramp approximation given by

$$y = \frac{x+1}{2\pi}(\arctan(10^4(x+1)) - \arctan(10^4(x-1))) + \frac{1}{\pi}\arctan(10^4(x-1)) - \frac{1}{2}, \tag{6}$$

which has no discontinuities, thereby avoiding such problems.

The unusual representations of discontinuous curves discussed here can be made to undergo continuous transformations in higher dimensional spaces, extending their range of application to representations of discontinuous surfaces and volumes, as well.

Acknowledgements

Thanks go to B. Selander, F. Marsiglio, and G. Pusch for suggesting (1), (4), and (6), respectively.

GLUBFIT: Interactive Graphic Curve Fitting Program

H. Keech
Math and Computation
AECL Research

ABSTRACT

GLUBFIT was developed for rapid primary analysis and fitting of Neutron and Solid State Physics (NSSP) spectrometer data. TRIUMF low-level graphics routines are used.

1. Introduction

The interactive menu-driven program GLUBFIT is a general curve fitting program for a user selectable combination of the fitting functions: Gaussian, Lorentzian, User-written, and Background. It is written in Fortran for a MicroVax VMS 5.4 system, for terminals using VT100 text mode and Tektronics 4014 graphics mode.

The spectrum input system is designed specifically for the internal structure used by NSSP spectrometer data files. However, the code is modular and for different data storage one only need substitute the proper input routines.

The feature of most general interest for workshop attendees is the use of the low-level TRIUMF graphics library. The original work proposal concentrated on the standard curve fitting features. We have found that the graphics features introduced to give the user visible hands-on control over fitting operations have become in themselves an important and desirable end-product.

2. Overview

The input data consists of any linear combination of spectrometer data runs. One may select a subset of data in a fit window. The program permits a sum of 6 base functions and a total of 18 fitting parameters. The parameters are allowed to vary freely or to be fixed.

The calculated fit is stored on a user file that may be edited and used as input for a new fit. This allows minor perturbations to previous fits. One may add or remove a base function from the linear combination.

An undo or backup feature allows users to move both directions in the interactive program. One may very quickly test and revise initial estimates. An error trap is active during the least-squares fitting to prevent aborts on arithmetic overflows.

3. Conclusions

The Gauss-Jordan curve-fitting algorithm has produced some excellent test results. It is important to start with reasonable initial values. A typical fit CP time is 15 seconds for a window with 6 peaks.

QUANTUM ALGEBRA AND QUANTUM HOLONOMY

H.C. Lee
Theoretical Physics Branch
AECL Research

ABSTRACT

We present a brief discussion of several interrelated topics: Stokes' law, classical holonomy, quantum holonomy, link and tangle invariants, quantum algebras.

1. Stoke's Law in Electromagnetism

Recall classical electromagnetism. Consider a space with magnetic field $\vec{B}$. Let $\vec{S}$ be a surface. Then

$$\Phi = \int_{\vec{S}} \vec{B} \cdot d\vec{S}, \tag{1}$$

the number of fluxlines piercing the surface $\vec{S}$, measures the magnetic field strength.

Let $\vec{A}$ be the vector potential and ∂S be the boundary of $\vec{S}$. Then

$$\vec{B} = \nabla \times \vec{A} \tag{2}$$

and, from Stoke's law, the flux Φ is given (in appropriate units) by the line integral of the vector potential along the boundary of $\vec{S}$:

$$\Phi = \int_{\partial S} \vec{A} \cdot d\vec{l}. \tag{3}$$

The flux is not changed when $\vec{A}$ is changed by a *gauge transformation*

$$\vec{A} \rightarrow \vec{A} + \nabla f, \tag{4}$$

where f is an arbitrary function.

The boundary $\vec{S}$ is just a closed contour C, or loop, in space. Let x_0 be a point in space and $\{C_1, C_2 \ldots C_N\}$ be a series of loops beginning and ending at x_0. Then $\{\Phi_1, \Phi_2 \ldots \Phi_N | \ \Phi_i = \oint_{C_i} \vec{A} \cdot d\vec{l}, \ i = 1, 2, \ldots N\}$, gives a series of measurement of the field strength. Barring pathological situations, for any x_0, the set of measurements with $N \leq \infty$ gives a complete description of the magnetic field $\vec{B}$. Equivalently, it gives a complete description of the vector potential $\vec{A}$, modulo gauge transformations.

2. Phase Factor and Holonomy

The measurement can be carried out by transporting a charged particle (say, an electron with charge e) slowly around a loop C_i. One can make the transportation sufficiently slow that the energy of the electron does not change. Then the wavefunction of the electron can at most change by a *phase factor*. One part of the phase depends on details (such as length) of the loop. Another part is just e times the flux encircled by C_i, and gives a geometric phase factor

$$\exp(ie\Phi_i). \tag{5}$$

This is a topological result [1], and, because the electron would acquire the factor (if $\Phi \neq 0$) even when the loop lies entirely in a region where the electric and magnetic fields are zero, it shows that the vector potential plays a more fundamental role than the field strengths in electromagnetism.

The phase factor is a simple realization of a mathematical construction called *holonomy*, which is a fundamental kind of sampling, done by sending a 'test' particle around a contour in space, of the local properties of a system with a spatially dependent group structure.

3. Quantum Holonomy

In a more general setting, the space is generally some manifold $\mathcal{M}$, and the vector potential is replaced by a matrix $A(x)$ that transforms as a representation of some group G at each point x in $\mathcal{M}$. In particular vector potentials at two different point do not commute:

$$[A(x), A(y)] = A(x)A(y) - A(y)A(x) \neq 0. \tag{6}$$

Theories with this kind of vector potentials are said to be nonabelian; the fields are known as Yang-Mills fields [2]. The electroweak force (the Standard Model) and the strong force (Quantum Chromodynamics, or QCD) are nonabelian theories with Yang-Mills fields plus matters particles such as electrons and quarks.

As in electromagnetism, the nonabelian theory depends on $A(x)$, modulo gauge transformations

$$A(x) \rightarrow \Omega^{-1}(x)A(x)\Omega(x) + \Omega^{-1}(x)\partial\Omega(x), \tag{7}$$

where $\Omega(x)$ is a matrix-valued function. (Indices attached to A and Ω are suppressed.)

In a nonabelian quantum field theory with action $I[A]$, the system is described statistically by the formal partition function

$$Z = \int \mathcal{D}A \exp(iI[A]). \tag{8}$$

The path integral $\int \mathcal{D}A$ integrates over (each component of) A at each point x as an independent integration variable, modulo gauge transformations. The expectation value of an A-dependent operator $\mathcal{O}$ is then given by

$$\langle \mathcal{O} \rangle = \frac{1}{Z} \int \mathcal{D}A \exp(iI[A])\mathcal{O}[A]. \tag{9}$$

In this setting, the generalization of holonomy is a matrix-valued *quantum holonomy*,

$$\Psi[C] = \langle P \exp(i \oint_C A dx) \rangle, \tag{10}$$

where C is a closed contour in $\mathcal{M}$ and P means path ordering, which is needed to define the integral because two A's at two different points along C do not commute. Because Yang-Mills fields self-interact, unlike its counterpart in electromagnetism, quantum holonomy is nontrivial even when there are no matter particles or other external fields. In the absence of such, the set of all independent quantum holonomies corresponding to the set of all contours tells us everything about the self-interaction of Yang-Mills fields.

4. Chern-Simons Theory, Topological Invariants and Quantum Algebra

In general, we do not know how to exactly calculate Z, nor the quantum holonomy, nor any $\langle \mathcal{O} \rangle$; instead, we use elaborate (but well established) purterbative methods to obtain approximations. There is one known exception to this rule, first discovered by Witten [3]. Witten pointed out that owing to the topological symmetry of the *Chern-Simons theory* in three dimensions, which has an action

$$I[A] = \int_{\mathcal{M}} dx^3 (A \wedge \partial A + \frac{2}{3} A \wedge A \wedge A), \tag{11}$$

($\wedge$ is the antisymmetric wedge product) the matrix trace of the quantum holonomy, also known as the Wilson line,

$$W[C] = Trace(\Psi[C]), \tag{12}$$

can be exactly computed by *algebraic* means - no explicit integration needs to be carried out.

This result implies that $W[C]$ is determined only by the representation of the group G and the topological property of C. The topological property of C in two dimensions is very restricted and in four and higher dimensions is trivial. But it can be highly nontrivial in three dimensions. In

particular, in three dimensions C can wind around itself to form *knots*, or around other loops as well as around itself to form *links*.

So we can think of $W[C]$ as a mapping, specified by a representation of G, of knots or links to number valued functions, namely, link invariants [4]. Loosely speaking, if we know the maps for all links, then we almost (because of trace taking) know everything about the Chern-Simons theory in three dimensions.

The algebra we use to calculate $W[C]$ exactly is a Hopf algebra that may be viewed as a deformation of the Lie algebra of G. Some Hopf algebras are also called *quantum groups* [5], or *quantum algebras*, because they act on 'quantum' spaces with noncommuting coordinates. Nontrivial Hopf algebras were discovered only a few years ago; the best known ones are deformations of the Lie algebras of classical Lie groups.

The Wilson line $W[C]$ is not a quantum holonomy, but only the trace of a quantum holonomy. What is the quantum holonomy in the Chern-Simons theory? Recall that in an algebra there are central elements that commute with other element in the algebra. For example, in $su(2)$ there is only one central element J^2. It has eigenvalue $J(J+1)$ for the irreducible spin-J representation. The centre of an algebra is the set of all its central elements. Recently, we [6] have shown that in every representation of G each quantum holonomy commutes with all the elements of G. This means that a quantum holonomy is just a scalar function times a unit matrix. Therefore, quantum holonomy may be given the the same physical interpretation as holonomy in electromagnetism: for a given C, every state in an irreducible representation has the same phase factor.

An application of this result to Chern-Simons theory in three dimensions leads to the following: quantum holonomy is a mapping of tangles (a tangle is a link cut in one place, with its two open ends held fixed on the surface of a sphere enclosing the tangle) to the centre of the Hopf algebra. Since there are an infinite number of tangles, there are also an infinite number of central elements in a Hopf algebra. It follows that if a physical system has a Hopf algebra symmetry, then the system has an infinite number of conserved quantum numbers (which are not integers or half integers, but are tangle invariants). This partly explains why such systems are integrable.

Although the need is great, especially for the study of phase transitions, few nonperturbative methods applicable to realistic field theories such as QCD are known. These results on quantum holonomy raise the hope that some topological properties of such theories may be exactly computable by algebraic means.

References

[1] Y. Aharonov and D. Bohm, Phys. Rev. **115** (1959) 485.
[2] C.N. Yang and R.L. Mills, Phys. Rev. **96** (1954) 191.
[3] E. Witten, Comm. Math. Phys. **121** (1989) 351.
[4] V.F.R. Jones, Bull. Am. Math. Soc. **12** (1985) 103.
[5] V. Drinfeld, *Quantum groups*, in Proc. Int. Cong. Mathematicians (Berkeley, 1986), **I**, 798.
[6] H.C. Lee and Z.Y. Zhu, Phys. Rev. **44** (1991) 942.

Generalized quantum groups

H.P. LEIVO
Theoretical Physics Branch
CRL

ABSTRACT

The algebraic approach to quantum groups is generalized to include what may be called an anyonic symmetry, reflecting the appearance of phases more general than ± 1 under transposition.

1. Quantum Groups

The notion of quantum group[1], a special type of *bialgebra*, originally abstracted from studies of integrable or exactly solvable physical systems, has been found to be quite pervasive in many diverse fields of physics, such as inverse scattering theory, solitons, statistical spin models, lattice gauge theory, conformal field theory and gravitation.

There now exists a great deal of elegant mathematical machinery to unify the various historical approaches to quantum groups, but a straightforward algebraic approach[2] which led to one of the earliest incarnations of the concept is also very directly linked to interesting physical systems. A method of studying such solvable statistical systems[3] as the Heisenberg antiferromagnetic chain, the 2-d Ising model, the 1-d XY-model, the XYZ model, the hard-hexagon model, and the general eight-vertex model, centers on the existence of a *transfer matrix* T_{ij} satisfying the equation†

$$\hat{R}_{ab|mn} T_{mk} T_{nl} = T_{am} T_{bn} \hat{R}_{mn|kl} \tag{1.1}$$

for some invertible $\hat{R}$. A consistency condition for this structure is the Yang-Baxter relation

$$\hat{R}_{ab|mn} \hat{R}_{nc|pk} \hat{R}_{mp|ij} = \hat{R}_{bc|mn} \hat{R}_{am|ip} \hat{R}_{pn|jk}. \tag{1.2}$$

It can be shown[2] that the associative algebra generated by the non-commuting T_{ij}, subject to the relations (1.1), obtains the additional structure of a bialgebra when a *coproduct* is introduced of the form

$$\Delta(T_{ij}) = T_{ik} \otimes T_{kj}. \tag{1.3}$$

A coproduct is, in a sense, the opposite of a product: instead of combining two elements to yield a third, it distributes an element into a sum of pairs. A simple example is the Lie coproduct which may be defined for any Lie algebra:

$$\Delta(X) = X \otimes 1 + 1 \otimes X. \tag{1.4}$$

In elementary physics the essential physical role of a coproduct is easy to overlook, since in the theory of angular momentum, for example, the Lie coproduct translates into the simple additive relation between the angular momentum operator of a compound system and the operators of the constituent systems,

$$J_z = j_z^{(1)} + j_z^{(2)}, \tag{1.5}$$

which one is tempted to take as intuitively obvious.

The continuous deformation of Lie algebras away from their natural Lie product and the coproduct (1.5), while retaining a bialgebra structure and hence such important consequences as being able to generate all states from one 'highest weight' state using raising and lowering operators, is an important approach[4] to obtaining quantum groups of potential physical interest. The quantum groups so obtained are, in fact, a subset of those obtained by considering a structure dual to that defined by equations (1.1) and (1.3). In the following we describe this structure and present a generalization.

† Implicit summation on all repeated indices.

2. More Details

The index acrobatics involved in (1.1) and (1.2) may be eliminated by using the transposition operator $P_{ij|kl} = \delta_{il}\delta_{jk}$. Then (1.1) may be written as $\hat{R}T_1PT_1P = T_1PT_1P\hat{R}$, where $T_{1\,ij|kl} = (T \otimes 1)_{ij|kl} = T_{ik}\delta_{jl}$ and the implicit summations are simply of the form $\sum_{p,q} A_{ij|pq}B_{pq|kl}$.

The dual algebra (to which the term 'quantum group' is strictly applicable) is generated by non-commuting quantities $L^{\pm}_{ij}$ with a coproduct of the same form as (1.3). The duality pairing obtained from

$$\langle L^{\pm}_{ij}, T_{ab}\rangle = R^{\pm}_{ia|jb}, \tag{2.1}$$

where $R^+ = \hat{R}P$ and $R^- = \hat{R}^{-1}P$, requires the $L^{\pm}$ to satisfy the relations

$$\begin{aligned} \hat{R}PL^{\pm}PL^{\pm} &= L^{\pm}PL^{\pm}P\hat{R} \\ \hat{R}PL^{+}PL^{-} &= L^{-}PL^{+}P\hat{R} \end{aligned} \tag{2.2}$$

analogous to (1.1).

3. An Anyonic Generalization

In analogy with the supersymmetric generalization[5] of the above structure, which replaces the transposition operator P with the graded transposition operator $\overline{P}_{ij|kl} = (-1)^{\bar{i}\bar{j}}P_{ij|kl}$, we seek a generalization involving a transposition operator of the form $\tilde{P}_{ij|kl} = \mu_{ij}P_{ij|kl}$. Unlike the regular and supersymmetric transposition operators, $\tilde{P}$ is not *a priori* assumed to be symmetric, nor does $\tilde{P}^{-1} = \tilde{P}$. There are thus a great many 'natural' generalizations of the equations in §2, in which one replaces P's with some selection of $\tilde{P}$'s, or its inverses or their transposes. Elimination of inconsistent choices is best done with a symbolic manipulation program such as Mathematica[6]. A consistent generalization, so derived, requires the μ_{ij} to satisfy $\mu_{ij}\mu_{jk}\mu_{ki} = \mu_{ik}\mu_{kj}\mu_{ji}$ and replaces the corresponding equations in §2 with

$$\begin{aligned} \hat{R}T_1\tilde{P}T_1\tilde{P} &= T_1\tilde{P}T_1\tilde{P}\hat{R}, \\ R^+ = \hat{R}\tilde{P} \quad , \quad R^- &= P\tilde{P}\hat{R}^{-1}P, \\ \hat{R}\tilde{P}^{-1}L^{\pm}\tilde{P}L^{\pm} &= \tilde{P}^{-1}L^{\pm}\tilde{P}L^{\pm}\hat{R}, \\ \hat{R}\tilde{P}L^{+}\tilde{P}^{T}L^{-}\tilde{P}^{T} &= \tilde{P}^{T}L^{-}\tilde{P}^{T}L^{+}\hat{R}\tilde{P}. \end{aligned} \tag{3.1}$$

The utility of such an introduction of 'anyonic' symmetry in the context of solvable models is currently under investigation.

References

1. V.G. Drinfeld, *Proc. Int. Congress Math. Berkeley* 1 (1987)798.
2. L.D. Faddeev, N.Yu. Reshetikhin, L.A. Takhtajan in *Algebraic Analysis, ed. Kashiwara et al.* (Academic, 1989)129.
3. cf. R.J. Baxter, *Exactly Solved Models in Statistical Mechanics* (Academic Press, 1982).
4. M. Jimbo, *Lett. Math. Phys.* 10(1985)63.
5. L. Liao, X.C. Song, *Mod. Phys. Lett.* 11(1991)959.
6. S. Wolfram, *Mathematica - A System for Doing Mathematics by Computer* (Addison Wesley, 1991).

MANY-BODY PROBLEMS IN CONDENSED MATTER PHYSICS

F. Marsiglio

Theoretical Physics Branch
Chalk River Laboratories

In condensed matter physics the type of problem one often addresses contains of order 10^{23} particles. A typical example is electronic properties of a metal, where the relevant entities are the conduction electrons. Besides interacting with the lattice (a complication which is often dismissed by resorting to the "jellium" model whereby the positive ions of the lattice act only to balance overall charge) electrons interact with one another through the long-range (but screened) Coulomb repulsion. It is the interactions with both the positive ions and with one another that greatly complicates the many-electron problem.

In this brief report, it is my intention to give the reader a taste of some of the techniques which are useful in attacking these kinds of problems. Generally speaking there are perhaps three approaches: exact solutions, variational techniques, and perturbation theory. In most of what follows I will discuss a particular aspect of (self-consistent) perturbation theory as applied to the phenomenon of superconductivity. Before doing so, however, it is perhaps useful to mention the difficulties involved in exact solutions. First of all, analytical exact solutions are few and far between. There are a number of analytical results involving model spin systems. Such models are useful for describing electrons which are localized (non-conducting) since only the spin (and not the charge) degree of freedom remains. Moreover, in one dimension analytical results do exist for the Hubbard model, for example, a result worked out by Lieb and Wu[1] using "Bethe Ansatz" techniques.[2] Beyond one dimension, however, it has proven necessary to resort to numerical techniques. For definiteness, we consider the paradigm of correlated electron systems, the Hubbard Hamiltonian:

$$H = -\sum_{\substack{<ij> \\ \sigma}} t_{ij}(c^{\dagger}_{i\sigma}c_{j\sigma} + \text{ h.c.}) + U\sum_{i} n_{i\uparrow}n_{i\downarrow}. \tag{1}$$

The Hamiltonian (1) is written in second-quantized notation; the operator $c^{\dagger}_{i\sigma}$ creates an electron at site 'i' with spin 'σ', while $c_{j\sigma}$ annihilates an electron of spin 'σ' at site 'j'. Hence the first term in the Hamiltonian is the kinetic part, whereby, an electron 'hops' from site 'j' to site 'i' or vice versa, with hopping amplitude t_{ij}. The indices 'i' and 'j' label sites on a periodic lattice, for example a two dimensional square lattice. In the second term, $n_{i\sigma}$ is the number operator, $n_{i\sigma} \equiv c^{\dagger}_{i\sigma}c_{i\sigma}$. Hence, if two electrons (necessarily of opposite spin due to the Pauli exclusion principle) occupy a single site 'i' then there is an energy cost U. Clearly, only the very short range (and most dominant) part of the electron-electron Coulomb potential has been retained. Note that we have assigned a single orbital to each site, thus making this a single band model. One can diagonalize the Hamiltonian (1) analytically in either of two limits; *(i)* the non-interaction limit ($U = 0$) or *(ii)* the strong-coupling limit ($t_{ij} = 0$). In between, an exact solution requires a computer. To enumerate the Hilbert space is quite simple if one begins in the localized (Wannier) representation. Each site can be in one of four states, *1)* occupied, *2)* occupied with a spin up electron, *3)* occupied with a spin down electron, or *4)* doubly occupied. The size of the Hilbert space is then 4^N, where N is the number of sites. Currently, a 4×4 lattice ($N = 16$) exhausts the capability of modern day computers, so that only small systems can be (or ever will be!) tackled by this method. Nonetheless, exact diagonalizations provide useful insight and checks on more approximate methods.[3] A second approach is Quantum Monte Carlo simulation.[4] The computer time requirements of this approach are significant; however the time required increases algebraically with the size of the system (as

opposed to exponentially) so that as computers become faster, larger and larger systems can be tackled (workers in the field have used 16×16 lattices to study the Hubbard model).

Since exact results are readily available in particular limits (*i.e.*the non-interacting limit), it becomes useful to perform perturbation theory. A systematic means of doing this is provided by Green function methods. The reader is referred to several books on this subject, in the many-body context.[5] For our purposes it is necessary only to realize that the Green function (or propagator, as it is sometimes called) contains most of the relevant information about a system. The single electron Green function is defined:

$$G(\vec{k}, \tau - \tau') = \begin{cases} - < c_k(\tau) c_k^\dagger(\tau') >, & \tau > \tau' \\ + < c_k^\dagger(\tau') c_k(\tau >, & \tau' > \tau \end{cases} \tag{2}$$

The angular brackets denote quantum mechanical expectation values. Similarly, the phonon (quantized ion vibration) propagator is given by

$$D(\vec{q}, \tau - \tau') = \begin{cases} - < u_q(\tau) u_q(\tau') >, & \tau > \tau' \\ - < u_q(\tau') u_q(\tau >, & \tau' > \tau \end{cases} \tag{3}$$

where $u_q(\tau)$ is the ion displacement operator. The non-interacting propagators, $G_0(k, \tau)$ and $D_0(\vec{q}, \tau)$, are both known analytically. For technical reasons, it is simplest to think of the variable 'τ' as imaginary time, so that the Fourier transform is in the imaginary frequency domain. We have

$$G_0(\vec{k}, i\omega_m) = \frac{1}{i\omega_m - \epsilon_k} \tag{4a}$$

and

$$D_0(\vec{q}, i\nu_n) = \frac{2\omega_q}{(i\nu_n)^2 - \omega_q^2} \tag{4b}$$

where $i\omega_m (\equiv i\pi T(2n-1))$ and $i\nu_n (\equiv i\pi T 2n)$ are the Fermion and Boson Matsubara frequencies, and ϵ_k (ω_q) is the one-electron (phonon) energy. From general considerations one can derive Dyson's equations:

$$G^{-1}(\vec{k}, i\omega_m) = G_0^{-1}(\vec{k}, i\omega_m) - \Sigma(\vec{k}, i\omega_m) \tag{5a}$$

and

$$D^{-1}(\vec{q}, i\nu_n) = D_0^{-1}(\vec{q}, i\nu_n) - \Pi(\vec{q}, i\nu_n) \tag{5b}$$

$\Sigma(\vec{k}, i\omega_m)$ and $\Pi(\vec{q}, i\nu_n)$ are the electron and phonon self-energies, respectively, which, through eq. (5), give the exact electron and phonon propagators. The theory is perturbative because we use approximations for Σ and Π which involve expansions in the electron-phonon coupling constant. In order to understand superconductivity, we need two added ingredients: *(1)* anomalous Green functions,

$$F(\vec{k}, \tau - \tau') = \begin{cases} - < c_{k\uparrow}(\tau) c_{-k\downarrow}(\tau') >, & \tau > \tau' \\ + < c_{-k\downarrow}(\tau') c_{k\uparrow}(\tau >, & \tau' > \tau \end{cases} \tag{6}$$

and *(2)* infinite order perturbation theory for a select set of processes. The expectation values in eq. (6) are non-zero only in the superconducting state.

Omitting all details, we write down the equations for the superconducting order parameter, $\Delta(i\omega_m)$ (which is related to the electron self-energy):

$$Z(i\omega_m)\Delta(i\omega_m) = \pi T \sum_{m'=-\infty}^{\infty} \lambda(i\omega_m - i\omega_{m'}) \frac{\Delta(i\omega_{m'})}{\sqrt{\omega_{m'}^2 + \Delta^2(i\omega_{m'})}} \tag{7a}$$

$$Z(i\omega_m) = 1 + \frac{\pi T}{\omega_m} \sum_{m'=-\infty}^{\infty} \lambda(i\omega_m - i\omega_{m'}) \frac{\omega_{m'}}{\sqrt{\omega_{m'}^2 + \Delta^2(i\omega_{m'})}} \tag{7b}$$

where

$$\lambda(z) \equiv \frac{\lambda \nu_E^2}{\nu_E^2 - z^2}, \tag{8}$$

and ν_E is the phonon frequency and λ is the electron-phonon coupling constant. Several assumptions have gone into eqs. (7), which we will not discuss here.[6] The order parameter function $\Delta(i\omega_m)$ is related to the anomalous amplitude in eq. (6), while the renormalization function $Z(i\omega_m)$ is related to the "normal" electron Green function given in eq. (2). These equations are solved numerically to self-consistency, giving $\Delta(i\omega_m)$ and $Z(i\omega_m)$ for all m, and for various temperatures. The self-consistency requirement is due to the fact that we are doing perturbation theory to infinite order. This information can then be used to calculate various superconducting properties, such as the free energy, the penetration depth, and the critical temperature. In many cases dynamical information ($\Delta(\omega)$ and $Z(\omega)$, where ω is real) is also required. Then, an analytical continuation is required. This can be accomplished either by using Padé approximants,[7] or by solving another set of equations[8] based on the imaginary axis equations. The alternative (used originally) is to self-consistently solve the analogue of eqs. (7) written on the real axis. It turns out that the new procedure is roughly two orders of magnitude faster on a computer. An appreciation of this difference can be gained by considering a simple function, $f(z) \equiv \sec(z)$. $f(z)$ has poles on the real axis, at $z = (2n-1)\frac{\pi}{2}, n = 0 \pm 1, \pm 2, \ldots$, whereas $f(z)$ is very smooth (*sech* function) on the imaginary axis. Hence, if a function with this structure is involved in an iteration, the equation will converge much more rapidly on the imaginary axis.

In summary, I have tried to give a feeling for the kind of mathematics and numerical techniques required for solving many-body problems in condensed matter physics.

References

1. E.M. Lieb and F.Y. Wu, Phys. Rev. Lett. **20** (1976) 1445.
2. H.A. Bethe, Z. Phys. **71** (1931) 205.
3. E. Dagotto *et al., Phys. Rev.* B41, (1990) 9049.
4. D.J. Scalapino, in *High Temperature Superconductivity*, edited by R.S. Bedell, D. Coffey, D.E. Meltzer, D. Pines, and J.R. Schrieffer (Addison-Wesley) 1989.
5. A.A. Abrikosov, L.P. Gorkov, and I.E. Dzyaloshinski, *Methods of Quantum Field Theory in Statistical Physics* (Dover) 1963; G.D. Mahan, *Many-Particle Physics* (Plenum Press) 1981.
6. See, for example, D.J. Scalapino, in *Superconductivity*, edited by R.D. Parks (Marcel Dekker) 1969, Vol. 1, p.449, or P.B. Allen and B. Mitrovic, Solid State Physics **37** (1982) 1.
7. H.J. Vidberg and J.W. Serene, *J. Low Temp. Phys.* **29** (1977) 179.
8. F. Marsiglio, M. Schossmann, and J.P. Carbotte, *Phys. Rev.* **B37** (1988) 4965.

Iteration of Aitken's Δ^2 Process as an Alternative to Padé Approximants and the Problem of Using Rational Fractions to Parameterize Experimental Data

Glenn A. McRae
Physical Chemistry Branch

Abstract

It is shown that iterating Aitken's Δ^2 process, or equivalently, Shanks' ϵ algorithm, on the partial sums of a Taylor series can lead to a dramatic convergence of the series. This method is compared to the standard technique of accelerating the convergence of series by constructing Padé Approximants. Also, the problem of determining Taylor expansion coefficients from experimental data fitted to Padé Approximants is reviewed, and it is suggested that a method based on this iteration scheme may be better.

Introduction:

In numerical analysis, methods that are useful in accelerating the convergence of a slowly converging procedure are important; this is especially true in high speed computing, where time is money. In this paper we shall consider ways to accelerate the convergence of Taylor series. Generally, an attempt to a better approximation of the function is constructed, from the known Taylor series coefficients, using Padé Approximants (PAs). This technique derives its name from Henri Padé who, in 1892, published an article on the approximate representation of e^x by rational fractions [1]. Much later, Shanks showed many advantages of Padé's method [2]. Since then, there has been a growing interest in PAs as an alternative to the standard representation of functions by power series, and the method is now well established in such fields as scattering theory, field theory, computer science and critical phenomena [3-6].

Another application of PAs is in the parameterizing of experimental data. For many situations where physical observables are measured experimentally as functions of some variable, the functional form is not known. In this instance, it is often opportune to expand the function as a Taylor, or power, series. A useful expansion is one that converges, to the level of the noise in the measurements, sufficiently rapidly. This is the inverse of the standard problem outlined above; now the Taylor expansion coefficients are not known and are to be determined from the experimental observations.

Ultimately, to make such a determination, the power expansion must be truncated. This introduces two problems. First, if the series is slow to converge, then the amount of data required to determine the expansion parameters might be impractically large, or in the extreme, a datum might be required for each successive expansion coefficient. Second, the determined parameters will contain the effects of the higher order parameters that have been constrained to zero by the truncation. PAs are sometimes used in an attempt to alleviate these problems.

In this paper a practical scheme is introduced to accelerate the convergence of power series expansions. This method is compared with PAs.

1. Theory:

For an iterative solution of some general equation, say $g(s) = 0$, it is often convenient to define a generator G such that

$$G(s_i) = s_{i+1} \tag{1}$$

where each application of G gives a better approximation to the real root r. It follows that

$$G(r) = r \tag{2}$$

Expanding this as a Taylor series and truncating after the linear term

$$G(s_i) = G(r) + (s_i - r)G'(r) \tag{3}$$

and rearranging

$$r - s_{i+1} = G'(r)(r - s_i) \tag{4}$$

In the same way

$$r - s_i = G'(r)(r - s_{i-1}) \tag{5}$$

Dividing equation 4 by equation 5 and solving for r yields

$$r = \frac{s_{i+1}s_{i-1} - s_i^2}{s_{i+1} + s_{i-1} - 2s_i} \tag{6}$$

This is the Δ^2 formula of Aitken. Given a series of three successive iterants, equation 6 will produce a better approximation to the true root. Equation 6 is a good approximation for *geometric* series, amongst others [3].

In the present work, the sequence of successive iterants, A_n, is defined by the partial sums of the general Taylor series expansion of some arbitrary function.

$$A_n = \sum_{j=0}^{n} a_j x^j \tag{7}$$

Following equation 6 we write

$$B_i \equiv \frac{A_{i+1}A_{i-1} - A_i^2}{A_{i+1} + A_{i-1} - 2A_i}. \tag{8}$$

Specifically, given the first three partial sums

$$B_1 = \frac{a_0 + [a_1 - a_0a_2/a_1]x}{1 - (a_2/a_1)x}. \tag{9}$$

It is interesting to note that by expanding equation 9

$$B_1 = a_0 + a_1x + a_2x^2 + \frac{a_2^2x^3}{a_1 - a_2x}. \tag{10}$$

The fraction term of equation 10 acts like a correction to the truncated Taylor series.

The B_1 above is also the [1/1] PA. For the function $f(x) = A_\infty$ the PA is defined as

$$[L/M] = \frac{\sum_{\alpha=0}^{L} p_\alpha x^\alpha}{1 + \sum_{\beta=1}^{M} q_\beta x^\beta} \tag{11}$$

where the standard normalization $q_0 = 1$ has been adopted. The coefficients, p_α and q_β, can be calculated from the formal identity

$$f(x) - [L/M] = \mathcal{O}(x^{L+M+1}) \tag{12}$$

The sum of the greatest power of x in the numerator and denominator, $L + M$, is equal to the greatest power of x in the Taylor expansion used to calculate the PA. The most powerful PAs are the diagonal ones where $L = M$.

1.1 The Iteration Algorithm:

The algorithm we wish to consider consists of successive application of the Δ^2 formula. The method was proposed by Shanks and used to accelerate the convergence of geometric series [2]. From one sequence of numbers, a second sequence is formed by taking in turn each successive 3-tuple and calculating the appropriate B_i. This second sequence, of B_i's, is then taken three at a time, in the same way, to produce a third sequence, C_j, and so on. This process produces series, each of which is two shorter than the previous one, until the final series, which has only one or two members. In this paper we consider the advantages of this iterative method when the initial sequence is given by the partial sums of a general power series expansion.

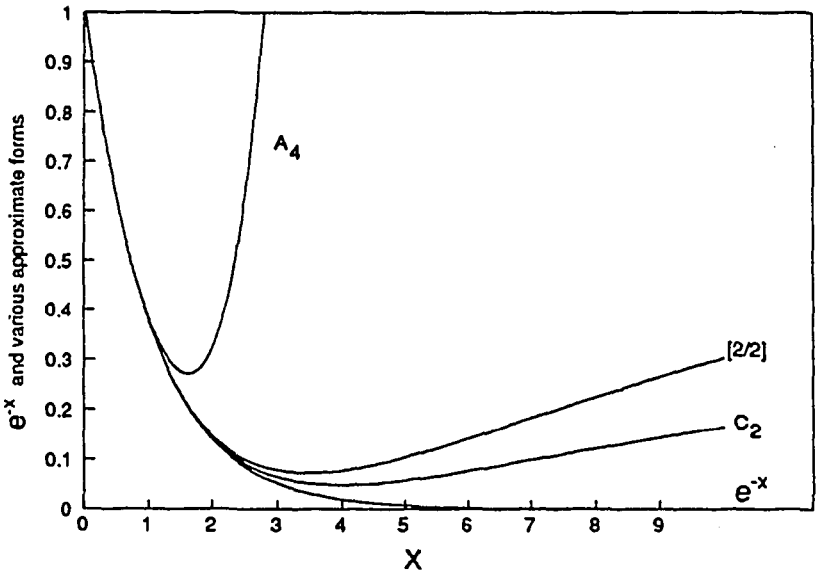

Figure 1: Approximating e^{-x} with A_4, [2/2] and C_2. Clearly, the iteration algorithm deviates the least from the true value.

2. An Example: Calculating the Approximate Value of e^{-x}

As an example we shall reconsider the problem posed by Padé: to find a better method than the standard Taylor expansion to calculate the function e^{-x}. The series expansion is well known

$$e^{-x} = 1 - x + \frac{1}{2!}x^2 - \frac{1}{3!}x^3 + \frac{1}{4!}x^4 + \ldots \tag{13}$$

The best PA, given the expansion coefficients up to fourth order in x, is

$$[2/2] = \frac{x^2 - 6x + 12}{x^2 + 6x + 12} \tag{14}$$

The expansion of this in powers of x agrees up to fourth order with equation 13. Also, the greatest powers of x in the numerator and denominator sum to four, which is the greatest power in the Taylor expansion from whence came the PA (see equation 12).

Using the same five coefficients, the iterated Δ^2 algorithm gives

$$C_2 = \frac{x^3 - 2x^2 - 18x + 72}{2(x^3 + 8x^2 + 27x + 36)} \tag{15}$$

Like the PA, expanding this in powers of x produces a series that agrees with the Taylor series up to fourth order. However, unlike the PA, the sum of the greatest powers of x is greater than the order of the Taylor expansion.

In Figure 1 is plotted e^{-x} and the approximate forms: A_4, [2/2] and C_2. It is important to remember that all three approximants were derived from the same five Taylor coefficients. Clearly, the iteration method produces a more precise approximation to the function than either the trucated Taylor series or the Padé Approximant.

Similar observations are made for higher order series. From the coefficients in the Taylor expansion, up to powers of six in x, we can construct the [3/3] PA and the D_3 iterated Δ^2 approximant. Given terms up to eighth order we can calculate [4/4] and E_4. From these functions, plots like Figure 1 can be produced that show similar trends; again, the algorithm presented in this work clearly gives the better estimate. Furthermore, the iterated algorithm is progressively better than the PA as the order of the expansion increases. For example, at $x = 1$ the C_2, D_3 and E_4 approximants are, respectively, 3, 15 and 100 times better at aproximating e^{-x} than the corresponding PA.

3. Determining Taylor Expansion Coefficients from Experimental Data

The introduction outlined the inverse problem of empirically determining the power series expansion terms given the value of the function, in this instance measured experimentally. In an attempt to avoid contamination of lower order coefficients with higher order effects and to accelerate the convergence of the power series expansion, experimental results are often fitted, for instance, in some least squares sense, to rational fractions.

The problem is that there is a possible ambiguity in how to solve for the Taylor series coefficients. It is important to obtain these coefficients since they are the derivatives of the function we are investigating.

As an example, consider some dependent variable fitted to a rational fraction of order three in both the numerator and denominator. If this is a [3/3] PA, then the rational fraction parameters should be linear combinations of the first seven Taylor expansion parameters. On the other hand, this rational fraction could instead represent the C_2 approximant. In this instance, the rational fraction parameters will be linear combinations of only the first five Taylor coefficients. In light of the economy of determinable parameters, and the relative efficiency of the method demonstrated in the preceeding section, it is proposed that the iterated Δ^2 algorithm could replace the Padé Approximant for experimental data analysis.

Concluding Remarks:

PA's are a generalization of B_1, defined in equation 9. Recall that the sum of the highest powers of x in the numerator, L, and denominator, M, equals the highest power of x in the appropriate Taylor series. The generalization to PAs, equations 11 and 12, is to allow more terms in powers of x in both the numerator and denominator while still maintaining the above constraint on the sum $L+M$. Given the example of approximating e^{-x}, it is clear that this generalization is not necessarily optimum.

In contrast, the iteration method described in this work relies upon no such generalization; it only requires that equation 8 be valid.

Finally, when experimental observables are parameterized by power series, it is suggested that the iterated Δ^2 algorithm may work better than the Padé Approximant for empirical determinations of Taylor expansion coefficients. However, there is still cause for concern over the proposed iteration algorithm as a solution to the inverse problem, since even higher order rational fractions might be constructed whose coefficients are linear combinations of even fewer Taylor expansion parameters. Until an optimum algorithm can be found, the fitting of experimental data to rational fractions should prove difficult.

In the end, the data will determine which approximate gives the best correction of the truncation error. If using a rational fraction results in a better fit, then something new has been learned about the convergence properties of the Taylor expansion. The PA may be the most popular rational fraction formulation, but the iteration scheme presented here may do a better job, and with fewer parameters.

References

[1] H. Padé, *Scientific Tranactions of the Ecole Normale Superieure in Paris*, (1892).

[2] D. Shanks, *J. Math. and Phys.*, 34, 1, (1955).

[3] G.A. Baker and J.L. Gammel eds., "The Padé Approximant in Theoretical Physics", Academic Press, (1970).

[4] P.R. Graves-Morris ed., "Padé Approximants and their Applications", Academic Press, (1975).

[5] G.A. Baker, "Essentials of Padé Approximants", Academic Press, (1975).

[6] E.B. Saff and R.S. Varga eds., "Padé and Rational Fraction Approximation", Academic Press, (1977).

CLASSICAL AND NOTSOCLASSICAL ANALYSIS

M. Milgram
Reactor Physics Branch
Chalk River Laboratories

1. Content

The applications of classical analysis are manifold and ubiquitous, yet there exists a large gap in people's familiarity with some of the great unifying concepts in this field. In particular I refer to the Mellin-Barnes formulation of functions as contour integrals, a formulation that contains most of the results of classical analysis as special cases, and permits otherwise difficult results to be obtained with surprising ease. The special application to which I refer here is the Meijer G-function, whose properties and relationships are well set out in ref. 1.

Consider the following form that arises anywhere a geometric field quantity or probability needs to be evaluated

$$I = \iiint_V e^{-\sigma R}\, \hat{\Omega}\cdot\hat{n}\; ds\; dr\; dR$$

where the integration is over a volume V. This integral describes the attenuated effect at a point, of an interaction at some distance R in some specified direction $\hat{\Omega}$ from that point. For example, in neutron transport problems integrals of the form

$$I = \int_0^1 dt\; t^{\xi+\eta}(1-\kappa^2 t^2)^{(\epsilon-1)/2}(1-t^2)^{\delta/2} R_{\pm}^{\mu+n}$$

often appear, where $R_{\pm} \equiv (1-\kappa^2 t^2)^{1/2} \pm \kappa(1-t^2)^{1/2}$ is the third side of the interaction triangle defined by $t = \cos\theta$, and $\epsilon = (0,1)$. The "n" index arises from expansion of the attenuation factor $\exp(-\sigma R_{\pm})$ as a convergent power series. Such integrals can be identified as Meijer G-functions[2] and hence simplified; manipulated or evaluated in a large variety of ways, sometimes with recourse to computer algebra for particularly tedious simplifications – surely a non-classical tool.

An instance that is particularly enlightening arises in the theory of neutron transport, where it is known[3] that the flux behaves as $x^n \log^j x$ at a distance x from the boundary. The integrals resulting from the analysis can be written[4]

$$E_n^j(z) = \int_1^\infty t^{-n} e^{-zt} (log\ t)^j dt$$

and are natural generalizations of the exponential integral. For a simple, yet elegant analysis, consider the usual exponential integral generalized to $n = s$, a continuous variable

$$E_s(z) \equiv \int_1^\infty t^{-s}\, e^{-zt}\, dt = G_{1,2}^{2,0}\left(z\Big|_{0,s-1;}^{;s}\right) = \frac{1}{2\pi i}\int_L \frac{\Gamma(-t) z^t\, dt}{s-1-t}$$

where the contour L encloses the non-negative integers and the pole at $s-1$. It is only the identification as a G-function that makes the computation tractable when $s \neq n$ an integer. With this result, we have

$$E_n^j(z) = \frac{(-)^j}{j!}\lim_{s\to n}\frac{\partial^j}{\partial s^j} E_s(z) = \frac{1}{2\pi i}\int_L \frac{\Gamma(-t) z^t\, dt}{(s-1-t)^{j+1}}$$

which is expressible as a sum of residues by elementary or notsoelementary (*i.e.* computer algebraic) techniques.

2. Summary

The principles discussed here are applicable to a wide variety of problems in a large number of fields, and should be better known to all.

References

1. Y. Luke, *The Special Functions and their Approximations*, Vol. 1, Academic Press (1969).
2. M.S. Milgram, J. Math. Phys. **18**, 2456 (1977).
3. K. Case and P. Zweifel, Linear Transport Theory, Addison-Wesley (1967).
4. M.S. Milgram, Math. & Comp. **44**, 443 (1985).

Theory and Applications of Differential Algebra

Gordon D. Pusch

TASCC Accelerators & Development Branch
Chalk River Laboratories

ABSTRACT

Differential algebra (DA) is a new method of automatic differentiation. DA can rapidly and efficiently calculate the values of derivatives of arbitrarily complicated functions, in arbitrarily many variables, to arbitrary order, via its definition of multiplication. I provide a brief introduction to DA, and enumerate some of its recent applications.

1. What is DA ?

Differential Algebra[1,2] is a method of automatic differentiation[a] capable of calculating the *values* of derivatives for arbitrarily complicated functions, with arbitrarily many variables, to arbitrarily high order, and machine precision. Differential Algebra is *not* finite differencing, nor is it symbolic manipulation. The immense power of DA is that it reduces *differentiation* to *multiplication*; its algebraic operations — $+$, $\cdot$, and $\circ$ — faithfully represent the *sum*, *product*, and *chain* rules of differential calculus.

Differential algebras in their most abstract form were first introduced by J. F. Ritt[4] in his study of the properties of partial differential equations, and foreshadowed the theory of *jets*.[5] Since all nontrivial representations of Ritt's DAs are infinite-dimensional, there is a practical barrier to implementing them on a computer. M. Berz's[1,2] *quotient* DAs overcame this barrier in 1986. Berz's DAs may be viewed as sub-rings of the "hyperreal numbers" of nonstandard analysis, consisting of the reals, and infinitesimals through some finite order. In Berz's notation, ${}_nD_v$ denotes a differential algebra of order n in v variables. Since I can only give a glimpse of the power of DA in this paper, I will only discuss quotient DAs in *one* variable: ${}_nD_1$; however, the extension to ${}_nD_v$ is straightforward.

2. DA and the Generalized Leibnitz (Product) Rule

The simplest way to understand how DA works is to consider the generalized *Leibnitz*, or *"product"* rule:

$$\begin{aligned}
(FG)' &= F'G + FG' \\
(FG)'' &= F''G + 2F'G' + FG'' \\
(FG)''' &= F'''G + 3F''G' + 3F'G'' + FG''' \\
&\vdots \\
(FG)^{(n)} &= \sum_{j=0}^{n} \frac{n!}{(n-j)!\,j!} F^{(n-j)} G^{(j)}.
\end{aligned} \tag{1}$$

The generalized Leibnitz rule shows that, in a sense, differentiating a product is a purely "algebraic" operation, in that the n^{th} derivative of (FG) is an algebraic combination of the first n derivatives of F and G.

If one defines "normalized derivatives" by $F_{(k)} := F^{(k)}/k!$, then the generalized Leibnitz rule simplifies to a *convolution*, $(FG)_{(k)} = \sum_{j=0}^{k} F_{(k-j)}\, G_{(j)}$, $0 \le k \le n$. Convolution is a commutative, associative *product operation* between two $(n+1)$-tuples, $(f_0, \ldots, f_n)$ and $(g_0, \ldots, g_n)$. The "convolution product," plus scalar multiplication and componentwise addition, together define an *algebra* on $(n+1)$-tuples, whose addition and multiplication are equivalent to the generalized "sum" and "product" rules; this algebra is in fact a faithful representation of ${}_nD_1$.

[a]Ref. (3) contains an alternative development of DA, along with references to other methods of automatic differentiation.

I use Df to denote a general DA-valued quantity,[b] $Df = (f_0, f_1, f_2, \ldots, f_n)$, and f and df to denote the "real" and "differential" parts of Df, *viz* $f = f_0 := \mathcal{R}\{Df\}$ and $df = (0, f_1, f_2, \ldots, f_n) := \mathcal{D}\{Df\}$. The "real + differential split" will be of considerable importance in what follows.

The *multiplicative unit element* of ${}_nD_1$ is $e := (1, 0, 0, 0, \ldots, 0)$; one can easily show the algebra of real-scalar multiples of e to be isomorphic to the real numbers. However, the most important element of ${}_nD_1$ is the *unit first-order differential:*[c] $dx := (0, 1, 0, 0, \ldots, 0)$. The powers of dx generate a basis for ${}_nD_1$:

$$\begin{aligned} dx^0 &:= (1,0,0,0,\ldots,0), \qquad dx^n = (0,0,0,0,\ldots,1), \quad n \equiv \textit{the "order"} \\ dx^1 &= (0,1,0,0,\ldots,0), \qquad dx^m = (0,0,0,0,\ldots,0) \quad \forall\, m > n. \\ dx^2 &= (0,0,1,0,\ldots,0), \\ &\vdots \end{aligned} \tag{2}$$

Note that the unit differential is *nilpotent*: all powers of dx (or any other differential) higher than n vanish identically.

If one considers instead the powers of $(x + dx)$, one sees that:

$$\begin{aligned} (x+dx)^2 &= x^2 + 2x\,dx + dx = \left(x^2, 2x, 1, 0, 0, \ldots, 0\right) \\ (x+dx)^3 &= x^3 + 3x^2\,dx + 3x\,dx^2 + dx^3 = \left(x^3, 3x^2, 3x, 1, 0, \ldots, 0\right) \\ &\vdots \\ (x+dx)^k &= x^k + kx^{k-1}dx + \tfrac{k(k-1)}{2!}x^{k-2}dx^2 + \tfrac{k(k-1)(k-2)}{3!}x^{k-3}dx^3 + \cdots \\ &= \left(x^k, kx^{k-1}, \tfrac{k(k-1)}{2!}x^{k-2}, \tfrac{k(k-1)(k-2)}{3!}x^{k-3}, \ldots\right). \end{aligned} \tag{3}$$

From the above, one sees that the j^{th} *component* of $(x + dx)^k$ equals the j^{th} *normalized derivative* of x^k.

3. Analytic Functions of DA-valued Quantities

To motivate Berz's definition of analytic functions of DA-valued quantities, let $F : I \to R$ be a real-analytic function[d] over some open interval $I \subseteq R$. If $x_0 \in I$, then $F(x) = \sum_{j=0}^{\infty} F_{(j)}\big|_{x_0} (x - x_0)^j$. Replace x by $Dw = w + dw \in {}_nD_v$, with $w \in I$. After some work, one obtains:

$$F(Dw) = \sum_{j=0}^{n} \left\{ \sum_{k=0}^{\infty} F_{(j+k)}\Big|_{x_0} (w - x_0)^k \right\} dw^j. \tag{4}$$

Now, the coefficient of dw^j in (4) is just the Taylor expansion of $F_{(j)}$ about x_0; therefore as w approaches x_0, the expansion converges uniformly to $F_{(j)}(x_0)$, since by hypothesis F is analytic within I. The preceding should motivate:

Definition 1 (The Fundamental Theorem of DA)

For any $F : I \to R$, and for any $Dw \in {}_nD_v$ such that $w = \mathcal{R}\{Dw\} \in I$, if F is at least n-times differentiable at w, then the DA-extension of the function $F : {}_nD_v \to {}_nD_v$ is defined by:

$$F(Dw) := \sum_{j=0}^{n} \frac{1}{j!} \frac{d^j F}{dx^j}\bigg|_w dw^j. \tag{5}$$

---

[b] Berz writes $[f]_n$ instead of my Df, because it describes an *equivalence class*. I choose to use "Df" and "df" instead, because Df also extends the concept of "derivative as tangent-map" to higher-order tangency, while df has the formal properties of an *infinitesimal*. The DA-vector Df is also closely related to $j_x^n F$, the *n-jet prolongation* of the function $F(x)$; Omohundro[6] has shown that a jet-space is the natural geometric arena of perturbation theory.

[c] In ${}_nD_v$, one has v commuting first-order unit differentials, $dx_1, dx_2, \ldots, dx_v$. A basis is generated by taking all possible products of the dx_i of order less than or equal to n.

[d] To help distinguish functions from their values, I will use uppercase letters for functions, and lowercase letters for values.

DA function evaluation automatically incorporates the n^{th}-order generalized "chain" rule for composite functions (Faà di Bruno's formula). For example, the DA extension of a Gaussian is:

$$\begin{aligned}\exp\left[-a(x+dx)^2\right] &= \exp\left[-ax^2 - 2ax\,dx - a\,dx^2\right] = \exp(-ax^2)\exp(-a(2x+dx)dx) \\ &= e^{-ax^2}\left[1 - a(2x+dx)dx + \tfrac{1}{2!}a^2(2x+dx)^2dx^2 - \ldots\right] \\ &= e^{-ax^2}\left[1 - 2ax\,dx + a(2ax^2-1)dx^2 - \ldots\right] \\ &= \left(e^{-ax^2}, -2axe^{-ax^2}, a(2ax^2-1)e^{-ax^2}, \ldots\right) \end{aligned} \tag{6}$$

— which is exactly what one would get by applying the generalized "chain" rule.

4. Differentiation as Algebra

While one could in principle use the "fundamental theorem" to reduce the evaluation of complicated functions to DA-products of simpler ones, in practice even this is often unnecessary. For most elementary functions, one can use various "tricks" instead, such as algebraic identities, addition theorems, inverse addition theorems, contractive maps, and recurrence relations. Using such tricks, one can beat the "combinatoric explosions" which often occur during repeated symbolic differentiation. For example, to calculate the multiplicative inverse of Dw, we can use the binomial theorem:

$$\begin{aligned} Dw^{-1} &= [w+dw]^{-1} = \frac{1}{w}\left[1+\frac{dw}{w}\right]^{-1} \\ &= \frac{1}{w}\left[1 - \left(\frac{dw}{w}\right) + \left(\frac{dw}{w}\right)^2 - \cdots + (-1)^n\left(\frac{dw}{w}\right)^n\right]; \end{aligned} \tag{7}$$

it is easy to show that $Dw \cdot Dw^{-1} \equiv 1$. This example illustrates a general approach: split Dw into "real + differential" parts, and manipulate $F(w+dw)$ into a form with a known series expansion; the series will *always* terminate at order n, because of the nilpotence of dw.

Another approach is to use "addition theorems," *i.e.* expressions of the form $F(a+b) = G(a,b)$. If the expansion of $G(a,b)$ about b has a simple form, then the "real + differential split" gives $F(Dw) = F(w+dw) = G(w,dw)$; the expansion will again terminate at order n. For example:

$$\begin{aligned} \cos(Dw) &= \cos(w+dw) = \cos(w)\cos(dw) - \sin(w)\sin(dw) \\ &= \cos(w)\left[1 - \tfrac{1}{2!}dw^2 + \ldots\right] - \sin(w)\left[dw - \tfrac{1}{3!}dw^3 + \ldots\right] \\ &= \left(\cos(w), -\sin(w), -\tfrac{1}{2!}\cos(w), \tfrac{1}{3!}\sin(w), \ldots\right) \end{aligned} \tag{8}$$

Each addition theorem implies an "inverse-function difference theorem," $F^{-1}(a) - F^{-1}(b) = F^{-1}(\,G(\,F^{-1}(a), -F^{-1}(b)\,)\,)$, which may be used if the r.h.s is tractable — *vide*:

$$\begin{aligned} \arctan(Dw) &= \arctan(w) + (\arctan(Dw) - \arctan(w)) \\ &= \arctan(w) + \arctan\left(\frac{dw}{1+wDw}\right). \end{aligned} \tag{9}$$

Another useful approach is that of *contractive maps*. For example, one can apply the implicit function theorem to invert the DA-extension of an equation $u = F(w)$ as follows. By the "fundamental theorem," (5),

$$u + du = F(w) + F_{(1)}(w)\,dw + \sum_{j=2}^{n} F_{(j)}(w)\,dw^j. \tag{10}$$

Assume that one has first solved $u = F(w)$ to sufficient accuracy, either analytically or numerically. One may then solve (10) for the first-order part:

$$dw = \frac{1}{F_{(1)}(w)}\left[du - \sum_{j=2}^{n} F_{(j)}(w)\,dw^j\right] \tag{11}$$

which has the form of a *fixed-point problem* for dw. Now one can show that if $dw \in {}_nD_v$ is a first-order differential accurate through order k, then for $m \geq 2$, dw^m is an m^{th}-order differential accurate through order $k+1$; because $\mathcal{R}\{dw\} \equiv 0$, the unknown $(k+1)^{th}$ order part of dw will make no contribution, so one may obtain an additional derivative, yet no "feed-down" of error will occur. Therefore, the recursion formula:

$$dw_{[k+1]} = \frac{1}{F_{(1)}(w)} \left[du - \sum_{j=2}^{k} F_{(j)}(w)\, dw_{[k]}^{j} \right], \tag{12}$$

with initialization $dw_{[1]} := du/F_{(1)}(w)$, gains *one order of accuracy with each iteration*, and converges after *exactly* n iterations. Since in each iteration of (12), the error in $Du = F(Dw)$ becomes an infinitesimal of one order higher — and therefore "infinitely smaller" — the recursion (12) is a "contractive map" which contracts "infinitely rapidly." If $du = dx$, the resulting dw will be the *reversion* of the Taylor expansion of F. Generalizations of the above method may be used to calculate DA-extensions of implicitly defined functions or maps in arbitrarily many variables, compute Legendre transforms of functions, interchange the roles of any subset of the dependent and independent variables (*e.g.* "partial" inversion of generating-function-based canonical transformations), *etc.*

5. Further Applications and Conclusion:

Given that many numerical methods were developed largely to *avoid* the use of analytic derivatives because they were either unavailable or too hard to compute, DA cannot help but alter the *status quo*. The list of successful applications of DA is already long[c] and continues to grow: derivatives of "hopelessly complicated" functions or maps, new methods of numerical integration, automatic "prolongation" of ODEs (equivalent to the "multiple scales" perturbation method), Lie transforms, normal forms, numerical solution of the Hamilton-Jacobi equation, solution of stochastic differential equations, *etc.*, *etc.* In summary, DA provides us with an ideal vehicle to "seek out new methods — new algorithms ... to boldly compute what no one has calculated before!"

References

1. M. Berz. The method of power series tracking for the mathematical description of beam dynamics. *Nucl. Inst. and Methods*, A258:431–436, 1987. Presented at the 2^{nd} International Conference on Charged Particle Optics.

2. M. Berz. Arbitrary order description of arbitrary particle optical systems. *Nucl. Inst. and Methods*, A298:426–440, 1990.

3. S. R. Douglas. Automatic differentiation of functions. Report AECL-10139, Chalk River Labs, 1990.

4. Joseph Fels Ritt. *Differential Algebra*, volume 33 of *AMS Colloquium Publications*. American Mathematical Society, New York, 1950.

5. Peter J. Olver. *Applications of Lie Groups to Differential Equations*. Springer-Verlag, New York, 1986.

6. Stephen M. Omohundro. *Geometrical Perturbation Theory in Physics*. World Scientific Publishing, Singapore, 1986.

[c] Albeit mostly within particle accelerator theory — one example being the DACYC orbit dynamics program currently being developed by TASCC.

COMPUTER SIMULATION WESTERN

H. Rasmussen
Department of Applied Mathematics
University of Western Ontario
London, Ontario, Canada
(519) 679-2111 Ext 8800, Fax (519) 661-3292

ABSTRACT

Computer Simulation Western is a unit within the Department of Applied Mathematics. The purpose of it is the development of computational and mathematical methods for practical problems in industry and engineering and the application and marketing of such methods. We will describe the unit and our efforts in obtaining research and development grants. Some representative projects will be presented. Finally we will discuss our future plans.

1. Computer Simulation Western

This unit within the Department of Applied Mathematics, University of Western Ontario was formed about four years ago by a group of researchers within the department. Members of other departments, such as engineering and statistics, may participate in particular projects for which their expertise is required. The research experience of the members of the unit is mainly in the modelling of physical phenomena and the analysis of these models using a mixture of analytic and computational methods. The final project is usually some form of a computer simulation package.

The purpose of the unit is to encourage the development of numerical and mathematical methods for practical problems in industry and engineering and the application of such methods. We do this by soliciting projects from industry and government agencies and form teams to carry out the required research and development. Usually this has required the employment of a full time research associate.

There are several reasons why the department is involved in such activities.

a) We feel that it is beneficial that at least some of our graduate students work on thesis topics of a practical orientation.

b) We will obtain contacts in industry and government agencies which can be used in assisting students in finding employment.

c) This is a method for obtaining additional research funds which in the present climate of government constraint can be valuable.

d) This will bring some new and interesting research problems to our attention which will lead interesting publications.

2. Marketing

The process of obtaining contracts has been long and arduous, but has led to some very interesting research projects. However, it should be pointed that in average a large amount of time will be spent in obtaining a contract.

The marketing of the services of Computer Simulation Western consists of two parts.

a) Personal contacts

We have approached all the personal contacts we had in industry and government agencies, such as former colleges, former graduate students, etc and made them aware of the aims of CSW and what we thought we could do for their organizations. This led to several invitations to visit the organizations and describe our expertise in more details.

b) Cold calls

The main part of our marketing was to approach companies in which we had no contacts. This consisted of sending a letter to the relevant director of research or similar position describing CSW and informing the particular person that we would phone him a week later in order to see if it would be mutually advantageous for us to visit the company. If a project of interest to both could be found and the company had the necessary money, a proposal would then be prepared. In general our experience shows that

- One out of ten phone calls results in visit
- One out of 25 visists results in a proposal
- One out of two proposals results in a contract
- Best success with foreign owned companies

3. Examples of contracts

We will describe in more detail some of the research projects that we have completed. I will be happy to supply more details of these projects.

Adsorption simulation software

Canmet at Energy, Mines, and Resources

This program simulated the removal of unwanted nitrogen and sulphur compounds from the feedstock during the early stages of fuel production via an adsortion process using zeolites. Both batch and column models were simulated.The mathematical model consists of a coupled system of nonlinear partial differential equations which was solved using a method of lines. This resulted in a coupled nonlinear system of ordinary equations using the LSODI package. The numerical program was successfully run on a 386 microcomputer.

Production of fibre glass

Fiberglas Canada

Glass fibres for insulation purposes are manufactured by pouring molten glass into rotating drums,called spinners, with perforated cylindrical walls. We modelled the production of a single glass fibre. The glass comes out of a spinner at roughly 1000 degrees and is reduced in thickness by a factor of 1000. The model is a system of ordinary and partial differential equations which must be solved numerically. The main effort in this project was in the development of the mathematical model.

Simulation of an airbag crash sensor

Siemens Automotive Products

The sensor consists of a steel ball bearing in a steel tube. The ball is normally kept in one end by a permanent magnet while in the other end of tube there are two spring contacts. When the car is involved in a crash, the magnet cannot hold the ball in position and it rolls down the tube and closes the contact. This sends an electric signal to the airbag which is then inflated. After a considerable amount of analysis the model is reduced to a system of ordinary differential equations.

4. Present Stategy

We have concluded from our experience over the last four years that we should change our strategy. In the future we plan to develop simulation packages for industrial problems on our own time. We will then sell these packages to organizations who can use them. Quite often these packages will have to be customized for a particular project and this will create additional income for us.

This approach will have two advantages over our present approach

i) We can spread the development cost over several projects, and thus offer a lower price

ii) We think it will be easier to sell an existing product rather than a contract for developing the project with delivery at a later time.

At the moment we are in the process of carrying out the following development projects.

a) Simulation of passive ground water pollution

Since the pollutant is passive, the model effectively consists of the three-dimensional diffusion-convection equation. We have developed a fast and efficient procedure for solving it consisting of a Crank-Nicolson procedure for the time derivatives and a sparse matric techique for the resulting system of linear algebraic equations. The novel part of our work consists of

i) An efficient visualization technique

ii) Use of optimal control to design the placement and strength of pumping.

b) School bus scheduling

We are in the process of completing a software package for the optimal routing of school buses. The optimization is carried out using the method of simulated annealing and we are now testing the program on large realistic problems. The final design of the package will be done in conjunction with one of the local school boards which will supply us with advice and data.

The package can easily be adjusted to treat other forms of transportation problems such as routing of emergency vehicles.

c) Inverse problem of resistivity or induced polarization surveys

We have developed a package for the direct problem where the structure of the ground is known and we calculated the resulting field on the surface. The package uses finite differences and a sparse matrix procedure for solving the resulting large system of linear equations. This program can be run for three dimensional problems on a 386 microcomputer. We plan to do the inverse part, where the surface field is known and we wish to find the corresponding subsurface structure, using the simulated annealing technique matrix procedure. The latter part has been completed and is now being tested. We expect to have a first version of the package ready in April.

We will be pleased to supply additional details of these packages and present a demonstration of them.

ISOTOPE-SELECTIVE LASER IONIZATION OF ATOMS USING INTERMEDIATE STATE ALIGNMENT

J.H. Rowat
CRL, Waste Management Systems
and
L.W. Green and G.A. McRae
CRL, Physical Chemistry

ABSTRACT

Experiments done at CRL and elsewhere have shown that isotopes with a nonzero nuclear spin can be selectively ionized by a sequence of broadband laser pulses. The process depends on hyperfine interactions and the relative polarizations of the laser pulses. A simple mathematical model for the process (and its application to isotope separation) will be outlined.

1. Introduction

The model to be presented here is illustrated by a three-level atomic system:

$$j_0 \xrightarrow{\nu_1} j_1 \xrightarrow{\nu_2} j_2$$

The laser pulses (~ 10 ns), υ_1 and υ_2, are plane-polarized, propagate in the same direction, and are separated by a time delay (~ 30 ns).

The mechanism for isotope-selective ionization is as follows. The population distribution for the j_0 sublevels (the ground state) is assumed to be uniform. An alignment in the intermediate level (j_1) is created by the first pulse, due to the selection rules for electric dipole transitions. During the time interval between pulses, hf coupling redistributes the population among the j_1 sublevels and destroys the alignment—if $I \neq 0$. Atoms that have $I=0$ retain their alignment. The second pulse "sees" either an aligned state, if the atom has $I=0$, or a state with an approximately uniform distribution of sublevel populations, if the atom has $I \neq 0$. This difference is the basis for the isotope selectivity. Decay and T_1-type relaxation of the intermediate sublevels are assumed to be negligible. In practice a third pulse is required to create the ion and unbound electron from the excited atom in the j_2 level. It is assumed that this step is not isotope selective, and that probability of ionization is proportional to the *total* population of the j_2 level. Hence, the total population of the j_2 level will be taken to represent the ionization rate.

2. Basis Sets and Notation

The $|F,m_F\rangle$ representation is the appropriate basis for a free atom with hyperfine (hf) structure

(i.e., an atom having $I \neq 0$), and the $|J,m_J\rangle$ basis is appropriate for atoms without hf structure. For the duration of a laser pulse, the strong atom/light interaction uncouples the weaker hf interaction—hyperfine uncoupling—and the $|J,m_J\rangle|I,m_I\rangle$ basis is appropriate even if the atom has $I \neq 0$. Conditions which ensure hyperfine uncoupling have been given elsewhere[1]. During the pulse the probability of a nuclear spin flip is small, so the basis can be simplified to $|J,m_J\rangle$. Of course, during the interval between pulses the hf interaction recouples J and I.

Two coordinate systems are used: (1) $\{x',y',z'\}$ for v_1, which is z'-polarized and propagates along y', and (2) $\{x,y,z\}$ for v_2, which is z-polarized and propagates along y. The y' and y axes coincide, and β is the angle between z and z'. To differentiate between coordinate systems, uppercase M is used to signify an eigenstate of $J_{z'}$ (e.g., $|J_1,M_1\rangle$); lowercase m signifies an eigenfunction of J_z (e.g., $|J_1,m_1\rangle$).

3. Transition Probabilities

The relative populations of the j_1 sublevels are calculated from Fermi's golden rule, therefore:

$$P(j_1,M_1) \propto \sum_{M_0=-j_0}^{+j_0} \begin{pmatrix} j_0 & 1 & j_1 \\ -M_0 & 0 & M_1 \end{pmatrix}^2 P(j_0,M_0)\ \delta_{M_0M_1} \tag{3.1}$$

where $P(j_1,M_1)$ is the population of $|J_1,M_1\rangle$ and $P(j_0,M_0)$ is the population of $|J_0,M_0\rangle$. Note that the population $P(j_1,M_1)$ could equally well be called a population rate, because the golden rule is a first-order calculation. The (x',y',z') and (x,y,z) frames are related by rotation about the y axis, therefore:

$$|j,m\rangle = \sum_{M=-j}^{+j} d^{(j)}_{M,m}(\beta)\ |j,M\rangle \tag{3.2}$$

where $d^{(J)}_{M,m}(\beta)$ is an element of the reduced rotation matrix. Sums over states can be represented by incoherent superpositions. Therefore, from Eq. (3.1) and Eq. (3.2) it follows that:

$$P(j_1,m_1) = \sum_{M_1=-K}^{+K} |d^{(j_1)}_{M_1,m_1}(\beta)|^2 \begin{pmatrix} j_0 & 1 & j_1 \\ -M_1 & 0 & M_1 \end{pmatrix}^2 P(j_0,M_1)\ ,\quad K=\min(j_0,j_1) \tag{3.3}$$

The expression for the $j_1 \rightarrow j_2$ transition follows from Eq. (3.1)—note the change of basis—and is:

$$P(j_2,m_2) \propto \sum_{m_1=-j_1}^{+j_1} \begin{pmatrix} j_1 & 1 & j_2 \\ -m_1 & 0 & m_2 \end{pmatrix}^2 P(j_1,m_1)\ \delta_{m_1m_2} \tag{3.4}$$

where:

(i) $P(j_1,m_1)$ is calculated from Eq. (3.3) if $I=0$, or

(ii) $P(j_1,m_1) = Avg.\{P(J_1,m_1)\}$, if $I \neq 0$.

Item (ii) is an approximation that accounts for population redistribution (within the intermediate level) that occurs between pulses due to hf coupling. It assumes a complete (i.e., uniform)

redistribution of the intermediate sublevel populations.

4. Results

Figure 1 shows the total population of the j_2 level, $P(j_2)$, as a function of β for a $\{j_0=5, j_1=6, j_2=5\}$ model system. This system has been realized in the lab by a system that is comprised of U-235 ($I=7/2$) and U-238 ($I=0$). The model calculations compare favourably with measurements[2].

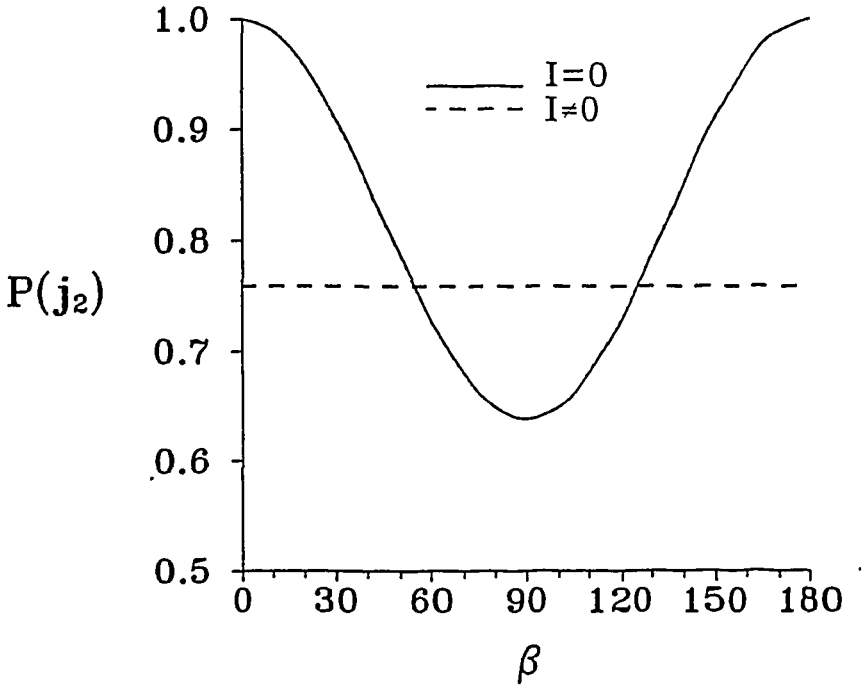

Fig. 1 Total population of the j_2 level as function of β, the angle between the polarization planes of the electric fields of υ_1 and υ_2.

5. References

1. W. Gawlik, "Hyperfine interaction versus strong laser field-optical Back-Goudsmit (Paschen-Back) effect", *Am. J. Phys.* **59** (1991) 706.

2. L.W. Green, M.H.C. Smyth, P.A. Rochefort and G.A. McRae, "Polarization and isotope shift effects in uranium isotope ratio measurements by resonance ionization mass spectrometry", *Inst. Phys. Conf. Ser. No 114, Varese, Italy, 16-21 September 1990*, pp. 243-246. Also published as AECL report: AECL-10274.

MATHEMATICS IN COMPUTED TOMOGRAPHY AND RELATED TECHNIQUES

BARBARA D. SAWICKA
Nondestructive Testing Development Branch
AECL Research, Chalk River Laboratories, Chalk River, Ontario K0J 1J0

Computed Tomography (CT) is a nondestructive imaging technique that produces cross-sectional views of an object. Nondestructive evaluation of an object determines its internal structure or property from measurements made outside of it without damaging or altering it in any way. The imaging technique allows the internal structure or property to be presented in the form of an image or a map that presents object morphology in its correct geometry.

The mathematical basis of tomographic techniques was formulated in 1917 by Radon (1). His theorem states that the 2-D function f(x,y) can be determined at all points from a complete set of its line integrals $m_l = \int f(x,y)dl$. In practical implementation, f(x,y) is a physical property and a line integral is a result of an interaction between radiation used for imaging and the substance of which the object is composed. A set of line integrals measured at one angle is called a projection. Tomography can be practiced using different types of radiation, but X- or γ-ray and NMR tomography are the techniques most used until now. In X- or γ-ray transmission tomography, line integrals of photon attenuation in the object under investigation are measured, and a computed CT image is a map of attenuation coefficients in the measured cross section, which can be transformed to a map of density variations.

The current excitement of tomographic imaging started in the early 1970's (Nobel prize for Hounsfield and Cormack in 1972), when Hounsfield constructed an X-ray scanner and obtained the first useful CT image. The breakthrough was to show that, although projection data do not strictly satisfy theoretical models, and very many measurements with fairly complex mathematical operations are needed to construct a CT image, using the efficiently implemented reconstruction algorithms one can get incredibly accurate images. CT images have been dramatically improved since then owing to developments in reconstruction algorithms, and various versions of scanners have been constructed. This can be considered a second phase of CT development (the first was the formulation of the theorem by Radon).

We are presently in the third phase of CT: CT is a standard diagnostic technique in medicine (most hospitals have CT scanners), the technique is spreading in scientific laboratories and industry, and further developments are being made in experimental techniques, equipment construction and mathematical methods. The experimental techniques progress from, on the one hand, constructing relatively inexpensive scanners for a variety of uses, and on the other, to building sophisticated equipment. The latter includes very high resolution

detectors (for materials analysis), employing synchrotron radiation sources (for 3-D tomography of small objects), very fast scanning (to image dynamical processes), and complex machines that incorporate such extra features as scanning objects under high pressure or radioactive materials. In both cases, high reconstruction accuracy is required and mathematical/computational techniques have to follow. In the first case, there is a switch to the use of personal computers; in the second case, dedicated fast processors are usually employed. CT techniques also progress towards very high resolution coupled with very high accuracy (i.e., high contrast) imaging, 3-D imaging, and tomography with truncated projection data; this requires not only fast computation techniques capable of handling large amounts of data, but also more precision in calculating CT images and new or improved mathematical approaches. CT using diffracting sources (for example for acoustic and electromagnetic refractive index measurements), an alternative to straight-ray (X- or -ray) tomography, is also being developed.

Modern methods of image reconstruction include three approaches (2-4): (i) ART (algebraic reconstruction technique) with modifications SIRT (simultaneous iterative reconstruction technique) and SART (simultaneous algebraic reconstruction technique), (ii) convolution back-projection, and (iii) the Fourier transform method. There is no one best approach. There is always a compromise between how accurate reconstruction can be and how fast it can be done, and how well experimental data can be approximated by mathematical models. Most scanners employ convolution back-projection methods, using various convolution functions (or so-called convolution kernels that filter the projection data before the back-projection process, in order to obtain a true representation).

The image reconstruction algorithm must be formulated in the geometry of the beam/detector configuration, which is defined by scanner geometry. There are four basic types of scanner geometry, which classify the scanners into four generations. First-generation scanners measure projections consisting of sets of parallel, pencil-beam rays. The use of divergent ray-beams speeds up the process of data collection, and this geometry is used in scanners of higher generations. Second- to fourth-generation scanners employ a fan beam geometry, with various modifications in the source-detector movement. Independent of the scanner geometry, 2-D images created from sets of 2-D data measured in parallel planes can be used for a 3-D reconstruction. A novel approach in 3-D imaging has been proposed (5) that uses a cone beam geometry coupled to a 2-D detector and a single-axis rotational stage, and permits a direct 3-D reconstruction from the data collected in this way; this can be considered fifth-generation scanning.

Because the experimental data do not strictly satisfy theoretical models, a number of effects have to be taken into account, which require mathematical solutions and add to the complexity of the problem. In particular, the problems of beam geometry, finite beam dimensions and distribution (causing partial volume effects), beam scattering, and the radiation source spectrum (multienergy sources causing beam hardening effects) have to be addressed. In high-accuracy, high-resolution CT imaging, the problems of data accuracy,

image noise, detectability limits for various types of features, imaging of inhomogeneously distributed multielement materials, etc., also have to be addressed.

Tomography with truncated data is of interest, when it is impossible or undesirable to collect the complete set of data required by the Radon transform of the object. This arises in a variety of cases and forms a field in itself. Mathematical approximations are used to compensate for the unmeasured projection data; otherwise, images are strongly distorted and a clear understanding of the limitations of the reconstructed images is needed. Examples of the use of truncated data tomography are mapping of underground resources via cross-borehole imaging and region-of-interest tomography (i.e., high-resolution imaging of a portion of an object). CT images reconstructed using incomplete data present features in the object with varying degrees of accuracy, depending on which data were missing, and the accuracy of the approximations used to compensate for the unmeasured projection data. To avoid image distortion, when reconstructing CT images from truncated data, one must use some approximations to compensate for the unmeasured projection data. The techniques of incomplete data tomography have recently been applied to calculate laminographic images (6). Laminography provides a tomographic-type image in one plane, using a series of about a dozen radiographic images. Traditionally, the image is measured with film as the imaging medium: the film is exposed to a series of radiographic shots while moving the source and detector in a correlated way, to obtain an image focused in one plane and thus separate overlying features. Computed laminography provides digital laminographic images that are more exact and can be calculated in various planes in the object from one series of digital radiographs.

Finally, because CT data are obtained as numerically measured images, mathematical techniques in image processing and data analysis are extensively used, such as image data filtering, algebraic operations on images, data profiling and statistical calculations.

The CT laboratory at AECL's Chalk River Laboratories practices CT for a variety of nonmedical applications (7, 8, and references therein). The experimental bases are two first-generation and one multidetector (a hybrid of second and third generation) scanners, with Co-60 and Ir-192 used as radiation sources (7, 9). The reconstruction algorithm used for image reconstruction employs a filtered back-projection technique in a pencil-beam geometry. Presently used algorithms have to be adapted to faster computers and a greater amount of data (larger images). Mathematical techniques have been developed to incorporate beam hardening effects for Ir-192 sources (10), and to employ truncated data approximations in cases of high resolution imaging of central parts of objects (region-of-interest tomography, 11). Issues such as detectability limits for detecting small ("point") defects and low-amplitude density gradients, depending on the scan parameters, have been addressed to some extent (12, 13), but these issues require more thorough approaches. Our goal is the construction of a multidetector scanner facility, based on the newest detection technology, with a 2-D imaging detector. Image reconstruction procedures must be developed for the divergent beam and a multienergy spectrum of an X-ray tube. Because we are aiming for CT imaging of high accuracy, such issues of technique limitations as

sensitivity, resolution and defect detectability have to be further addressed, and in general should be considered for particular types of scanner configurations, beam conditions and reconstruction algorithms. Image processing is currently performed for 2-D images, using satisfactory image analysis programs. However, the capability to handle large data matrices will be needed for high-resolution tomography, and 3-D image processing is required.

References

1. J. Radon, "Uber due bestimmung von funktionen durch ihre integralwerte langs gewisser mannigfaltigkeiten" ("On the determination of functions from their integrals along certain manifolds"), Berichte Saechsische Academie der Wissenschaften **69** (1917) 262.
2. A.C. Kak and M. Slaney, *Principles of Computerized Tomographic Imaging*, (IEEE Press, The Institute of Electrical and Electronics Engineers, Inc., New York, 1988).
3. A. Rosenfeld and A.C. Kak, *Digital Picture Processing*, (Academic Press, New York, NY, 1982).
4. G.T. Hermann, *Image Reconstructions from Projections*, (Academic Press, New York, NY, 1980).
5. L.A. Feldkamp, D.J. Kubinski and G. Jesion, "3-D X-ray computed tomography", *Review of Progress in Quantitative NDE*, edited by D.O. Thompson and D.E. Chimenti (Plenum Press, New York, 1986), Vol. 5A, pp. 555-566; L.A. Feldkamp and G. Jesion, "Practical cone-beam algorithm", *J. Opt. Soc. Am.* A/Vol.1, No 6/ June (1984) 612-619.
6. M.D. Barker, "Laminographic reconstruction from real-time radiographic images", *Review of Progress in Quantitative NDE*, edited by D.O. Thompson and D.E. Chimenti (Plenum Press, New York, 1989), Vol. 8A, pp. 457-464. Also, private communication.
7. B.D. Sawicka, R.V. Murphy, G. Tosello. P.W. Reynolds and T. Romaniszyn, "Computed tomography of radioactive objects and materials", *Nuclear Instruments and Methods in Physics Research A* **299** (1990) 468-479.
8. B.D. Sawicka and B.J.F. Palmer, "Application of computed tomography to the development of advanced ceramics", *Journal of Canadian Society for Nondestructive Testing*, Vol. **10**, No.2 (1989) 24-33.
9. T. Taylor and L.R. Lupton, "Resolution, artifacts and the design of computed tomography systems", *Nuclear Instruments and Methods in Physics Research A* **242** (1986) 603-609.
10. P.D. Tonner, G. Tosello, D.S. Hall, L.R. Lupton and B.D. Sawicka, *unpublished report*, (September 1988).
11. P.D. Tonner, B.D. Sawicka, G. Tosello and T. Romaniszyn, "Region-of-interest tomography imaging for product and material characterization", *Industrial Computerized Tomography* (published by the American Society for Nondestructive Testing, Inc., 1989), pp. 160-165. ISBN 0-931403-89-8.
12. B.D. Sawicka and R.L. Tapping, "CAT scanning of hydrogen induced cracks in steel", *Nuclear Instruments and Methods in Physics Research A* **256** (1987) 103-111.
13. B.D. Sawicka and B.J.F. Palmer, "Density gradients in ceramic pellets measured by computed tomography", *Nuclear Instruments and Methods in Physics Research A* **263** (1988) 525-528.

Generalized Pauli Operators

N.C. Schmeing
Theoretical Physics Branch
Chalk River Laboratories

ABSTRACT

A new description of the Lie algebras A_n generalizes the Pauli matrix representation of A_1. Properties analogous to the Lie algebraic and group properties of the Pauli matrices are retained by matrices representing the generators of A_n in the new decomposition. The new decomposition also carries a Hopf algebraic structure and is used to express new solutions to the Yang-Baxter equation.

1. Introduction

Patera and Zassenhaus have proposed[1] a new decomposition of all Lie algebras A_n and formulated their Lie algebraic and group properties in analogy with those of the two-dimensional Pauli matrices:

$$\sigma_0 = N' \begin{pmatrix} 1 & 0 \\ 0 & 1 \end{pmatrix}, \ \sigma_1 = N \begin{pmatrix} 0 & 1 \\ -1 & 0 \end{pmatrix}, \ \sigma_2 = N \begin{pmatrix} 0 & i \\ i & 0 \end{pmatrix}, \ \sigma_3 = N \begin{pmatrix} i & 0 \\ 0 & -i \end{pmatrix}.$$

A generator basis for A_1 is σ_1 to σ_3 with fixed N. The eight matrices given by the above with $\{N, N'\} = \pm 1$ is a group $\mathcal{P}_2$. For the rank 2 algebra, the matrices:

$$A_k = \omega^k \begin{pmatrix} 0 & 1 & 0 \\ 0 & 0 & 1 \\ 1 & 0 & 0 \end{pmatrix}, \ B_k = \omega^k \begin{pmatrix} 0 & \omega & 0 \\ 0 & 0 & \omega^2 \\ 1 & 0 & 0 \end{pmatrix}, \ C_k = \omega^k \begin{pmatrix} 0 & \omega^2 & 0 \\ 0 & 0 & \omega \\ 1 & 0 & 0 \end{pmatrix}, \ D_k = \omega^k \begin{pmatrix} 1 & 0 & 0 \\ 0 & \omega & 0 \\ 0 & 0 & \omega^2 \end{pmatrix},$$

$$A_k^- = \omega^{-k} \begin{pmatrix} 0 & 0 & 1 \\ 1 & 0 & 0 \\ 0 & 1 & 0 \end{pmatrix}, \ B_k^- = \omega^{-k} \begin{pmatrix} 0 & 0 & \omega \\ 1 & 0 & 0 \\ 0 & \omega^2 & 0 \end{pmatrix}, \ C_k^- = \omega^{-k} \begin{pmatrix} 0 & 0 & \omega^2 \\ 1 & 0 & 0 \\ 0 & \omega & 0 \end{pmatrix}, \ D_k^- = \omega^{-k} \begin{pmatrix} 1 & 0 & 0 \\ 0 & \omega^2 & 0 \\ 0 & 0 & \omega \end{pmatrix},$$

with $\omega = \exp(2\pi i/3)$ and k fixed are a basis of generators. To be specific, define $\mathbf{A} = A_0$, *etc.*, above. Then $\mathbf{A}$ to $\mathbf{D}^-$ are the eight generators of A_2, which is $g\ell(3)$. Along with $I_k = \omega^k I$, with $\mathbf{I}$ the identity matrix and k any integer mod 3, the above 3×3 matrices form a group $\mathcal{P}_3$. A Hopf structure inherent in this decomposition for any A_n has been formulated[2] by this author. We will discuss this new basis as an example of the generalized Pauli matrices.

2. Group Properties

The two-dimensional Paul matrices with $\omega = \exp(2\pi i/2) = -1$ are seen to be analogous to the three-dimensional ones in their form. Calling the dimensionality of the matrices d, the following group properties hold for $\mathcal{P}_d$.

The adjoint action is diagonal. If X_k, $Y_{k'}$ are in $\mathcal{P}_d$, $X_k Y_{k'} X_k^{-1} = \omega^j Y_k$, for some j depending on the two matrices. The group $\mathcal{P}_d$ is generated by the matrices which are in the Lie algebra, plus the identity, via the group-operation of matrix multiplication. Its order is $d^3 = 8$ or 27. Except for multiples of unity, which form the center, all elements are in the conjugacy class of lowest order regular elements, of order d^d. Thus there exists an equivalence relation between all operators. The quotient group of $\mathcal{P}_d$ is abelian, so $\mathcal{P}_d$ is a nilpotent subgroup.

3. Lie Algebraic Properties

The Pauli matrices that form the basis of generators for the Lie algebras are quite remarkable in that they provide a finest grading of the algebra, as seen by the commutation relations above. The space of the generators decomposes into a direct sum of one dimensional subspaces labelled by the eigenvalues under

commutation with a fixed set of two generators, *e.g.* **A** and **D**. The algebras also decompose into a direct sum of Cartan subalgebras. They are equivalent to one another and pairwise orthogonal. The r elements in each subalgebra are equivalent to one another. Their fundamental representation is not modular, but cyclic. It may be chosen such that the operator **A** transforms from one state into the "next" on the circle, while **D** changes the state by a phase. Other operators do both. Thus[2] the enveloping algebra is generated by **A** and **D** alone, in contrast to the root space decomposition where in principle all generators are needed.

4. Hopf Algebraic Properties

The Hopf algebra axioms are clearly stated in our paper.[2] For the Patera-Zassenhaus decomposition, the homomorphisms in that definition imply that the Hopf algebra is determined entirely by the properties of **A** and **D**. Best understood in the context of the theory of categories, the three mappings forming Hopf algebra (in addition to the multiplication within the enveloping algebra on which it is based) will be explained briefly and intuitively. The comultiplication Δ maps an operator into an expression which shows how it acts on a system computed of two objects. The familiar cases are that the operator assigns a value to the first object and a value to the second object and adds, or else multiplies, to get the value for the system. The counit ϵ is 0 for operators if additive and 1 if multiplicative. The antipode is an additive or multiplicative inverse in these familiar cases. For the decomposition considered here, the following defines the Hopf structure:

$$\Delta\mathbf{A} = \mathbf{D}\otimes\mathbf{A} + \mathbf{A}\otimes 1; \Delta\mathbf{D} = \mathbf{D}\otimes\mathbf{D}$$

$$\epsilon(\mathbf{T}) = \epsilon(\mathbf{D}) = 1; \epsilon(\mathbf{A}) = 0$$

$$\gamma(\mathbf{D}) = \mathbf{D}^{-1}; \gamma(\mathbf{A}) = -\mathbf{D}^{-1}\mathbf{A}.$$

We refer the interested reader to our paper for several solutions to the Yang-Baxter equation given there for the first time. They are not quasiclassical, and one case is a limit of the non-standard braid group representation given by Couture & Lee.[3]

References

[1] J. Patera and H. Zassenhaus, The Paul matrices in n dimensions and finest gradings of simple Lie algebras of type A_{n-1}, *J. Math. Phys.* **29***(1988)665-73.*

[2] N.C. Schmeing, A Hopf algebra based on the Patera-Zassenhaus grading of A_n, *J. Phys. A: Math. Gen.* **24***(1991)1971-77.*

[3] M. Couture, H.C. Lee and N.C. Schmeing (1990), A new family of N-state representations of the braid group, *Proc. NATO Advanced Study Institute on Physics, Geometry, and Topology* (New York: Plenum).

Performance Assessment Methodology (PAM) For Low Level Radioactive Waste (LLRW) Disposal Facilities

W.N. Selander

Waste Management Systems
Chalk River Laboratories

ABSTRACT

An overview is given for Performance Assessment Methodology (PAM) for Low Level Radioactive Waste (LLRW) disposal technologies, as required for licensing and safety studies. This is a multi-disciplinary activity, emphasizing applied mathematics, mass transfer, geohydrology and radiotoxicity effects on humans.

1. Introduction

Facilities for the permanent disposal of LLRW must be engineered and built to protect the public from radiological exposure for many years. Over time, radionuclides can migrate from the facility and enter the environment by various pathways. The overall performance assessment requires that these rates of migration and their consequences be predicted.

The accepted methodology that has evolved world-wide for such predictions is pathways analysis. Pathways and mechanisms are identified which may expose the waste in the facility to some future individual, called the critical individual, who lives near the facility. The methodology includes a mass transfer model for radionuclide migration along the pathway, and a dose model to predict radiological exposure effects on the critical individual.

The special problems of LLRW, including its treatment and permanent disposal options, are described in other AECL publications. In the remainder of this paper, the analysis of long-term migration of radionuclides from an engineered underground vault to the underlying aquifer, and the resulting impact on humans, will be described.

2. The IRUS Facility

AECL's choice for permanent disposal of LLRW is IRUS (Intrusion Resistant Underground Structure), a concrete vault buried in a sandy site above the local aquifer.[1] For this discussion, it is sufficient to note that the floor of the vault is permeable; it is free-draining to prevent possible flooding. The roof is designed for a service life of 500 years; however, it will eventually fail allowing rainwater to infiltrate the vault. The dominant mass transfer mechanism for a wet vault is convection, a relatively fast process. In the dry vault with the roof intact, the slower process of diffusion is the dominant mechanism. Hence, the time and rate of roof failure will be important features in the mass transfer model. The waste placed in the facility will be conditioned and packaged, and appropriate parameters for these processes are included in the system model.

3. Mass Transfer Equations

The various parts of the system (waste, vault, geosphere) where mass transfer of radionuclides occurs, are porous media. These are unconsolidated particles with pore water acting as the conduit for the migration of atoms. Although it is misleading to consider such a system as constituting a single medium with designated properties, the concept does lead to a practical set of equations. The physical processes governing mass transfer are diffusion in pore water, convection by movement of pore water, adsorption on the solid phase and radioactive decay. An equivalent Fick's law is assumed for the medium, which when combined with the continuity equation and a linear adsorption model, leads to the one-dimensional transfer equation for the pore water concentration $C(x,t)$,

$$R\frac{\partial C}{\partial t} = D'\frac{\partial^2 C}{\partial x^2} - V\frac{\partial C}{\partial x} - R\lambda C \qquad (1)$$

where

R	retardation factor due to adsorption, which may be in the hundreds or thousands,
D'	equivalent diffusivity resulting from the form assumed for Fick's law
V	pore water velocity
λ	radioactive decay constant

The last term may be left out of (1) and applied as a decay factor $\exp(-\lambda t)$ at the end of the mass transfer calculation.

Equation (1) applies to the flux of atoms as well as their concentration. Appropriate initial and boundary conditions complete the problem.

A computer code, COSMOS-3, has been written to generate solutions of (1) for various parts of the system. Some details of this model will be described next.

4. The Vault Model and Source Term

The rate of release of radionuclides from the engineered facility to the geosphere, called the source term, is an important feature of the performance assessment model. To calculate the source term, a mathematical model of the mass transfer process in the vault is constructed. Within the IRUS vault, mass transfer is assumed to occur in two stages. Diffusive radionuclide leaching from the waste to the surrounding backfill represents the first stage. The second stage consists of a mixture of diffusion and convection (depending on vault conditions) from the vault as a whole. The atoms move downward through the permeable bottom of the vault, crossing a buffer layer and an unsaturated layer that retard their migration relative to the water, then enter the aquifer. The first stage acts as a driver for the second stage. The resulting nuclide flux from the second stage is the source term. The vault concentration equation is thus of the form,

$$R\frac{\partial C}{\partial t} = D'\frac{\partial^2 C}{\partial x^2} - V\frac{\partial C}{\partial x} + S(t) \tag{2}$$

where,

$$S(t) = \sigma[exp(\frac{-t}{t_W}) + \alpha exp(\frac{-t}{t'_W})] \tag{3}$$

is the driving term resulting from leaching, which consists of a principal exponential representing long-term behaviour, and a secondary term representing rapid initial transients. The respective time constants are t_W and t'_W, where t_W exceeds t'_W by about an order of magnitude. In the COSMOS-3 code, (2) is solved with appropriate initial and boundary conditions, and the solution is represented by an analytical approximation. Finally, the concentration at the base of the vault is converted into the vault flux or source term, $J_S(t)$.

The COSMOS-3 code assumes the roof of the facility eventually fails, allowing the entry of increasing amounts of rainwater. Therefore, while diffusion in the dry vault is the initial mass transfer process, an increasing area of the vault becomes subject to convection. This transition is handled in the time-step loop of COSMOS-3. The characteristic time scale for vault mass transfer, t_V, will be large for diffusion (D' dominates (2)), and small for convection (V dominates (2)). Since the waste leaching may also be fast or slow, there are four possible situations within the vault:

- fast leaching, dry vault $(t_V > t_W, V = 0)$
- slow leaching, dry vault $(t_V < t_W, V = 0)$
- fast leaching, wet vault $(t_V > t_W, D = 0)$
- slow leaching, wet vault $(t_V < t_W, D = 0)$

The four corresponding solutions, whose details are given in Ref. 2, are combined to construct the source term at each time step.

5. The Geosphere Response

Parabolic transport equations for adjoining regions are theoretically linked in both directions. To allow a sequential solution with undirectional linking only, fictitious boundary conditions are used, in which the response of each section of the geosphere to any radionuclide flux which enters it is the same as if the medium were semi-infinite. The flux at any finite distance L into a section of geosphere is then the convolution,

$$J(L,t) = \int_0^t J_0(t-\tau)\, G(L,\tau)\, d\tau \tag{4}$$

where the Green's function for simple diffusive / convective transport, Eq. (1), is

$$G(x,t) = xR^{1/2}\,(4\pi Dt^3)^{\frac{-1}{2}}\; exp[\frac{-(xR-Vt)^2}{4DRt}] \tag{5}$$

and where $J_0(t)$ is the flux entering at the boundary, $x = 0$. COSMOS-3 uses the analytical source term $J_S(t)$ to start the solution, one region at a time, and each calculated function $J(L,t)$ is used as the driving term in Eq. (4) for the next.

The final step in the mass transfer calculation is to give an expression for the concentration in the aquifer or surface water body. Either of these may be regarded as a source of water for human use, depending on the scenario chosen. In the aquifer, the flux and concentration are related by the equation,

$$J = VC \tag{6}$$

In a lake, a simple mixing model determines the diluted concentration.

6. The Biosphere Response

The impact on human health of radionuclides which migrate from the vault into the biosphere will depend on the human scenario assumed; that is, on the type and extent of groundwater usage by humans. The common "worst case" scenario is the assumption that the critical individual is a subsistence farmer who uses the water for all his needs. These include bathing, drinking, crop irrigation and livestock watering, fishing and recreation. This leads to a complex web of pathways by which the farmer may be exposed to radioactivity, including direct ingestion, inhalation and external exposure. The dose rate incurred via each pathway is typically expressed by multiplying the radionuclide concentration in the water by a transfer factor (PTF), which represents the rate of water utilization in the pathway, and by a dose conversion factor (DCF);

Dose Rate	=	Concentration	*	PTF	*	DCF
(Sv/a)		(Bq/m3)		(m3/a)		(Sv/Bq)

These are summed over all pathways to give either a whole body effective dose or various organ doses. Since concentrations vary with time during the simulation, the dose rate will also vary with time.

Acknowledgements

The author wishes to thank all members of the Waste Management Systems Modelling Group; D.S. Rattan, J.H. Rowat, S.R. Wilkinson, B.L. Briden, F.E. Lane and V.R. Ruddock for their assistance in the work relating to COSMOS-3, and V.R. Ruddock for her assistance in preparing this presentation.

References

1. D.G. Hardy, K.E. Philipose, L.P. Buckley, G.W. Csullog, W.N. Selander, J. Torok and D.M. Wuschke. Preliminary Safety Analysis Report for the Intrusion Resistant Underground Structure (IRUS). AECL Unpublished Report AECL-MISC-295 Rev.1. 1990 August; available from Scientific Document Distribution Office, Chalk River Laboratories, Chalk River, Ontario, K0J 1J0.
2. S.R. Wilkinson, W.N. Selander, J.H. Rowat, V. Ruddock, B. Briden, F. Lane. The COSMOS-3 Assessment Code for LLRW Repositories. AECL Report, AECL-10380. 1991 November.

COMPUTER MODELLING OF EDDY CURRENT PROBES

S.P. Sullivan
NDT Development Branch
Chalk River Laboratories
Chalk River, Ontario K0J 1J0

ABSTRACT

Computer programs have been developed for modelling impedance and transmit-receive eddy current probes in two-dimensional axis-symmetric configurations. These programs, which are based on analytic equations, simulate bobbin probes in infinitely long tubes and surface probes on plates. They calculate probe signals due to uniform variations in conductor thickness, resistivity and permeability. These signals depend on probe design and frequency.

A finite element numerical program has been procured to calculate magnetic permeability in non-linear ferromagnetic materials. Permeability values from these calculations can be incorporated into the above analytic programs to predict signals from eddy current probes with permanent magnets in ferromagnetic tubes.

These programs were used to test various probe designs for new testing applications. Measurements of magnetic permeability in magnetically biased ferromagnetic materials have been performed by superimposing experimental signals, from special laboratory ET probes, on impedance plane diagrams calculated using these programs.

1. Introduction

Eddy current testing (ET) probes are composed of coils of wire as depicted in Figure 1. Time harmonic magnetic fields are generated by AC excitation current driven through a transmit coil. The time harmonic fields interact with metallic conductors by generating electrical eddy currents in the conductors in accordance with Faraday's law of electromagnetic induction. Variations in the magnetic field pattern that may be caused by changes in the conductor geometry, permeability, or conductivity are detected by detector coils, shown in Figure 1. An eddy current impedance probe uses one coil as both transmitter and detector. In this case, the conductor may be characterized by examining the coil's impedance. Transmit-receive probes use separate transmit and detector coils.

Eddy current probe signals are typically presented on a 2-dimensional display, which plots the quadrature component of the detector coil voltage (component which is 90° out of phase with the transmitter coil current) as a function of the in-phase component. Theoretically, these components are treated with complex mathematics, where the in-phase component corresponds to a "real" value and the quadrature component corresponds to an "imaginary" value.

2. Analytic Modelling

Computer programs based on equations developed by Dodd and Deeds[1] are used to simulate impedance and transmit-receive ET probes. These equations are closed form analytic solutions to geometries such as bobbin coils with infinitely long coaxial tubes, shown in Figure 1(a), and surface coils with plates, shown in Figure 1(b). These programs also predict how coil geometry affects probe signals. These programs cannot simulate probe signals from real three-dimensional (3-D) defects. They only model probe response due to uniform wall loss.

An example of the output produced by these programs is shown in Figure 2, which is a plot of the in-phase and quadrature components of an eddy current probe signal. Signals are plotted which correspond to changes in tube wall thickness and magnetic permeability.

Programs based on analytic equations by Burrows[3], when combined with the equations of Dodd et al., can

predict eddy current probe response from small spheroidal defects[1,2].

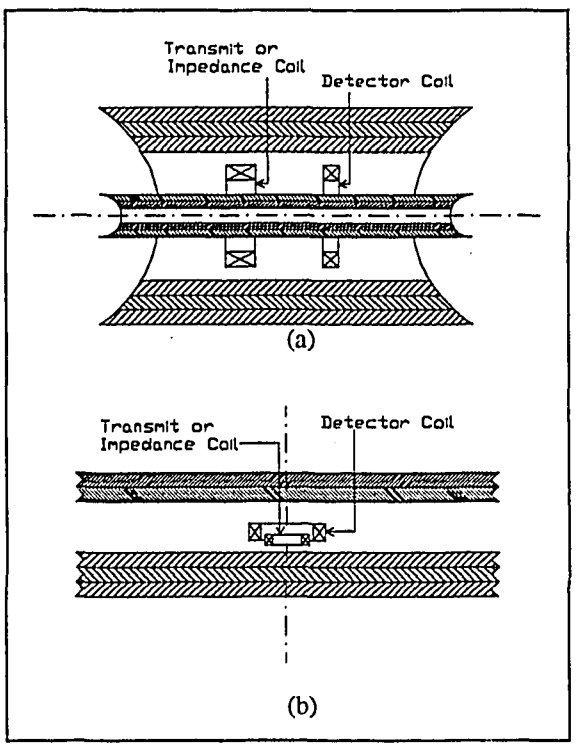

Figure 1: Eddy current probes modelled by analytic equations. (a) Bobbin coils with coaxial tube conductors. (b) Surface coils with plates.

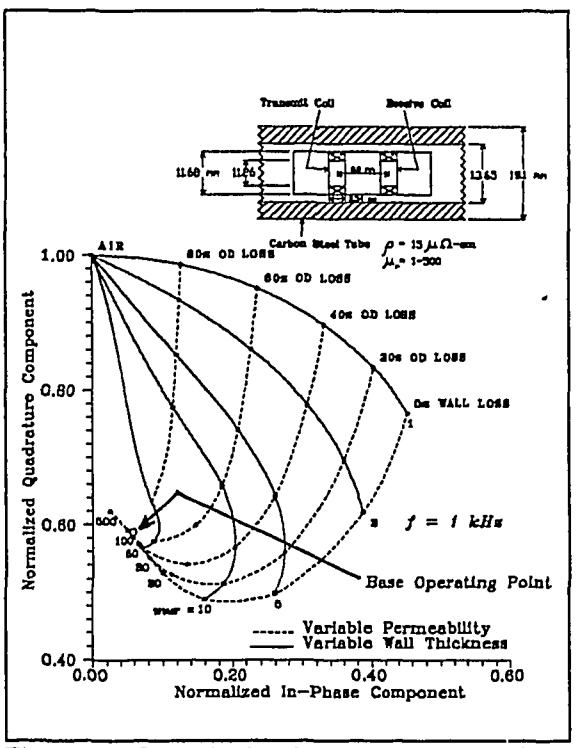

Figure 2: Normalized voltage plane display for a transmit-receive probe in a carbon steel tube with variable permeability and wall thickness.

3. Numerical Finite Element Modelling

A 2-D finite element modelling (FEM) package for IBM PC compatibles was purchased from Infolytica Corp. of Montreal. It has programs for solving nonlinear magnetostatic problems and linear low-frequency time-harmonic electromagnetic problems. So far, these programs have been used for analyzing permanent magnet configurations on magnetic biasing probes used for inspecting ferromagnetic tubes. These probes are composed of eddy current coils and permanent magnets. The field from the permanent magnets alters the permeability of the test material. With a proper permanent magnet configuration, noise from variable permeability in the test material can be significantly reduced and defect signals can be enhanced.

4. References

1. Dodd C.V. and Deeds W.E., "Analytical Solutions to Eddy-Current Probe-Coil Problems", Journal of Applied Physics, Vol.39, No.6, 1968 May, pp. 2829-2838.

2. Dodd C.V., Cheng C.C. and Deeds W.E., "Induction Coils Coaxial with an Arbitrary Number of Cylindrical Conductors", Journal of Applied Physics, Vol.45, No.2, 1974 February, pp. 638-647.

3. Burrows M.L., "A Theory of Eddy Current Flaw Detection", (University Microfilms, Inc., Ann Arbor, Michigan 1964).

COMPUTER SIMULATION OF ULTRASONIC WAVES IN SOLIDS

GORDON A. THIBAULT
Professional Experience Year Student
University of Toronto

and

KEN CHAPLIN
Non-Destructive Testing Development Branch
AECL Research

ABSTRACT

A computer model that simulates the propagation of ultrasonic waves has been developed at AECL Research, Chalk River Laboratories. This program is called EWE, short for Elastic Wave Equations, the mathematics governing the propagation of ultrasonic waves. This report contains: a brief summary of the use of ultrasonic waves in non-destructive testing techniques, a discussion of the EWE simulation code explaining the implementation of the equations and the types of output received from the model, and an example simulation showing the abilities of the model.

1. Use of Ultrasonics in Non-Destructive Testing

Ultrasonic waves are used in the non-destructive testing of materials to discover any defects or discontinuities inside the material. This is achieved by creating a wave using a piezoelectric transducer, which converts an electrical signal to an oscillating pressure with a frequency in the megahertz range. This wave travels through the material, interacting with any defects or discontinuities in its path, and is then received by either the same transducer, or a transducer in a different location. The signal is then converted back to electrical energy, and is displayed as an amplitude or A-scan, which is a graph of the electrical signal as a function of time.

2. EWE (Elastic Wave Equations)

2.1 *Explanation of the Equations and Their Implementation*

The EWE model was designed to perform all the operations of a real ultrasonic test. To explain how this is accomplished, here are the Elastic Wave Equations calculated by the model:

$$\rho \frac{\partial \dot{u}}{\partial t} = \frac{\partial X_x}{\partial x} + \frac{\partial X_y}{\partial y} \tag{2.1}$$

$$\rho \frac{\partial \dot{v}}{\partial t} = \frac{\partial X_y}{\partial x} + \frac{\partial Y_y}{\partial y} \tag{2.2}$$

$$\frac{\partial X_x}{\partial t} = (\lambda+2\mu)\frac{\partial \dot{u}}{\partial x} + \lambda \frac{\partial \dot{v}}{\partial y} \tag{2.3}$$

$$\frac{\partial Y_y}{\partial t} = (\lambda+2\mu)\frac{\partial \dot{v}}{\partial y} + \lambda \frac{\partial \dot{u}}{\partial x} \tag{2.4}$$

$$\frac{\partial X_y}{\partial t} = \mu \frac{\partial \dot{u}}{\partial y} + \mu \frac{\partial \dot{v}}{\partial x} \tag{2.5}$$

where $\dot{u}$ and $\dot{v}$ are velocities, and X_x, X_y, Y_x, and Y_y are stresses. These equations hold true for an isotropic, uniform medium. Note that in (2.1) and (2.2), the derivatives of the velocities $\dot{u}$ and $\dot{v}$ depend on the derivatives of the stresses X_x, X_y, and Y_y, and in (2.3), (2.4) and (2.5), the derivatives of the stresses X_x, X_y, and Y_y depend on the derivatives of the velocities $\dot{u}$ and $\dot{v}$. Using these equations, two grids are established containing velocity and stress data. These grids then interpenetrate in space to form the given region. Velocities are calculated at grid points from stresses on surrounding grid points. Similarly, the stress grid is calculated to find the new velocity grid. This repeats to propagate the wave through the grids. Additional formulas are used to calculate velocity and stress data for cracks, slots, and absorbing or reflecting boundaries. Data is also collected at the surface closest to the transducer, over the time period of the simulation, to allow the calculation of the signal displayed in an A-scan.

2.2 *Output Types From the Model*

These calculations generate considerable amounts of data. A realistic simulation produces files on the order of 250MB, and could take 24 hours of CPU time to execute on the Cyber 990 mainframe. To analyze these results, graphical visualization techniques are implemented. The data files consist of values of $\dot{u}$ and $\dot{v}$ for the region stored at several regular time intervals. The data is then put into a commercially-provided graphics package available on the Cyber, such as CA-DISSPLA or NCAR. These packages create contour plots of the data to show the waves. The output capabilities of the model include:

- Energy Displays; created from the velocity data, displayed in Fig. 1.
- Compression Wave Velocity Displays; created by employing a DIV operator on the wave fields, which attenuates the shear waves.
- Shear Wave Velocity Displays; created by employing a CURL operator on the wave fields, which attenuates the compression waves.
- Vector Displays; created from the velocity data.
- Focal Point Displays; created from the maximum energy at each point over the duration of the simulation.
- A-Scan graphs; similar to experimental data from ultrasonic instruments.

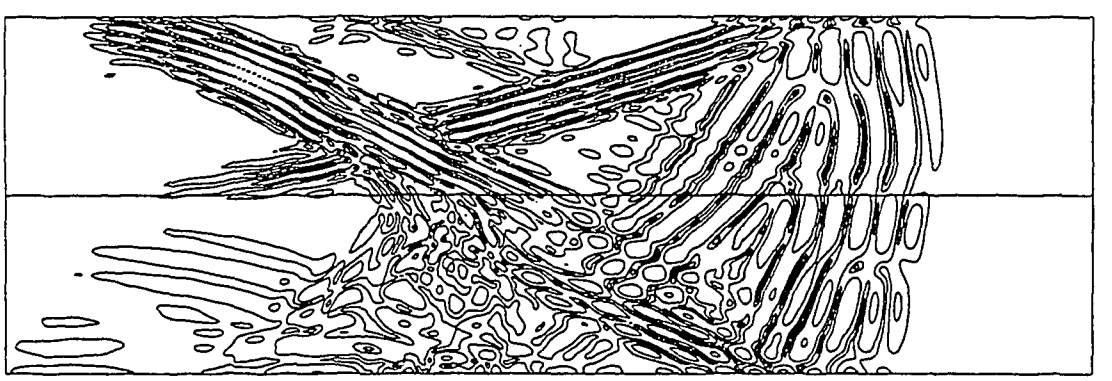

Fig. 1 Energy Display output from the EWE model. The waves with large wavelengths are compression waves, and the small wavelength waves are shear waves.

There are some capabilities to produce colour contour displays, and animated simulation is among our present endeavors. All these tools are useful in analyzing the interaction of ultrasonic waves with defects and discontinuities, and in interpretation of inspection results such as an A-scan.

3. Application Example

Materials have a property known as a critical angle, which represents the angle of total internal reflection. This means that if a wave hits a boundary at an angle below the critical angle, it will split into different types of waves and divide its energy among these new waves. This division process is called mode conversion. If a waves hits a boundary above the critical angle, it will completely reflect from the boundary.

Through a previous simulation, an interesting effect was observed. When a shear wave hit the backwall surface at just below the critical angle of the material, some energy is mode converted into a compression wave travelling parallel to the surface. This compression wave then mode converted back to a shear wave at the backwall surface, and travelled along side the original shear wave, which reflected the rest of the energy.

We decided to see if this phenomena occured in real materials, so we tried this technique using zirconium as the material. In zirconium, the critical angle is 29°, so we chose a smaller angle of 26°, and ran the simulation. It exhibited many of the same effects as the first simulation, except more energy converted to compression wave, therefore there was a significant drop in amplitude of the shear wave upon reflection. Through the study of this case, it was hypothesized that if a layer of material with a critical angle of less than 26° was placed inside the backwall surface of the zirconium, the shear wave would not mode convert to compression wave. It would just reflect off the backwall surface entirely. Such a material did exist in zirconium hydride, a material found in blister defects on pressure tubes. Zirconium hydride has a critical angle of about 20°.

We ran the new simulation with a zirconium hydride layer in place. As predicted, most of the energy did reflect back from the boundary. A comparison between the plain zirconium and the zirconium hydride layer case was performed to see the effect on the amplitude of the reflected shear wave in detail. This was done by moving the receive transducer along the near surface of the region and finding the amplitude of the wave for each position. In a few spots, the shear wave was three times larger in the zirconium hydride than the plain zirconium. Another wave exhibited different effects in the two cases. This wave is caused partially by a compression wave converting to shear wave at the backwall surface, and partially by the initial shear wave converting to a compression wave at the backwall surface. Both these waves meet the near surface of the region at the same time, creating a single wave. Its amplitude decreased slightly in the zirconium hydride case compared to the zirconium case.

Since in the zirconium case, this compression-shear wave was about half the size of the shear wave, simple mathematical manipulation of the signals could be used to give a result that is near zero for the case of pure zirconium, and large for a case with zirconium hydride. By subtracting twice the amplitude of the compression-shear wave from the amplitude of the shear-shear wave, this effect is realized. The zirconium hydride signal is 10 times the size of the zirconium signal using this method, as shown in Fig. 2.

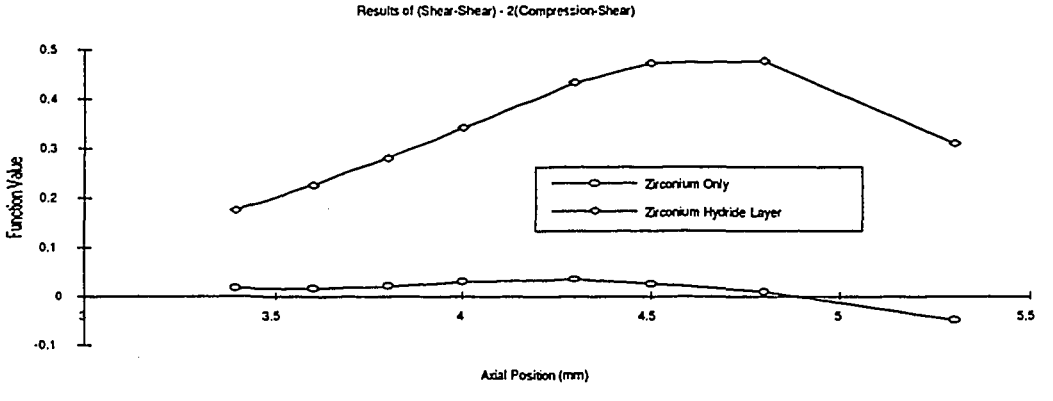

Fig. 2 Graph of possible function to improve detection of zirconium hydride .

All the ideas for this example were triggered and analyzed by simulation with the computer model. In this way, we hope to be able to develop new techniques for inspection, as well as further understanding and explanation of existing inspection results.

Acknowledgements

The support of COG, WP#34, WPIR 6542 for this work is gratefully acknowledged.

Bibliography

1. S.R. Douglas and K.R. Chaplin, *EWE: A Computer Model for Ultrasonic Inspection*, AECL-10507/COG 91-261.
2. K.R. Chaplin, S.R. Douglas, A.W. Leung, and G.A. Thibault, 1992, *unpublished report.*

MATHEMATICAL MODELLING OF HOT FORMING OF METALS

J. J. M. Too
Metals Technology Laboratories, CANMET,
Energy, Mines and Resources Canada
Ottawa, Canada

ABSTRACT

In recent years, mathematical models are gaining significant recognition in the improvement of metal forming processes. Methods for the modelling of the physical phenomena in hot forming are presented; the complexity of the interdependent relations between the macro-behaviour and micro-structural changes is discussed. A modelling approach to account for these interwoven relations is proposed. The need for coupling of macro and micro models is emphasized.

1. INTRODUCTION

The technology of hot rolling of metals has been in existence for decades. Significant progress made over the years on this technology has mainly relied upon the accumulated experience of expensive and time consuming trial-and-error methods. However, the ever increasing competitiveness in the world market, the demands for tighter tolerance on mechanical properties and the call for energy conservation have necessitated the development of methods for improvement. Mathematical modelling has thus gained wide-spread recognition in the metals industry. Progress has been made specifically in the areas of mathematical description of the behaviour of metal deformation, heat transport phenomena, constitutive relations, and to a lesser degree, in the area of microstructural evolution during and after forming processes. Due to the complexity of the processes many difficulties remain to be resolved for achieving further improvements in cost reduction and in the control of mechanical properties of products.

It is well known that the most critical factors in controlling the final properties of metals are the rate of strain, accumulated strain, temperature and the cooling path subsequent to rolling. These factors are by no means homogeneous and time invariant in a deforming metal. The temporal and spatial variation in grain size, crystallography, phase, and solubility of alloy elements are generally dependent upon strain, strain rate and temperature path. Among the wide range of parameters that may affect the rolling process, only the modelling of heat conduction, thermomechanical coupling, visco-plastic flow, and phase transformation will be briefly discussed.

2. MACRO- AND MICRO-SCOPIC MODELLING

The mathematical description of the coupling behaviour of metal flow and heat and mass transport can be deduced from the principles of conservation of momentum, energy and mass which lead to the following differential equations:

(i) for the viscoplastic flow of metal we have

$$L^T\left[D\dot{\tilde{\varepsilon}} + \tilde{\sigma}_m\right] + \tilde{\chi}_0 + \rho\dot{\tilde{u}} = 0$$

or

$$\rho\dot{\tilde{u}} + L^T D L\tilde{u} + L^T M P = \chi_0 \qquad (1)$$

in which the volumetic stress, $\tilde{\sigma}_m$, is expressed in terms of hydrostatic pressure P, whereas ' L ' denotes $(\partial/\partial x, \partial/\partial y)$ in the material coordinates. $\tilde{\chi}_0$ is the externally applied force vector, ρ is the density of the material. The notations ' ~ ' and ' · ' respectively denote a vector quantity and a time derivative. D denotes

the material compliance which can itself be temperature, stress and strain/strain rate dependent. It should be mentioned here that a microstructural based constitutive law is required to model the flow behaviour correctly;

(ii) for the heat transport phenomenon we have

$$\rho c\dot{T} + \rho\dot{H} = \nabla(k\nabla T) + Q \tag{2a}$$

$$k\frac{\partial T}{\partial x_i} = h_f(T - T_e) \tag{2b}$$

where h_f denotes the heat transfer coefficients for the convective, radiative or conductive transfer depending upon the nature of the boundary; c, k and H are respectively the specific heat, the thermal conductivity and the enthalpy related to the phase transformation. The second term on the left hand side of Eq. (2a) represents the heat adsorbed or generated due to a phase transformation, and Q represents the heat generated in a unit time by the plastic energy dissipation per unit volume which is: $Q = f\tilde{\sigma}'\dot{\tilde{\varepsilon}}$. In a multicomponent system H becomes: $H=\sum H_i n_i$, where H_i is the partial molar enthalpy, and n_i is the molar flux of species i;

(iii) for the microstructural evolution (particle or matter transport) it is assumed that microstructural changes during hot rolling are diffusion-like processes driven by the free energy stored in the distorted grains and at the grain boundaries. The migration of dislocations, vacancies and solute particles in a material matrix and at a interface are expressed mathmetically as:

$$\dot{\eta} = \nabla(B\nabla\eta) + \tilde{u}\cdot\nabla\eta \tag{3}$$

where η is a generalized state variable, to which a physical meaning can be assigned, such as the represention of the concentration of migrating solutes, dislocations, etc. B is the diffusion coefficient. It is important to note that the diffusion coefficient is a function of temperature, cooling rate, dislocation density, chemical potential and mean path length of the migrating particles. Also in a deforming metal, dislocation density and free energy are directly related to the local stresses, strains and strain rates. The second term on the right hand side in Eq. (3) accounts for the effect of the rate of deformation on the rate of microstructural changes. It is through these dependencies that the microstructure is coupled with the flow of metal and heat as described by Eq.s (1) and (2). Note that Eq.(3) is a general expression to account for the microstructural evolution. Specifics relating phase transformation is given in the next section.

Eq.s (1-3) together with the contact interface models provide a description of the thermomechanical processes including the microstructural changes during hot forming. These equations can be solved simultaneously by the finite element method.

3. Modelling of Phase Transformation of Metals

Phase transformation in a general sense encompasses nucleation, precipitation, recrystallization, grain growth and other microstructural evolution. Theoretically, they have been all treated as diffusion processes.

In hot forming, phase transformation depends strongly upon the temperature and the rate of temperature change. The resulting phase structure directly affects the strength, hardness, toughness, ductility and other physical properties of the products. This effect on the properties is further complicated because phase transformation is always accompanied by heat production or absorption, which in turn, causes temperature changes. Moreover, since metal surfaces are in contact with cold forming tools and cooling agents, the temperature of the metal surface is likely to be significantly lower than that of its interior. This difference can create large thermal gradients and can cause non-uniform temperature distribution and rate of temperature changes in the metal piece. Thus the resulting transition products may differ from location to location in a hot-formed metal. Phenomenological models for phase transformation without the considerationn of thermal diffusion have been derived analytically by Kirkaldy and others[1-2].

However, Hillert and Agren[3] pointed out that analytical solutions for the diffusion controlled transformations have very limited applicability, and they indicated that the use of numerical methods to solve the basic diffusion equations is a natural alternative.

The fact that phase transformation is a rate process makes the conventional macroscopic, thermodynamic treatment of the phenomenon inappropriate. The modelling of this physical phenomenon requires consideration of the microscopic, atomic or particle interaction and the rate of reaction, and a connection between macro- and microscopic properties.

In phase transformation of metals, there are two types of transport phenomena which occur simultaneously: the transport of substance of various components and the readjustment of lattice sites, and the transport of energy due to the accompanied heat production and to the initial and imposed thermal-boundary conditions. To account for these phenomena let us consider a system in a state of non-equilibrium. This can be described by the phenomenological theory and the principle of microscopic reversibility introduced by Onsager[4]. Experimental evidence has shown that thermal flux J_u can be set up by a local fluctuation of concentration of solutes; and a flow of substance J_i can be set up by the fluctuation of a temperature field or an externally-imposed thermal gradient. These fluxes flow in and out across a phase interface under the action of driving forces X_i and X_u. Such a movement will be accompanied by an entropy production:

$$T\frac{\partial s}{\partial t} = \sum_{i=1}^{n-1} J_i\{X_i - X_n\} + J_u X_u \tag{4}$$

where

$$J_i = \sum_{k=1}^{n-1} L_{ik}\{X_k - X_n\} + L_{iu}X_u \tag{5a}$$

$$J_u = \sum_{k=1}^{n-1} L_{uk}\{X_k - X_n\} + L_{uu}X_u \tag{5b}$$

The cross coefficients L_{ik} and L_{uk} represent the interference of all components.

By choosing J_i and X_i based upon the Gibbs' Equations and by satisfying Onsager's reciprocity relation requirement, we obtain the following equations after some algebraic manipulations:

$$\begin{aligned} J_i &= \sum_{k=1}^{n-1} L_{ik}T\{\nabla g'_k - \nabla g'_n\} + L_{iu}T^{-1}\nabla T \\ J_u &= \sum_{k=1}^{n-1} L_{uk}T\{\nabla g'_k - \nabla g'_n\} + L_{uu}T^{-1}\nabla T \end{aligned} \tag{6}$$

where $g'_k = g_k/T$ and g_k is the Gibbs free energy of substance k. As previously mentioned, phase transformation is a transient, rate process and the model must take into consideration the kinetics of the process. For the flow of substance, this process is described by the reaction rate, which in this case, can be interpreted in two ways. In a microscopic sense, it can be described as frequency of jumps of component i to the nearest neighboring locations in a unit time, and in a macroscopic sense, it can be described as the rate of change in concentration of solutes in a unit volume. For the flow of heat, the process is described by the rate of heat stored in or released from a unit volume. These changes must be equal to the net fluxes of the substance/heat entering the volume, we may therefore write:

$$\dot{\eta}_i = \nabla J_i \tag{7}$$

where η_i represents, in this case, the concentration of component i and the temperature at and near i. Introducing Eq. (6) into Eq.(7) leads to a set of rate equations consisting gradient terms of Gibbs free energy and temperature. While this set of equations represents the statistical micro-changes, it is inconvenient for practical applications. It is more convenient to convert Eq. (7) in terms of concentration and thermal gradients. This is readily obtainable by comparing the rate equation with the Fick's Second law

$$\dot{c}_i = \sum_{j=1}^{n-1} \nabla B_{ij} \nabla c_j + \nabla K_{iu} \nabla T \tag{8a}$$

$$\dot{T} = \sum_{j=1}^{n-1} \nabla B_{uj} \nabla c_j + \nabla K_{uu} \nabla T \tag{8b}$$

with the coefficients given as

$$B_{ij} = \sum_{k=1}^{n-1} L_{ik} T \partial (g'_k - g'_n) / \partial c_j \tag{9a}$$

$$K_{iu} = L_{iu} / T \tag{9b}$$

It is interesting to note that Eq.s (8) and (9) have effectively linked a microscopic description of a phase-transformation problem with macroscopic quantities c_i and T. This is achieved through the definition of B_{ij} and K_{iu} given in Eq. (9). In this equation, the microscopic parts are reflected by the Gibbs free energy g_i which is the cause for atoms to jump to and from locations. The frequency of these jumps directly determines the net flux of a component across a phase interface. Eq. (8) consists of a set of n simultaneous Eq.s with n state variables. It furnishes a description of the coupled thermal and substance transport phenomena in a phase transformation for an n-component system. The solution of this set of equations provides the values of (n-1) state variables along with temperature values at any location at a time point (i.e., $c_i(t)$ and T(t)) which is needed for the prediction of phase transformation processes. The n th component is eliminated from the equation due to its dependence on other variables. The closed solution for these types of Eq.s is not readily available and we must rely upon finite element method solution. Details of finite element formulation is here omitted. In Eq. (9), L_{ij} is the cross coefficient representing the interaction between the components i and j. The coefficient L_{ui} is defined as the heat flux transported across a phase interface due to a unit increase in chemical potential over a unit distance; and coefficient L_{iu} is the flow of atoms of component i due to an unit increase in temperature over a unit distance. Eq. (8) provides a theoretical description of a coupled heat and mass transport phenomena in phase transition. It permits the evaluation of the needed state variables, such as the evolution of concentrations of solutes, temperatures and rate of temperature changes at any location in time, for the determination of fractions transformed at a given state. The entropy production and temperature changes and rate of transition are rigorously accounted for. It should be noted that for austenite/ferrite/pearlite transformation, the transformation mechanism is known to be controlled by carbon diffusion. In this case, the interstitials can be considered as one of the alloy components, and Eq. (8) remains equally applicable. The application of the present formulation requires the knowledge of the cross coefficients, L_{ij} and L_{uj} which may be calculated theoretically for certain cases. However, they are also obtainable experimentally.

4. REFERENCE

(1) Lane, L.E. and Kirkaldy, J.S., Can. J. Phys. 42, 1643, (1964).

(2) Agren, J., Acta Metall., 30, 841-851, 1982.

(3) Hillert, M. Agren, J., Advances in Phase Transformations, ed.by Embury et al Pergamon Press,1988.

(4) Onsager, L. , Phys. Rev., 38, 12, 2265-79 (1931).

TOPICS IN INDUSTRIAL MATHEMATICS

S.R. Vatsya
Thermalhydraulics Branch, Whiteshell Laboratories
Pinawa, Manitoba R0E 1L0

ABSTRACT

Mathematical methods are widely used to solve practical problems arising in modern industry. This article outlines some of the topics relevant to AECL programmes. This covers the applications of Transmission and Neutron Transport Tomography to determine density distributions in rocks and two phase flow situations. Another example covered is the use of variational methods to solve the problems of aerosol migration and control theory.

1. Introduction

Mathematics may have first developed out of our need to solve practical problems, but it has evolved into an independent discipline. While the aim in pure mathematics is to find all possible implications of the underlying assumptions, the relevance and acceptability of the final results impose constraints in applied mathematics. Industrial mathematics is essentially applied mathematics characterized by serving the needs of industry. The field of industrial mathematics is quite wide. A few examples are described below.

2. Nonintrusive Imaging Techniques

For some measurements, probe-based (intrusive) techniques are impractical, leaving nonintrusive ones as the only alternatives. Most nonintrusive techniques are based on the principle of tomography. Transmission tomography has been used to determine the local density of rocks[1], X-ray and γ-ray transmission tomography, to determine the density distribution of fluids[2], industrial products and for medical diagnosis. Neutron transport topographic methods are better suited for some fluid flow situations.[3] Methods developed and in use at Whiteshell are described here.

2.1 Geophysical tomography

Seismic tomography is used to determine density variations in rocks. Measured quantity is the travel time $T_i = T(L_i)$ of sound along each of many paths $L_i, i = 1, 2, \ldots n$, given by

$$T_i = \int \eta(r) d\ell(r) \tag{1}$$

where $\eta(r)$ is the slowness to be computed at point r and $d\ell(r)$ is the infinitesimal-length. All of the transmission tomographic problems reduce to an equivalent problem. Standard methods may be classified as algebraic reconstruction, and the transform methods. A new method, called the areal basis inversion technique (ABIT) reduces (1) to a Fredholm-type integral equation of the first kind and solves it by the L_2-inversion theorem.[1] A comparison of results produced from synthetic data demonstrates that ABIT defines the anomaly more accurately.

2.2 Gamma-ray densitometer

The phase-distribution is needed to understand many physical situations involving two-phase flow. Multibeam gamma densitometers are commonly used for this purpose; they measure, essentially, the chordal void fractions. An algorithm developed recently[2] to extract the phase-distribution is outlined below.

The chordal void fraction $\alpha(\phi)$ along $L(\phi)$ is given by

$$\alpha(\phi) = \frac{1}{d(\phi)} \int_{r_0(\phi)}^{r_1(\phi)} \Gamma(s(\phi), r) dr \tag{2}$$

where $\Gamma(s(\phi), r) = 1$ for r in $s(\phi)$, and zero otherwise, $d(\phi) = (r_1(\phi) - r_0(\phi))$ and $s(\phi)$ is a subset of $[r_0(\phi), r_1(\phi)]$ defined by the phase distribution. The points $r_0(\phi)$ and $r_1(\phi)$ are the intersections of the γ-ray

with the circumference of the pipe. The purpose here is to approximate Γ. The procedure used was based on the series expansion method; *i.e.*, expand Γ as a linear combination of some basis functions β_j. The coefficients are determined by (2). For the three-beam densitometers in use at Whiteshell, the problem was reduced to solving one nonlinear equation: $h(\gamma) = 0$, after some manipulations. The method was verified for several realistic flow patterns and found to be a vast improvement over the existing methods.

2.3 Neutron transport tomography

While the quantities of interest are still the distribution of the phases and the void fraction, the system of interest is the heated section of an experimental test facility. The γ-rays are attenuated almost out of existence by this type of system, rendering the multi-beam gamma densitometers inapplicable. A method based on neutron transport tomography solves the technical problem satisfactorily, but the mathematical problem encountered is quite complex.

In addition to other difficulties in solving the inverse problem of nonlinear tomography, the number of detector locations in a realistic experimental situation is quite small, two or three at the most. As was the case with gamma densitometry, the series expansion method is, therefore, better suited in this kind of situation. This procedure was used to reduce the problem to solving $\phi(\gamma) = 0$. The D vector $\phi(\gamma)$ is defined by $\phi_d(\gamma) = u_d - \mu_0(r_d), d = 1, 2, \ldots, D$, and γ is the D vector to be computed, u_d is determined by the measured count and

$$\mu_i(r) = \int \frac{d^2r'}{|r-r'|} exp\left[-\kappa_1 \sum_{i=1}^{3} \gamma_i \xi_i(r,r')\right] \left\{ \sum_{c=1}^{3} \frac{a_c}{|r_c - r'|} + \lambda \left[\sum_{i=1}^{3} \gamma_i \beta_i(r')\right] (A\mu(r')) \right\}_i \qquad i = 0, 1, 2, \cdots$$

where $\xi_i(r, r')$ is the line integral of the basis vectors β_i along the straight line joining r and r'.

The solution γ yields the void fraction and the phase distribution in a straightforward manner. The method was verified by using experimental neutron counts for a number of void fraction values in a stratified flow pattern. Agreement between the experimental and computed values of the void fraction is excellent for most of the measured values. The present method also identifies the flow pattern quite well.

3. Variational Methods

Variational calculus is one of the major tools used to formulate physical problems. Fermat's "least time" and Hamilton's "least action" principles have enjoyed widespread applications in the framework of variational calculus. On the other hand, variational methods such as the Rayleigh-Ritz method, the Bubnov-Galerkin method and the method of moments provide powerful tools to solve differential, integral and integro-differential equations. Both types of applications are indicated here.

3.1 Geophysical tomography

It was assumed in Section 2.1 that a signal travels along straight lines joining the sources and the detectors. A more accurate model may be used to describe the signal path. According to Fermat's principle, the travel time along a ray path joining the given points is minimum compared to all of the neighbouring paths. The physical path is then described by the Euler equation of the associated variational problem, which reduces to

$$\nabla \eta = \frac{d}{d\ell}(\eta \frac{dr}{d\ell}) \tag{3}$$

Equation (3) forms the basis of the ray tracing and the shooting methods.[4]

3.2 Aerosol migration

The transport of aerosols is described by a multi-component, nonlinear integrodifferential equation. Here we consider a simplified version that is adequate enough to address most of the complications.

The number density, $C(m,t)$, of particles of mass m in size range $(0, M)$ at time t is the solution of

$$C'(m,t) = F(m,t,C(m,t))$$

where the prime denotes the derivative with respect to time, and F is a nonlinear operator. The value of $C(m,0)$ is known and $C(0,t) = C(M,t) = 0$. In the direct variational method, the solution $C(m,t)$ is treated as an element of an appropriate Hilbert space H with a scalar product (,). For the present case, H may be taken to be the space of square integrable functions over the interval $(0,M)$. The solution $C(m,t)$ may be approximated by a linear combination of basis functions $\{v_j(m)\}$:

$$C(m,t) = \sum_{j=1}^{n} \alpha_j(t) v_j(m).$$

This reduces the problem to solving

$$A\frac{\partial \alpha(t)}{\partial t} = g(\alpha(t))$$

where A is the normalization matrix, and the vector function $g(\alpha(t))$ is as defined above. Standard methods are used to integrate this equation. A commonly used basis set in this case is given by

$$v_i(m) = m^{i-1}e^{-\gamma m}$$

where γ is an arbitrary positive constant. This scheme was tested for a number of cases.[5] Variational approximations converge rapidly to the exact solution as the basis size increases.

3.3 Control theory

The dynamics of a large class of linear control systems is described by

$$dx/dt = A(t)x + B(t)u, \qquad x(0) = x_0, \tag{4}$$

where x and u are vectors, and A and B are matrices. It is required to find the value u^* of the control function u that optimizes a functional termed the performance index. It can be shown that u^* is related to the solution ξ^* of an operator equation of the form[6]

$$(1+K)\xi^* = g \tag{5}$$

where g is a given vector in a Hilbert space and K is an operator.

While the problem is solvable by the variational methods of the type described above, convergence rate is often poor. However, the set $\{K^{i-1}g\}$ may be used as a basis in the direct variational method. The method based on such a representation is called the moment method.[7] The rate of convergence of the method, when applicable, is usually better, and it may be applied to generate monotonically convergent upper and lower bounds to J[6].

The moment method was compared with the standard variational methods for several realistic problems. The method of moments required only a few basis functions, compared to tens in the other types.

4. Concluding Remarks

As a subfield of applied mathematics, industrial mathematics overlaps with a number of areas of pure mathematics. The applications of the non-intrusive imaging techniques illustrated here cover a small section of the tomographic methods. Other methods worth mentioning are positron emission tomography and ultrasound and magnetic resonance imaging.

The topics and applications discussed in this paper were selected for their significance to AECL Research. Also, these are some of the areas in which we have made substantial improvements over the techniques that were otherwise available. However, some further work is needed before these developments can be fully exploited.

5. References

1. G. Lodha, J.G. Hayles, S.R. Vatsya and M. Serzu, *A new approach to geophysical tomography using areal basis inversion technique,* to be published.
2. S.R. Vatsya, G.R. McGee and P.S. Yuen, *Use of a three-beam gamma densitometer to determine average void fraction and flow regime,* Tenth Annual Conference of Canadian Nuclear Society, Ottawa, 1989.
3. S.R. Vatsya and P.T. Wan, Unpublished report, (1991); S.R. Vatsya, Unpublished report, (1992).
4. W.L. Rodi and J.G. Berryman, *Notes on inversion,* Technical Report, *ER* Laboratory, Mass. Inst. Tech., 1991.
5. S.R. Vatsya and M. Razzaghi, *A solution scheme for aerosol transport models,* 14*th* Annual CNS Simulation Symposium, 1988.
6. S.R. Vatsya, *Optimization of spaces station and robotic control systems,* CASI Symposium on Space Station, Ottawa, 1989.
7. Yu V. Vorobyev, *Method of Moments in Applied Mathematics,* Gordon & Breach, New York, 1965.

MDPOLY: A Molecular Dynamics Simulation Code

P. Y. Wong
Math and Computation
AECL Research

ABSTRACT

MDPOLY is a molecular dynamics (MD) simulation code developed at the National Research Council of Canada. Unlike many early MD codes, which perform only constant volume calculations, MDPOLY uses the constant pressure method, which allows a solid to change its size and shape in response to a given pressure. As such, MDPOLY is particularly well suited for studying structural transformations of crystals. This talk gives an overview of MDPOLY's features and the mathematics involved.

What is molecular dynamics and how does it work?

Molecular dynamics (MD) is a well known technique for simulating liquids and solids by computer[1]. A basic ingredient of any MD simulation is a so-called MD box, usually cubic, which contains the particles (atoms or molecules) to be simulated. The particles move inside the box according to the equations of motion specified by the molecular dynamics. The MD box satisfies a periodic boundary condition (PBC), which means that when a particle moves out from one face of the box, its image from the opposite face enters so that the number of particles in the box is conserved at all times. A PBC also implies that the entire physical space can be filled with identical MD boxes so that only one box need be considered. This explains why an MD box with no more than a few hundred particles can be used to simulate a macroscopic ($\sim 10^{24}$ atoms) bulk system.

There are three basic steps involved in an MD simulation:
(i) Numerically integrate the equations of motion to an equilibrium around a given temperature.
(ii) Collect particle trajectories as a function of time in equilibrium.
(iii) Perform statistical averages from particle trajectories.

Early or conventional MD simulations are based on the classical equations of motion with a fixed MD box. An excellent example of such a simulation is described in a 1964 paper published by Rahman[2]. This paper demonstrates the power of MD simulations and plays an important role in opening up the field of molecular dynamics.

2. Constant Pressure Molecular Dynamics

A major shortcoming of conventional molecular dynamics is that the MD box volume must be kept constant, a condition which limits applications. Since 1980, a new molecular dynamics (NMD) has evolved which allows the box to change its size and shape in response to a given hydrostatic pressure (see Nosé and Klein[3] and references therein). Commonly called constant pressure molecular dynamics, the new MD opens up a way to explore structural transformations of crystals.

Following Nosé and Klein, the three equations of motion in NMD are:

$$\ddot{\mathbf{s}}_i = h^{-1}\mathbf{f}_i m_i^{-1} - \mathbf{G}^{-1}\dot{\mathbf{G}}\dot{\mathbf{s}}_i \tag{1}$$

$$\frac{d}{dt}(\mathbf{I}_i\omega_i) = \tau_i \tag{2}$$

$$\ddot{h} = W^{-1}(\mathbf{\Pi} - \mathbf{P}_{ex}1)\sigma \tag{3}$$

Eq.(1) gives a molecule's centre-of-mass translational motion, while Eq.(2) specifies the rotational motion about the centre-of-mass. The matrix h in Eq.(3) carries the size and shape of the MD box at any time t and, as shown, varies according to the imbalance between the internally generated stress tensor $\mathbf{\Pi}$ and the external pressure $\mathbf{P}_{ex}$. If h is not allowed to vary with time, these equations are reduced to the classical equations of motion.

3. MDPOLY

MDPOLY[4] is a polyatomic, rigid-molecule MD code developed at the National Research Council of Canada.

3.1 Key features

- constant pressure molecular dynamics,
- pairwise additive potentials plus distributed charges,
- forces are of the site-site form,
- orientations represented by quaternions[5],
- equations of motion solved by Gear's predictor-corrector method[6].

3.2 Quaternions

The standard method of solving the rotational equation (Eq.(2)) is to rotate the inertia tensor I in the space-fixed coordinates by the Euler angles (ϕ, θ, ψ) to the body-fixed coordinates. The angular velocity ω is then solved in the body-fixed frame. The method poses a difficulty in that the equations of motion of the Euler angles contain a singularity at $\theta = 0$. In MDPOLY, Evans'[5] method of quaternions is used to solve for the orientations, which is singularity-free.

3.3 Method of solution

The equations of motions are solved using Gear's predictor-corrector method.

3.4 Computer-time intensive

All MD codes are computer-time intensive and MDPOLY is no exception. This is due to the number of forces that need to be calculated in a timestep which goes as $N^2/2a$, where a is the reduction factor due to range cutoff, and N the number of atoms in a simulation. Computer time is the main constraint to larger simulations. An MDPOLY simulation typically takes many hours of Cyber-990 time.

3.5 Difficulty

MDPOLY is particularly well suited for modelling crystal structural transformations[7]. A major problem here is to find a good potential. While the Lennard-Jones type of potentials seem to work well with solid and liquid carbon tetrafluoride[8], so far they are not able to explain the crystal transformations of T_eF_6 or C_4F_8. How to find an effective potential, given the demanding computer time constraint, remains a very real challenge.

References

1. G. Ciccotti, D. Frenkel and I.R. McDonald, editors, *Simulation of Liquids and Solids*, (NORTH-HOLLAND, 1987).
2. A. Rahman, *Correlations in the Motion of Atoms in Liquid Agron*, Physical Review, Volume 136, No. 2A, 1964.
3. S. Nosé and M.L. Klein, *Constant Pressure Molecular Dynamics for Molecular Systems*, Molecular Physics, Vol. 50, No. 5, 1983.
4. R. Impey, *MDPOLY*, National Research Council of Canada, (undocumented).
5. D.J. Evans, *On the Representation of Orientation Space*, Molecular Physics, **34**, 317-25, 1977.
6. C.W. Gear, *Numerical initial value problems in ordinary differential equations*, (Prentice-Hall, Englewood Cliffs, NJ, 1971).
7. R.W. Impey, M. Sprik, and M.L. Klein, *Simulation of the cubic to orthorhombic phase transition in potassium cyanide*, J.Chem. Phys. **83**(7), 1985.
8. S. Nosé and M.L. Klein, *A study of solid and liquid carbon tetrafluoride using the constant pressure molecular dynamics technique*, J.Chem. Phys. **78**(11), 1983

A SELF-CONSISTENT MODEL OF IRRADIATION CREEP AND GROWTH

C.H. WOO, C. TOME and N. CHRISTODOULOU
Reactor Materials Research Branch
Reactor Materials Division

ABSTRACT

Irradiation creep and growth in zirconium alloys result in anisotropic dimensional changes relative to the crystallographic axis in each individual grain. Since the deformation of each grain is constrained by the collective deformation of neighbouring grains, anisotropic deformation generates internal stresses. As a result, the total deformation of a polycrystalline specimen cannot simply be taken as the average of the deformation of its individual grains under the action of only the external stresses. The aim of this paper is to demonstrate how intergranular interaction can be taken into account during irradiation creep and growth.

1. Introduction

Zirconium alloys are widely used as structural materials in nuclear reactors. During manufacturing and under reactor operating temperatures, most of these alloys have a hexagonal close-packed crystallographic structure. They tend to develop sharp textures because of the anisotropic properties of the single crystal. Many of their physical properties are anisotropic including irradiation creep (i.e. deformation under an applied stress) and growth (i.e. deformation under no load). Both creep and growth result in anisotropic dimensional changes relative to the crystallographic axes in each individual grain. Since a polycrystalline sample is a collection of many grains with different orientations, anisotropic deformation of the individual crystals generates internal stresses due to the constraint imposed on each grain by the collective deformation of the surrounding grains. These stresses cause elastic, plastic and creep deformation as each grain has to conform to the deformation of its neighbours to maintain the integrity of the entire sample.

2. Polycrystalline Model

The distribution of orientations of all the grains in space in a polycrystallline sample defines the crystallographic texture. A self-consistent polycrystalline deformation model developed by Woo [1] will be used to calculate the steady state deformation rate of the polycrystal. Each grain of the polycrystalline sample is considered to be an inhomogeneous ellipsoidal inclusion embedded in a continuum matrix with properties identical to those of the polycrystal. The intergranular compatibility condition can then be described by the elastic-plastic interaction between the inclusion and the matrix, using the 'constraint' tensor $\mathbf{K}^*$ introduced by Hill [2] for the continuum matrix. If σ^* is a uniform stress field producing a traction on the interface of the inclusion with the matrix, and $\dot{\varepsilon}^*$ is the corresponding uniform deformation rate due to the traction, then $\mathbf{K}^*$ is defined by

$$\dot{\varepsilon}^* = \dot{\varepsilon} - \dot{E} = \mathbf{K}^*.\, \sigma^* = \mathbf{K}^*.(\sigma - \Sigma) \qquad (1)$$

Here $\mathbf{K}^*$ is a function of the creep compliance of the polycrystalline matrix $\mathbf{K}$ and the aspect ratio of the inclusion, $\dot{E}$ and Σ are the strain rate of the polycrystal and external stress, respectively and $\dot{\varepsilon}$ is the strain rate of the individual grain. It is also implied in eq. (1) that σ^* is equal to the internal stress generated due to the anisotropic deformation of the single crystal and the constraint imposed by the collective deformation of the surrounding grains. For irradiation creep $\mathbf{K}$ and $\mathbf{K}^*$ are assumed to be independent of stress and are related by

$$\mathbf{K}^* = (\mathbf{S}^{-1} - \mathbf{I})^{-1}.\, \mathbf{K} \qquad (2)$$

Here $\mathbf{S}$, the 'viscous' Eshelby tensor, is a function of $\mathbf{K}^{-1}$ and the aspect ratio of the inclusion and can be calculated numerically [1]. The following expressions are also true

$$\dot{\varepsilon} = \mathbf{k}\,\sigma + \dot{\gamma} \tag{3}$$

$$\dot{\mathbf{E}} = \mathbf{K}\,\Sigma + \dot{\Gamma} \tag{4}$$

$$\dot{\mathbf{E}} = \{\dot{\varepsilon}\} \qquad\qquad \Sigma = \{\sigma\} \tag{5}$$

From equations (1-5) the macroscopic strain rate is given by

$$\dot{\mathbf{E}} = \{(\mathbf{k}+\mathbf{K}^*)^{-1}\}\ [\{\mathbf{k}+\mathbf{K}^*)^{-1}\mathbf{k}\}\Sigma + \{(\mathbf{k}+\mathbf{K}^*)^{-1}\dot{\gamma}\}] \tag{6}$$

where $\mathbf{k}$ and $\dot{\gamma}$ are the single crystal creep compliance and growth rate respectively, and $\{\}$ brackets denote weighted averaging over the grains. $\mathbf{K}$ can be expressed in terms of $\mathbf{k}$ by means of

$$\mathbf{K} = \{(\mathbf{k}+\mathbf{K}^*)^{-1}\}^{-1}\ \{(\mathbf{k}+\mathbf{K}^*)^{-1}\mathbf{k}\} \tag{7}$$

The effect of texture is accounted for in eqs. (6) and (7) through the weighted average and the fact that all the tensors have to be referred to the same set of axes. Eq. (7) is used in the numerical calculation for determining $\mathbf{K}$ given $\mathbf{k}$ and the crystallographic texture. $\mathbf{k}$ can also be calculated if $\mathbf{K}$ and the crystallographic texture are given. The latter technique is used to derive $\mathbf{k}$ for calandria and pressure tube materials. Then it is possible to correlate the calculated values of $\mathbf{k}$ with the predominant creep mechanisms taking place during reactor operation.

The manipulation of the tensors involved in the analysis can be handled more readily if the following basis of 2nd order orthonormal symmetric tensors $\mathbf{b}^n$ is defined

$$\boldsymbol{b}^1 = 1/\sqrt{6}\begin{pmatrix}1 & 0 & 0\\ 0 & 1 & 0\\ 0 & 0 & \overline{2}\end{pmatrix} \qquad \boldsymbol{b}^3 = 1/\sqrt{2}\begin{pmatrix}0 & 0 & 0\\ 0 & 0 & 1\\ 0 & 1 & 0\end{pmatrix}$$

$$\boldsymbol{b}^2 = 1/\sqrt{2}\begin{pmatrix}1 & 0 & 0\\ 0 & \overline{1} & 0\\ 0 & 0 & 0\end{pmatrix} \qquad \boldsymbol{b}^4 = 1/\sqrt{2}\begin{pmatrix}0 & 0 & 1\\ 0 & 0 & 0\\ 1 & 0 & 0\end{pmatrix}$$

$$\boldsymbol{b}^6 = 1/\sqrt{3}\begin{pmatrix}1 & 0 & 0\\ 0 & 1 & 0\\ 0 & 0 & 1\end{pmatrix} \qquad \boldsymbol{b}^5 = 1/\sqrt{2}\begin{pmatrix}0 & 1 & 0\\ 1 & 0 & 0\\ 0 & 0 & 0\end{pmatrix}$$

The fourth rank tensors can then be represented as follows:

$$\mathbf{k} = k_a\,\mathbf{b}^a\,\mathbf{b}^a \tag{8}$$

where k_1, k_2 ($=k_5$), k_3 ($=k_4$), k_6 ($=0$) are the corresponding eigenvalues.

References

1. C.H. Woo, "Materials for Nuclear Reactor Core Applications", British Nuclear Energy Society, (1987), p. 65.
2. R. Hill, J. Mech. Phys. Solids, **13** (1965) 89.

LOW-DIMENSIONAL DESCRIPTION OF PLANT CANOPY TURBULENT FLOW

Yahui Zhuang
Environmental Science Branch
AECL Research, Pinawa, Manitoba

Abstract

We propose that the large-scale airflow structures within forest canopies can be described by a relatively low-dimensional dynamical system. This research aims at simplifying a model of turbulence transport in the plant canopy.

1. Introduction

Over the last two decades, research on air turbulence in plant canopies has revealed that various transport mechanisms within the canopy are dominated by intermittent, large-scale coherent structures. They appear as sweep structures in the velocity signals and ramps in the scalar fluctuations. These organized motions are one of the causes of the inhomogeneity in canopy turbulence. It is well known that the traditional gradient transport theory does not work in describing canopy flow.[1] Although the higher-order closure models have provided some valuable information, they tend to smear the instantaneous large-scale flow structures considered to be very important in the turbulent transport processes. It is suggested that the coherent dynamics have to be incorporated to explain the flow phenomena observed. Most existing works on the coherent structure in canopy turbulent flow use the conditional sampling or VITA technique to extract the coherent structures. The averaging and smoothing procedures used in these methods prevent them from giving a complete description of the dynamics of the coherent structures.

On the theoretical side, recent applications of dynamical system theory to turbulence flow have shown that the transport properties of the turbulent flows, especially the ones that are obviously influenced by the coherent structures, may be described by a relatively low-dimensional strange attractor in phase space.[2] This suggests that the natural decomposition of the turbulent flow is to divide the flow into organized motions represented by the dominant orbits in phase space and the statistical fluctuations about these orbits.

In view of the abundant evidence of coherent structures in the canopy flows, we feel that a low-dimensional study of the canopy turbulent flow may provide the dynamical information about the transport processes that the experimental work cannot offer. In this study we will use a simple dynamical system theory to determine whether the canopy flow is low-dimensional, and if it is then find the suitable flow coordinates in phase space to represent the flow in physical space. The flow dynamics, especially the coherent structures, will be discussed in terms of this low-dimensional dynamical system.

2. Dimensional estimate of the canopy flow

Dissipative nonlinear dynamical systems, such as the one under study, that exhibit chaotic behaviour in the experimental signals sometimes have strange attractors characterized by their fractal dimensionality in phase space. To examine the possibility that the canopy turbulence is a low-dimensional one, we can try to estimate the dimension of the phase space region visited by this dynamical system. A simple method developed by Grassberger and Procaccia[3] will be used to measure the global geometrical properties; *i.e.*, the correlation dimension of this system. The definition of the correlation

$$C(r) = lim \frac{1}{N^2} \sum_{i,j=1}^{N} H(r - |X_i - X_j|) \qquad (1)$$

where $H(x)$ is the Heaviside function with $H(x) = 1$ for $x > 0$, $H(x) = 0$ for $x < 0$, the $\mathbf{X}$ are the phase space variables for this system and N the total number of the phase variables. The theory is that $C(r) \propto r^d$ for a certain range of r. The exponent d is closely related to the fractal dimension D. The phase variable, $\mathbf{X}$, can be constructed from a time series of a single experimental variable. With this technique, and using a vertical velocity time series obtained from an experiment within a canopy, we calculated the correlation

$C(r)$. Our analysis shows that the system has only six degrees of freedom and, in principle, one should be able to describe the velocity evolution using a closed set of ordinary differential equations with only six, and at most 15, independent variables. Although this gives no hint as to what the phase variables are and what the equations might look like, it provides an inspiration for seeking a low-dimensional description of the flow.

3. Identification of flow coordinates (Phase space)

Knowing that the flow can be decomposed into a small number of elementary components, one can expand the velocity field in the volume occupied by the fluid in a set of suitable orthogonal functions. A common choice of the orthogonal functions is the Fourier series as used in the spectral method of fluid dynamics. Such a selection of orthogonal functions, although elegant mathematically, is not very suitable for our purpose. Since we are interested in large-scale dynamics, the Fourier series representation, as Tennekes[4] pointed out, weighs too much on the small scales and is ineffective in representing the large scales. Furthermore, the large-scale structures are sensitive to the geometry of the boundary; *i.e.*, different flows have different large-scale structures. In this study, we will extract such orthogonal functions from the experimental data by the "Proper Orthogonal Decomposition" proposed by Lumley.[5] Once the orthogonal functions are extracted from the experimental data, the velocity signal can be decomposed as

$$V(x,t) = \Sigma \alpha_j \phi_j(x,t). \tag{2}$$

Here α_j are the general flow coordinates in phase space.

4. Governing equations

So far we have found a way to decompose the velocity field. To describe the evolution of the flow field, we need dynamical equations that can predict the variations of the decomposition coefficients, α_j, with time and the interactions among different orthogonal functions in space. We assume that the velocity variation at a fixed space is caused essentially by the large-scale turbulence given by Eq. (2), plus some small-scale random fluctuations which can be modeled. Substituting (2) into the Navier-Stokes equations,

$$\frac{\partial v}{\partial t} = D(v), \tag{3}$$

then projecting (Galerkin) this along the eigenfunctions, ϕ_n, we obtain the ordinary differential equations,

$$\frac{d\alpha_k}{dt} = F_k(\alpha), \qquad k = 1, 2, \ldots \tag{4}$$

The contribution from small-scale turbulence will be modeled by the eddy viscosity concept.

5. Numerical simulation of the flow field

The phase space evolution of the flow field will be obtained by numerically integrating Eq. (4) in time. Each set of α's represent a flow visualization at that moment by Eq. (2). It is hoped that such an instantaneous flow simulation will help us to understand the dynamics of the canopy flow, especially the coherent dynamics observed in the experiments.

Acknowledgements

I wish to thank B. Amiro and Phil Davis for reviewing this manuscript.

References

1. Raupach, M.R. *et al.* (1989): Coherent eddies in vegetation canopies, Proc. Fourth Australian Conference on Heat and Mass Transfer, Christchurch, New Zealand.
2. Newell, A.C. *et al.* (1988): Turbulent transport and random occurrence of coherent events, Physica $D, 33, 281 - 303$.
3. Grassberger, P. and Procaccia, I. (1982): Measuring the strangeness of strange attractors, Physica $9D, 189 - 208$.
4. Tennekes, H. (1976): Fourier-transform ambiguity in turbulence dynamics, J. of the Atmos. Sci. **33**, 1660-1663.
5. Lumley, J.L. (1970): Stochastic tools in turbulence, Academic Press, N.Y.

APPENDIX A

WORKSHOP ON APPLIED MATHEMATICS

PROGRAMME

FRIDAY, FEBRUARY 7	
8:30am	**Dolling:** Opening Remarks
8:55am	**Lee:** Rude Interruption
9:00am	**Baset:** Finite elements - theory and applications
9:30am	**Kobos:** F.E. Analysis of Duralcan™ MMC Brake Rotor
9:45am	**Rowat:** Isotope-selective laser ionization
10:00am	**Selander:** Performance assessment modelling
10:30am	◇◇◇ *Coffee and discussion break* ◇◇◇
11:00am	**McRae:** Shanks' iterated algorithm
11:15am	**Lina:** Parallel computations and CANDU reactors
11:30am	**Milgram:** Classical and notsoclassical analysis
11:45am	**Christodoulou:** Irradiation creep and growth
12:00pm	**Subrao:** Matrix computations
12:15pm	**Pusch:** Theory and applications of differential algebra
12:30pm	◇◇◇ *Lunch* ◇◇◇
1:30pm	**Diserens:** Eddy current simulations in 3d
2:00pm	**Sullivan:** Computer modelling of eddy current probes
2:15pm	**Sawicka:** Computed tomography and related techniques
2:30pm	**Thibault:** Ultrasonic waves in solids
2:45pm	**Chaplin:** Modelling ultrasonic inspection of pressure tubes
3:00pm	◇◇◇ *Coffee and discussion break* ◇◇◇
3:30pm	**Poulsen:** From calculus to numerics and back again
3:45pm	**Carver:** Overview of multidimensional two-fluid computation
4:15pm	**Banas:** Multiphase flows and computational fluid dynamics
4:30pm	**Vatsya:** Topics in industrial mathematics
5:00pm	◇◇◇ *End of session* ◇◇◇
6:30pm	CASH BAR – ELMS CAFE
7:00pm	**DINNER**

SATURDAY, FEBRUARY 8	
9:00am	**Too:** Mathematical modelling of hot forming of metals
9:30am	**Davis:** Pressure-tube sampler
9:45am	**Davies:** Normal form methods and resonances in particle accelerators
10:15am	**Zhuang:** Low-dimensional description of canopy turbulent flow
10:30am	◇◇◇ *Coffee and discussion break* ◇◇◇
11:00am	**Rasmussen:** Computer Simulation Western
11:30am	**Wong:** MDPOLY — A molecular dynamics simulation code
11:45am	**Woo:** Radiation damage modelling
12:00pm	**Jack:** Unusual representations of discontinuous curves
12:15pm	**Keech:** GLUBFIT — Interactive graphic curve fitting program
12:30pm	◇◇◇ *Lunch* ◇◇◇
1:30pm	**Schmeing:** Generalized Pauli Operators
1:45pm	**Marsiglio:** Electron correlations in solids
2:00pm	**Couture:** Quantum symmetries
2:15pm	**Leivo:** Quantum groups with Mathematica
2:30pm	**Lee:** Quantum algebra and quantum holonomy
2:45pm	◇◇◇ *Coffee and discussion break* ◇◇◇
3:15pm	**ROUND TABLE DISCUSSION**
5:30pm	**Lee:** Closing Remarks

APPENDIX B

List of Participants

Banas, Andrzej	*Thermalhydraulics Dev., CRL*
Baset, Saleh B.	*Math. & Comp., CRL*
Blair, Jim	*Math. & Comp., CRL*
Brewster, Peter	*Reactor Physics, CRL*
Buyers, W.J.L.	*NSSP, CRL*
Carey, Margaret	*Theoretical Physics*
Campagna, Alfio	*Thermalhydraulics Dev., CRL*
Carver, Mike	*Thermalhydraulics Dev., CRL*
Chaplin, Ken	*Non-D Test Dev., CRL*
Chatoorgoon, Vijay	*Thermalhydraulics Dev., CRL*
Christodoulou, Nick	*Reactor Materials Res., CRL*
Couture, Michel	*Theoretical Physics, CRL*
Creutzberg, T.	*Thermalhydraulics Dev., CRL*
Davies, Walter G.	*Nuclear Physics, CRL*
Davis, Ron	*Reactor Physics, CRL*
De Jong, Mark - Dr.	*Accelerator Physics, CRL*
Diserens, N.J.	*Math. & Compt., CRL*
Douglas, Stephen	*Math. & Compt., CRL*
Gracie, Brian	*Math. & Compt., CRL*
Jack, David	*Safety & Environmental, CRL*
Jateaonkar, Ravi	*Civil & Electrical Design*
Kalechstein, Wally	*Instrumentation & Control, CRL*
Keech, Howard	*Math. & Comp., CRL*
Kiteley, Jon	*Thermalhydraulics Dev., CRL*
Kobos, Andrew	*Alcan International Ltd.*
Lane, Fenella	*Waste Management, CRL*
LaPointe, Patrice	*Math. & Compt., CRL*
Laughton, Peter J.	*Reactor Physics, CRL*
Lee, Paul H.C.	*Theoretical Physics, CRL*
Lee-Whiting, Graham	*Deep River*
Leivo, Peter	*Theoretical Physics, CRL*
LeNeveu, Dennis	*Envir. & Safety Assess., WL*
Lidicky, Bernard	*Thermalhydraulics Dev., CRL*
Lina, Jean Marc	*University of Montreal*
Liner, Yakov	*Thermalhydraulics Dev., CRL*
Lone, M. Aslam	*NSSP, CRL*
Marsiglio, Frank	*Theoretical Physics, CRL*
McRae, Glenn	*Physical Chemistry, CRL*
Milgram, Mike	*Reactor Physics, CRL*
Pensom, Croombe	*Safety & Reliability Anal., CRL*
Poulsen, Niel B.	*Thermalhydraulics Dev., CRL*
Pusch, Gordon D.	*TASCC A&D, CRL*
Rasmussen, Henning	*Applied Mathematics, UWO*
Rowat, John	*Waste Management Systems, CRL*
Sawicka, Barbara	*Non-Destruc. Test Dev., CRL*
Schmeing, Nancy	*Theoretical Physics, CRL*
Sears, Varley F.	*Theoretical Physics, CRL*
Selander, Bill N.	*Waste Management, CRL*
Smellie, Don	*Deep River*
Subrao, Dore	*Comput. & Inform. Sys., WL*
Sullivan, Sean	*NDT Development, CRL*
Thibault, Gordon A.	*NDT Development, CRL*
Too, James	*CANMET, EMR*
Vatsya, S. Raj	*Thermalhydraulics, WL*
Wilkinson, Steven R.	*Waste Management Systems, CRL*
Wills, Anne	*Environmental Research, CRL*
Winfield, Dave	*Safety & Reliability Anal., CRL*
Wong, Peter Y.	*Math. & Comp., CRL*
Woo, C.H.	*Reactor Materials Res., WL*
Zariffeh, E.K.	*Thermalhydraulic Dev., CRL*
Zhuang, Yahui	*Environmental Science, WL*

* *CRL = Chalk River Laboratories, Chalk River, Ontario, K0J 1J0, Canada*
** *UWO = University of Western Ontario, London, Ontario, N6A 5B7, Canada*
*** *WL = Whiteshell Laboratories, Pinawa, Manitoba, R0E 1L0, Canada*

Cat. No. CC2-10748E
ISBN 0-660-15196-0
ISSN 0067-0367

To identify individual documents in the series we have assigned an AECL- number to each.

Please refer to the AECL- number when requesting additional copies of this document

from

Scientific Document Distribution Office
Atomic Energy of Canada Limited
Chalk River, Ontario, Canada
K0J 1J0

Price: B

No. au cat. CC2-10748E
ISBN 0-660-15196-0
ISSN 0067-0367

Pour identifier les rapports individuels faisant partie de cette série nous avons assigné un numéro AECL- à chacun.

Veuillez faire mention du numéro AECL- si vous demandez d'autres exemplaires de ce rapport

au

Service de Distribution des Documents Officiels
Énergie atomique du Canada limitée
Chalk River, Ontario, Canada
K0J 1J0

Prix: B

1638-93